nagra
National Cooperative for the
Disposal of Radioactive Waste

TECHNICAL REPORT 01-02

Experimental studies on the inventory of cement-derived colloids in the pore water of a cementitious backfill material

A contribution to the understanding of their rôle in the retardation of radionuclides in the near-field of a repository

August 2001

E. Wieland

Labor für Endlagersicherheit (LES/PSI)

Hardstrasse 73, CH-5430 Wettingen/Switzerland, Telephone +41-56-437 11 11

nagra
National Cooperative for the
Disposal of Radioactive Waste

TECHNICAL REPORT 01-02

Experimental studies on the inventory of cement-derived colloids in the pore water of a cementitious backfill material

A contribution to the understanding of their rôle in the retardation of radionuclides in the near-field of a repository

August 2001

E. Wieland

Labor für Endlagersicherheit (LES/PSI)

Hardstrasse 73, CH-5430 Wettingen/Switzerland, Telephone +41-56-437 11 11

This report was prepared on behalf of Nagra. The viewpoints presented and conclusions reached are those of the author(s) and do not necessarily represent those of Nagra.

PREFACE

The Laboratory for Waste Management at the Paul Scherrer Institut is performing work to develop and test models as well as to acquire specific data relevant to performance assessments of planned Swiss nuclear waste repositories. These investigations are undertaken in close co-operation with, and with the financial support of, the National Co-operative for the Disposal of Radioactive Waste (Nagra). The present report is issued simultaneously as a PSI-Bericht and a Nagra Technical Report.

ISSN 1015-2636

ABSTRACT

The potential rôle of near-field colloids for the colloid-facilitated migration of radionuclides has stimulated investigations concerning the generation and presence of colloids in the near-field of a repository for low- and intermediate level waste (L/ILW). The highly gas permeable mortar (Nagra designation: mortar M1) is currently favoured as backfill material for the engineered barrier of the planned Swiss L/ILW repository. The cementitious backfill is considered to be a chemical environment with some potential for colloid generation.

In a series of batch-style laboratory experiments the physico-chemical processes controlling the inventory of colloids in cement pore water of the backfill were assessed for chemical conditions prevailing in the initial stage of the cement degradation. In these experiments, backfill mortar M1 or quartz, respectively, which may be used as aggregate material for the backfill, were immersed in artificial cement pore water (a NaOH/KOH rich cement fluid). Colloid concentrations in the cement pore water were recorded as a function of time for different experimental settings. The results indicate that a colloid-colloid interaction process (coagulation) controlled the colloid inventory. The mass concentration of dispersed colloids was found to be typically lower than 0.02 ppm in undisturbed batch systems. An upper-bound value was estimated to be 0.1 ppm taking into account uncertainties on the measurements.

To assess the potential for colloid generation in a dynamic system, colloid concentrations were determined in the pore water of a column filled with backfill mortar. The chemical conditions established in the mortar column corresponded to conditions observed in the second stage of the cement degradation (a $Ca(OH)_2$-controlled cement system). In this dynamic system, the upper-bound value for the colloid mass concentration was estimated to be 0.1 ppm.

Implications for radionuclide mobility were deduced taking into account the experimental results of the study. Predictions of the colloidal effect on radionuclide mobility were based on the assumption that colloids dispersed in the pore water of the backfill material may reduce radionuclide sorption (R_d values) on cement. This effect was described in terms of a sorption reduction factor. The distribution ratios (R_c) of radionuclides between the cement pore water and the colloidal phase as well as the colloid mass concentration (m_c) are the two important colloidal parameters affecting sorption reduction. No significant sorption reduction is expected for weakly and moderately sorbing radionuclides ($R_d \leq 1$ m^3 kg^{-1}) up to a colloid concentration of 1 ppm. Moreover, no significant sorption reduction is anticipated for strongly sorbing radionuclides ($R_d > 1$ m^3 kg^{-1}) below colloid concentrations of 0.1 ppm. This value is considered to be representative for the backfill material. At higher colloid concentrations, however, sorption reduction may occur in case of the strongly sorbing radionuclides. Nevertheless, due to an extremely strong uptake of these elements by cement in the absence of colloids, the effective sorption values in the presence of colloids are predicted to be still high.

ZUSAMMENFASSUNG

Da Kolloide den Transport von Radionukliden beeinflussen können, wurden Untersuchungen zur Bildung und zum Inventar von Kolloiden im Nahfeld eines Endlagers für schwach und mittelaktive Abfälle (Endlager SMA) durchgeführt. Es ist geplant, einen hochpermeablen Mörtel (Nagra Bezeichnung: Mörtel M1) als Verfüllmörtel in einem Endlager SMA zu verwenden. Die in diesem zementgebundenen Verfüllmörtel erzeugten chemischen Bedingungen könnten die Bildung von Kolloiden im Nahfeld begünstigen.

In einer Serie von Experimenten wurden die physikalisch-chemischen Prozesse untersucht, die das Kolloidinventar im Zementporenwasser des Verfüllmörtels bestimmen können. Die Untersuchungen wurden in Batch Systemen unter solchen Bedingungen durchgeführt, wie sie während der ersten Phase der Zementdegradation auftreten. Dazu wurde Verfüllmörtel oder Quarz, der als Aggregatmaterial zur Herstellung des Verfüllmörtels verwendet wurde, mit synthetisch hergestelltem Zementporenwasser (ein NaOH/KOH reiches Zementporenwasser) in Kontakt gebracht. Die Kolloidkonzentrationen im Zementporenwasser wurden in Abhängigkeit der Zeit und für verschiedene experimentelle Auslegungen bestimmt. Die Resultate zeigen, dass ein Kolloid-Kolloid Wechselwirkungsprozess (Koagulation) das Kolloidinventar kontrolliert. In nicht gestörten Batch Systemen war die Massenkonzentration der im Zementporenwasser suspendierten Kolloide typischerweise unter einem Wert von 0.02 ppm. Unter Berücksichtigung der Messunsicherheiten wurde der Maximalwert für die Konzentration auf 0.1 ppm abgeschätzt.

Um die Möglichkeit einer Kolloidbildung in dynamischen Systemen beurteilen zu können, wurden in weiteren Untersuchungen die Kolloidkonzentrationen im Porenwasser einer mit Verfüllmörtel gefüllten Kolonne ermittelt. Das vom Verfüllmörtel kontrollierte chemische Milieu in der Kolonne entsprach Bedingungen, wie sie während der zweiten Phase der Zementdegradation (ein $Ca(OH)_2$ kontrolliertes Zementsystem) auftreten. In diesem dynamischen System wurde der Maximalwert der Kolloidmassenkonzentrationen auf 0.1 ppm abgeschätzt.

Die Auswirkungen von Nahfeldkolloiden auf die Radionuklidmobilität im Verfüllmörtel wurde anhand der experimentellen Resultate beurteilt. Der Einfluss von Kolloiden auf die Radionuklidmobilität wurde unter der Annahme, dass die im Zementporenwasser suspendierten Kolloide zu einer Reduktion der Radionuklidbindung am Zement (R_d Werte) führen können, abgeschätzt. Diese Sorptionsreduktion konnte unter Berücksichtigung des Verteilungskoeffizienten (R_c) eines Radionuklids zwischen dem Zementporenwasser und der kolloidalen Phase sowie der Kolloidmassenkonzentration (m_c) quantifiziert werden. Keine Reduktion der Bindung an Zement wird für schwach und mässig sorbierende Radionuklide ($R_d \leq 1\ m^3\ kg^{-1}$) bei Kolloidkonzentrationen von weniger als 1 ppm erwartet. Bei stark sorbierenden Radionukliden ($R_d > 1\ m^3\ kg^{-1}$) findet ebenfalls keine wesentliche Sorptionsreduktion bis zu einer Maximalkonzentration der Kolloide von 0.1 ppm statt. Diese Kolloidmassenkonzentration wird als typischer Wert für den Verfüllmörtel angesehen. Im Falle der stark sorbierenden Radionuklide wird bei höheren Kolloidkonzentrationen eine Reduktion der Radionuklidbindung an Zement erwartet. Wegen der sehr starken Bindung in Abwesenheit von Kolloiden wird jedoch für diese Radionuklide auch bei erhöhten Kolloidkonzentrationen noch ein hohes Rückhaltevermögen durch Zement vorausgesagt.

RÉSUMÉ

Le rôle potentiel des colloïdes du champ proche sur la migration des radionucléides est à l'origine de recherches sur la formation et la présence de colloïdes dans le champ proche d'un dépôt final pour déchets de faible et moyenne activité. Le mortier M1 (désignation donnée par la Nagra), fortement perméable au gaz, est actuellement le matériau envisagé pour les barrières ouvragées dans les sites de stockage final destinés aux déchets de faible et moyenne activité planifiés en Suisse. Ce mortier à base de ciment est considéré comme un environnement chimique propice à la formation de colloïdes.

Les processus physico-chimiques contrôlant l'inventaire des colloïdes dans les eaux interstitielles du ciment ont été étudiés. Pour cela, des expériences (méthodes de batch) ont été effectuées en laboratoire dans les conditions chimiques qui prévalent dans la phase initiale de dégradation du ciment. Pour effectuer ces expériences, du mortier M1 ou du quartz, qui est l'un des composants de ce mortier, ont été immergés dans une eau interstitielle synthétique de ciment (eau de ciment riche en NaOH/KOH). Les concentrations en colloïdes ont été enregistrées selon le temps écoulé pour différents arrangements expérimentaux. Les résultats indiquent que le processus d'interaction entre colloïdes (coagulation) contrôle l'inventaire des colloïdes. La concentration massique des colloïdes dispersés a été typiquement trouvée inférieurs à 0.02 ppm dans des systèmes en batchs non-perturbés. Une valeur limitée supérieur a été estimée égale à 0.1 ppm en prenant en compte les incertitudes des mesures.

Afin d'estimer la capacité d'un système dynamique à générer des colloïdes, les concentrations en colloïdes ont été mesurées dans l'eau interstitielle d'une colonne remplie de mortier M1. Les conditions chimiques régnant dans cette colonne étaient identiques à celles observées lors de la deuxième phase de dégradation du ciment (système de ciment contrôlé par le $Ca(OH)_2$). La valeur limitée supérieur de la concentration massique en colloïdes dans ce système dynamique à été estimée égale à 0.1 ppm.

Les résultats expérimentaux de cette étude ont permis d'évaluer les influences exercées par les colloïdes sur la mobilité des radionucléides. Pour estimer l'influence des colloïdes sur la rétention des radionucléides, on a supposé que les colloïdes dispersés dans les eaux interstitielles du mortier M1 réduisaient la sorption des radionucléides sur le ciment (R_d coefficent). La réduction de la sorption a été décrite sous la forme du coefficient de répartition des radionucléides entre l'eau interstitielle et la phase colloïdale (R_c) et la concentration massique en colloïdes (m_c). En présence de concentrations en colloïdes inférieures à 1 ppm, aucune réduction de la sorption n'est prévisible pour les radionucléides qui sorbent faiblement ou modérément sur le ciment ($R_d \leq 1\ m^3\ kg^{-1}$). De plus, la sorption des radionucléides sorbant fortement sur le ciment ($R_d > 1\ m^3\ kg^{-1}$) ne sera pas réduite de façon significative pour des concentrations en colloïdes inférieures à 0.1 ppm. Cette concentration est considérée comme typique pour le matériau de remplissage. Pour des concentrations en colloïdes plus élevées, cependant, une réduction de la sorption pourrait avoir lieu dans le cas de radionucléides qui sont fortement sorbés. Néanmoins, en raison de la forte affinité que présentent ces éléments pour le ciment en l'absence de colloïdes, leur sorption prévue en présence de colloïdes sera également élevée.

TABLE OF CONTENTS

LIST OF FIGURES

LIST OF TABLES

1 INTRODUCTION

1.1 The Rôle of Colloids in Radionuclide Migration

The retardation of contaminants in subsurface environments is believed to depend upon the distribution of the mobile species between a mobile aqueous phase (groundwater flow) and an immobile solid phase (rock or soil constituent). In the last years, numerous studies have, however, shown that colloids dispersed in the groundwater may enhance contaminant transport in subsurface aquifers (for reviews see McCARTHY & DEGUELDRE 1993; SWANTON 1995). Therefore, in the Swiss programme for the disposal of radioactive waste, colloid-facilitated radionuclide migration has been considered and addressed in performance assessments (NAGRA 1994a; NAGRA 1994b).

A series of sub-processes contribute to the impact of colloids on radionuclide transport: 1) the generation and release of colloids from the repository environment, 2) the physico-chemical stability of the colloidal material (growth, coagulation and disaggregation), 3) the interaction of colloids with the repository or rock material (colloid filtration), 4) adsorption/desorption of radionuclides onto the colloidal matter, and 5) the mobility and chemical stability of the colloids in the goundwater aquifer of the far field. Numerous models have been developed to describe the colloid-mediated transport of radionuclides in homogeneous porous or fractured media (e.g., TRAVIS & NUTALL 1985; BONANO & BEYELER 1985; GRINDROD 1990; SMITH & DEGUELDRE 1993; NUTALL & LONG 1993; ABDEL-SALAM & CHRYSIKOPOULOS 1995). For the performance assessment of the planned Swiss repositories, the effect of colloids on radionuclide migration in the near-field and far-field has been quantified using a simplified transport model (e.g., SMITH 1993; SMITH & DEGUELDRE 1993). The underlying model scenario is based upon solute transport in a dual-porosity system (fractured rock). It includes the physical and chemical processes relevant to colloid-facilitated transport of radionuclides.

Three criteria must be met for inorganic colloids to affect radionuclide migration: 1) colloids must be present at significant concentrations, 2) radionuclides must associate with the colloidal material in significant portion in comparison with the solid phase, and 3) colloids and associated radionuclides must be transported with the groundwater flow. The first criterion is met. Colloids are occurring in

groundwater samples originating form different geological and hydrogeochemical settings (e.g., McCARTHY & DEGUELDRE 1993). In stagnant groundwater aquifers, colloid concentrations were reported to be in the ppb to ppm concentration range. In principle, colloids may also exist in the pore water of a cementitious repository. The second criteria is also met as colloidal phases appear to be effective carriers of strongly sorbing radionuclides due to the relatively high specific surfaces (e.g., GRAUER 1990). Strongly sorbing radionuclides such as lanthanides and actinides are contained in radioactive wastes. The last criterion is fulfilled as well because numerous studies have shown colloid migration and associated contaminants in groundwater aquifers (e.g., RYAN & ELIMELECH 1996).

In this context, the terms "particle and colloids" require a few explanatory comments. There is no generally accepted view within the scientific community what constitutes particles and colloids (BUFFLE & VAN LEEUWEN 1992). The situation is complicated by the fact that the definitions are mostly based on experimental techniques used to discriminate the colloidal and particulate materials. Particles with size between 1 nm and 450 nm are usually classified as colloids. Chemical entities with diameter smaller than 1 nm have molecular weights of less than ~ 1000 daltons. This size range also includes small molecules and ions normally involved in chemical reactions. Therefore, the lower size limit is set to discriminate colloids from dissolved species. The upper size limit is arbitrary. Limnologists and oceanographers traditionally use the limit of 450 nm with the notion that 1) many organisms are larger than 450 nm, and 2) coagulation leading to sedimentation is effective in the size range above 450 nm. The upper size limit corresponds to the technical specification of the filters (nominal pore size) commonly used in these scientific disciplines. Hence, the chemical entity "colloid" is defined operationally by means of a procedure used to separate solids from solutes.

In this study, the main criteria for defining the terms "particles or colloids" is based on the presence of a chemical entity (inorganic particle) which 1) is generated or present in the system, 2) is chemically stable, and 3) small enough to be dispersed in the fluid by Brownian motion. Particles with diameters between 1 nm and 1000 nm, and a density of about 2 g cm^{-3}, are considered to fulfil the criteria. Cement-derived particles larger than 1000 nm are retarded effectively in a repository due to sedimentation or attachment to the near-field

material (filtration) and, moreover, require water turbulence to stay in suspension. Hence, the influence of larger cement-derived particles on colloid-facilitated radionuclide migration is assumed to be negligible due to their low mobility (VILKS & BACHINSKI 1994). The lower size limit of colloids is set to distinguish colloids from dissolved molecules and ions.

1.2 Previous Studies on Near-Field Colloids

In the context of this study, the term “near-field colloids” denotes cementitious or cement-derived colloidal matter present or generated in the near-field of a repository. Note, however, that colloids may originate from sources other than cementitious materials. For example, alteration processes affecting the waste materials, e.g., the corrosion of metals and the degradation of organic materials may produce colloidal matter. Despite an increasing interest in the rôle of colloids for radionuclide migration, however, only a few studies have addressed problems concerning the formation, characterisation and sorption characteristics of cement-derived colloids in the near-field of a repository.

Novel information on the properties of near-field colloids were drawn from the studies of RAMSAY et al. (1988) and (1991), and GARDINER et al. (1990). Ramsay and co-workers demonstrated the potential for cement-derived colloids to be generated under conditions encountered in the near-field of a repository. Colloidal material from cement leachates were collected to determine the chemical composition and microstructure of the particle aggregates. Ramsay and co-workers describe the generation of near-field colloids from cementitious material as a sequence of consecutive processes with the initial dissolution of the cement material as a first step, followed by supersaturating the cement pore water (CPW) with respect to the solubility-controlling phases and, finally, nucleation and growth of particle aggregates. The colloidal material was shown to have the chemical composition of calcium silicate hydrates (CSH), together with some calcium carbonate and calcium aluminates. According to RAMSAY et al. (1991), the generation of near-field colloids and their concentration in CPW critically depends on the silica content of the cementitious material. Moreover, the studies of Ramsay and co-workers show that radionuclides may be associated with cementitious near-field material as well as colloidal matter indicating that cementitious colloids may act as carriers for radionuclides in the near-field of a repository.

Supporting information concerning the characterisation and concentration of colloids formed under highly alkaline conditions was gained from the studies of natural analogues (WETTON et al. 1998). The authors report average colloid populations in the range 0.6 to 1.4×10^{7} coll mL^{-1} in the highly alkaline groundwater of the Maqarin site (T = 25°C, pH=12.7, $[Ca]_{tot}$ = 1.78×10^{-2} M, I ~ 0.07 M). Colloids were collected onto filters with nominal pore sizes of 50 nm, and different methods were applied to calculate the colloid population. The corresponding mass concentrations of the colloid populations were estimated to range from 0.06 to 0.09 mg L^{-1}. Thus, the study by WETTON et al. (1998) indicates the existence of colloids in high pH cement-type environments, although their concentration appears to be very low.

A great number of colloid concentration measurements result from studies of groundwater aquifers. The chemical regime of a groundwater aquifer is significantly different from that of a cementitious environment. For example, the pH of groundwater systems lies between pH 6 and 9 whereas the pH of CPW is typically ≥ 12.5. A comparison of the concentrations of near-field and far-field colloids, however, may allow us to assess the importance of the different sources on the colloid inventory in a repository environment. Within the framework of the Swiss programme for the disposal of radioactive waste, an extensive colloid sampling and characterisation campaign was carried out with the goal of evaluating the concentration of groundwater colloids in subsurface systems and quantifying colloid properties (DEGUELDRE et al. 1989; 1996a/b; DEGUELDRE 1994; 1997). The colloid concentrations reported were generally lower than 1 ppm for colloids in the size range 10 - 1000 nm. In deep granitic groundwater the colloid concentration were often below 0.1 ppm (size range 10 - 1000 nm). Thus, colloid concentrations appear to be in the ppb to ppm range in stagnant aquifers, which are geochemically and tectonically stable. Moreover, it was shown that the colloidal matter was mainly composed of phyllosilicates and silica, which are the dominating components of the aquifer material in granitic systems.

The literature review indicates substantial evidence for the generation and existence of colloids in cementitious environments whether these are laboratory or natural analogue systems (RAMSAY et al. 1988; GARDINER et al. 1990; WETTON et al. 1998). As yet, however, little attention has been given to elucidating the processes, which control inventories and size distributions of cemen-

titious colloids as well as the uptake of radionuclides by these colloids. Questions concerning the effect of the pore water composition on colloid generation and colloid stability under near-field conditions, the influence of the long-term degradation of cement and cementitious backfill material on colloid concentrations as well as the kinetics of radionuclide sorption and/or incorporation on or into in-situ generated colloids, respectively, still have to be addressed in more detail.

1.3 Effect of Colloids on the Retardation of Radionuclides

The uptake of a sorbing metal cation, M, by the cementitious bulk material, S, or the colloidal phase, C, are considered to be competitive reactions. Moreover, in the presence of a complexing agent, complexation of the metal by a ligand, L, competes with sorption of the metal cation onto either solid phases, that is the bulk material or colloids. Inorganic (e.g., OH^-, CO_3^{2-} etc.) and organic ligands (e.g., isosaccharinic acid, gluconic acid etc.) are among the most relevant complexing agents in the near-field of a repository. The distribution of a metal cation between a bulk phase, the colloidal phase and the ligand is governed by the stability of the aqueous metal-ligand complexes, the sorption mechanism (reversible or irreversible binding of the metal) and the stability of the metal-surface complex on the bulk and colloidal phases. The following considerations are based on the assumption that uptake is a reversible process.

In the absence of colloids, the distribution of a metal cation between solid and solution is described by:

$$M + S \Leftrightarrow MS. \qquad (1)$$

The extent of sorption can be expressed in terms of a macroscopic distribution ratio (R_d) given by:

$$R_d = \frac{M_{sorbed}}{M_{solution}} = \frac{\{MS\}}{[M]_{aq}} \qquad [m^3\ kg^{-1}]. \qquad (2)$$

Taking into account metal-ligand complex formation in solution, the R_d value can be written as

$$R_d = \frac{M_{sorbed}}{M_{solution}} = \frac{\{MS\}}{[M] + \sum_i \sum_n [ML_n^i]} \qquad [m^3\ kg^{-1}], \qquad (3)$$

where {MS} is the concentration of metal sorbed on the solid [mol kg^{-1}], [M] is the concentration of free, uncomplexed metal in solution [mol m^{-3}], and $[ML_n^i]$ represents the concentration of metal-ligand complexes with any ligand L^i in solution [mol m^{-3}].

The distribution of a metal cation between a colloidal phase and solution can be expressed in analogy to Eq.(3) as:

$$R_c = \frac{M_{sorbed}}{M_{solution}} = \frac{\{MC\}}{[M] + \sum_i \sum_n [ML_n^i]} \qquad [m^3\ kg^{-1}]. \qquad (4)$$

R_c is the macroscopic distribution ratio [m^3 kg^{-1}], {MC} is the analytical concentration of metal sorbed on the colloidal phase [mol kg^{-1}], and [M] and $[ML_n^i]$ represent the concentrations of metal concentrations in solution as given above.

In the presence of colloids, the distribution ratio for the partitioning of a metal cation between the bulk phase and the colloidal and aqueous phases can be described by

$$R_{d,eff} = \frac{M_{sorbed}}{M_{solution}} = \frac{\{MS\}}{[M] + [MC] + \sum_i \sum_n [ML_n^i]} \qquad [m^3\ kg^{-1}], \qquad (5)$$

with [MC] as the concentration of metal sorbed on the colloidal phase [mol m^{-3}]. Thus, $R_{d,eff}$ corresponds to the effective distribution ratio between solid and liquid phase in the presence of colloids.

Combining Eq. (4) and (5), and replacing [MC] by $m_c \times \{MC\}$ leads to:

$$R_{d,eff} = \frac{M_{sorbed}}{M_{solution}} = \frac{R_d}{(1 + R_c m_c)} \qquad [m^3\ kg^{-1}], \qquad (6)$$

with m_c as the concentration of colloids in the fluid [kg m^{-3}]. The effect of colloids on radionuclide sorption can then be interpreted in terms of a sorption reduction factor, which is defined as:

$$F_{red} = \frac{R_d}{R_{d,eff}} = (1 + R_c m_c) \qquad [-]. \tag{7}$$

Eq. (7) indicates that the effect of colloids on radionuclide sorption onto the bulk phase depends on the stability of the metal-colloid surface complex (expressed by R_c) and the colloid mass concentration (m_c). Hence, the key parameters for assessing the impact of near-field colloids on radionuclide migration are the concentration of near-field colloids and the affinity of radionuclides for the colloidal matter. Note again that Eq. (7) is based on the assumption that uptake processes on both the colloidal and the cementitious bulk phases are reversible.

1.4 Aim of this Study

The impact of colloids has consequently been addressed in performance assessment of the planned Swiss L/ILW repository. A transport model for colloid-facilitated radionuclide migration was developed which allows predictions to be made about the release of radionuclides from the near-field of a repository (SMITH 1993; NAGRA 1994b). In this model, an effective retention factor (R_{eff}) was derived to account for the contribution of near-field colloids to radionuclide transport in the fluid:

$$R_{eff} = 1 + \frac{m_z}{\varepsilon} \frac{K_d}{1 + m_c K_c}, \tag{8}$$

- R_{eff}: retention factor of a radionuclide affected by near-field colloids [-],
- K_d: distribution coefficient (or ratio) of a radionuclide between the bulk material (hardened cement paste) and the liquid phase [$m^3\ kg^{-1}$],
- K_c: distribution coefficient (or ratio) of a radionuclide between the colloidal and the liquid phase [$m^3\ kg^{-1}$],
- m_z: mass of cement paste per m^3 repository volume [$kg\ m^{-3}$],
- m_c: mass of colloids per m^3 pore water volume [$kg\ m^{-3}$],
- ε: porosity of the near-field [-].

Note that the terms K_d and $m_c \times K_c$ in Eq.(8) can be replaced by R_d and $m_c \times R_c$ on the assumption that sorption processes are linear and reversible. In NAGRA

(1994b) a scaling factor (S_c) was employed in order to relate the affinity of a radionuclide for near-field colloids to its affinity for the near-field material:

$$K_c = S_c \times K_d . \quad (9)$$

S_c = 100 and 1000 were taken as realistic-conservative and conservative values, respectively, in the transport model (NAGRA 1994b). The values were chosen with the notion to account for differences in the surface areas of the near-field and the colloidal materials. Note that VILKS et al. (1998) applied a similar model to estimate the effect of colloids on contaminant migration in a geologic medium.

Eqs. (8) and (9) reveal that colloid-specific input parameters are required in the transport models: First, the colloid source term, i.e., the mass concentration of colloids in the near-field pore water of a L/ILW repository (m_c), and, second, distribution coefficients (or ratios) of radionuclides to describe the partitioning between the pore water and the colloidal phase (K_c or R_c, respectively). Thus, experimental investigations focusing on the evaluation of the concentration of near-field colloids in a L/ILW repository and the determination of distribution coefficients (or ratios) between the colloidal and liquid phase are required to assess the impact of near-field colloids on radionuclide migration.

A highly permeable mortar is currently favoured as backfill for the engineered barrier of the planned Swiss L/ILW repository (see chapter 2). The backfill mortar was designed to contain accessible volume for gas formed in the emplacement cavern and to ensure mechanical stability through filling of voids between the waste containers (JACOBS et al. 1994). Thus, it is the most permeable component of the engineered barrier due to the needs of high porosity and high gas permeability. The mortar is composed of quartz and hardened cement paste. Colloidal material may be generated due to the interaction of quartz exposed to high pH pore water (chemical gradient) or released from the hardened cement paste. Thus, the backfill is considered to have a potential for colloid generation and, due to its high porosity, for colloid transport.

The aim of the study was to determine a range for colloid inventories to be expected in the pore water of backfill mortar and to assess possible impacts of near-field colloids on radionuclide migration. A review of the literature on colloi-

dal stability in natural systems shows that favourable chemical conditions for colloid removal, either due to colloid-colloid interaction (coagulation) or colloid-backfill interaction (deposition), prevail in a cementitious environment (see chapter 3). The setting up of an appropriate analytical tool was a prerequisite for accurate in-situ colloid concentration measurements (see chapter 4). The study includes investigations on the generation and physico-chemical stability of backfill-derived colloids in a static system and measurements of colloid concentrations in the pore water of a dynamic system. Batch-type experiments were performed to elucidate the physico-chemical processes controlling colloid inventories in the pore water of the backfill mortar (see chapter 5). Complementary to the lab-scale batch studies, colloid concentrations in the pore water of a dynamic system were measured (see chapter 6). Pore water samples were collected from a column filled with backfill mortar and used for large-scale flow experiments. The information gained from the experimental studies were then employed to assess potential effects of cement-derived near-field colloids on radionuclide migration and to discuss implications for the safety of a repository (see chapter 7).

With the present study it was not intended to elucidate colloid deposition and aggregation phenomena in the backfill of a repository to the last detail. Moreover, it was not foreseen to investigate the effect of temperature, redox potential, or the concentrations of natural organic matter on colloid concentrations as well as the effect of disturbances affecting colloid inventories on geological time scales such as tectonic movements. However, the results obtained from this study should allow a first assessment of the relevance of cement-derived near-field colloids for the safety aspects of repositories for nuclear waste.

2 THE BACKFILL MATERIAL

2.1 Composition and Characterisation

The backfill material (Nagra designation: mortar M1) is a like-grained mix prepared from quartz aggregates and Portland (Sulfacem PZHS) cement.

The chemical analysis of Portland PZHS cement, listed in Table 1, was reported by JACOBS et al. (1994). It agrees with the composition of Sulfacem cement given by BERNER (1990). The aggregate material is a commercial product with diameters of the quartz grains between 2 and 4 mm.

According to JACOBS et al. (1994), mortar M1 has the following composition (mass proportion) :

cement: water: aggregate = 1.00 : 0.40 : 5.33.

Table 1: Chemical analysis and mineralogy of Portland PZHS cement (JACOBS et al. 1994).

	Portland PZHS ("Sulfacem") cement
Chemical Compound	(wt.-%)
SiO_2	20.5
Al_2O_3	4.0
Fe_2O_3	7.3
MnO	0.06
CaO (total)	62.0
MgO	1.2
K_2O	0.6
Na_2O	0.1
SO_3	2.5
TiO_2	0.4
loss on ignition at 1000°C	1
insoluble residual	0.3
Mineralogy	
C_3S	48
C_2S	21
C_4AF	19
C_2F	1
C_3A	0
not determined	11

In the mixture hardened cement paste (HCP) was found to contribute to about 20 weight-% (wt.-%) of the mortar material after curing (JACOBS et al. 1994; MAYER et al. 1998). IRIYA et al. (1991) and JACOBS & WITTMANN (1992) describe gas transport properties and the effect of ageing of mortar M1 on the porosity and gas permeability.

2.1.1 Mortar Material used for the Batch Flocculation Studies

Batch-type flocculation studies were performed with crushed material of mortar M1 or quartz aggregates, respectively. The mortar M1 material was prepared as follows: Mortar M1 was cast in cylinders with diameters ranging from 5 to 17 cm and an overall length of about 100 cm and cured for approximately two months. The cylinders were stored at 90 % relative humidity to achieve an increased degree of hydration before being used in the experiments. The cylindrical blocks were then gradually and carefully crushed in a crusher. The bulk material was sieved to obtain like-grained specimens with diameters ranging from 2 to 4 mm. The material prepared in this manner consists of quartz grains, which were partially covered by HCP.

The quartz material used for the batch-type studies was obtained by sieving the bulk material and collecting grains with diameters ranging from 2 to 4 mm. The average diameter of the quartz grains was estimated to be 2.8±0.1 mm, and the geometric surface area of the quartz grains to be 7.8±0.1 $cm^2\ g^{-1}$. Note that the surface area of the aggregate material is low compared to the surface area of HCP (Table 4). The quartz material was used in the experiments without further pre-treatment.

During crushing of the mortar M1 a powered HCP residual was produced indicating that the HCP coverage was partially eroded from the quartz grains during sample preparation and, therefore, expected to be lower than the 20 wt.-% reported by JACOBS et al. (1994). Thus, it was decided to perform a few leaching tests to demonstrate the presence of HCP on the grains and to estimate the cement content of the crushed material. For this, the mortar grains were treated with 1 M HNO_3 as follows: After adding 30 g of grains to 200 mL 1 M HNO_3 (Merck, suprapur) gas production occurred presumably due to the presence of trace amounts of carbonates. After gas production had stopped, the bottle was tightly closed and shaken end-over-end over a period of 18 days.

The supernatant was filtered (0.2 µm pore size) and analysed by ICP-OES for major and trace elements. The same procedure was applied to evaluate the chemical purity of the quartz grains. The concentrations of cement-derived elements in the supernatant solution of the quartz and mortar samples are listed in Table 2. Note that concentrations were corrected for the background concentrations of HNO_3. The values were deduced by averaging the analytical results of duplicate samples.

The results indicate that quartz grains contain impurities at low but measurable concentration levels.

The cement content of crushed mortar M1 was estimated based on the chemical composition of Portland PZHS cement (wt.-% content of the chemical compounds CaO, MgO, Fe_2O_3 and Al_2O_3 as given in Table 1) and the concentrations of Al, Ca, Fe and Mg determined in the supernatant solution of the mortar M1 suspensions (Table 2). Al, Ca, Fe and Mg were selected as cement-derived tracers to minimise interference from quartz impurities.

Table 2: Chemical composition of the supernatant after contacting quartz (40 g L^{-1}) and mortar M1 grains (150 g L^{-1}) with 1 M HNO_3.

Element	Quartz [M]	Mortar M1 [M]
K	$(6.1\pm0.8)\times10^{-5}$	$(7.6\pm1.6)\times10^{-4}$
Na	$(4.1\pm3.3)\times10^{-5}$	$(7.8\pm3.9)\times10^{-4}$
Ca	$(6.9\pm2.5)\times10^{-5}$	$(1.4\pm0.1)\times10^{-1}$
Al	$(1.1\pm0.1)\times10^{-4}$	$(8.6\pm0.2)\times10^{-3}$
Si	$(2.2\pm0.1)\times10^{-4}$	$(1.3\pm0.3)\times10^{-2}$
Fe	$(1.6\pm0.1)\times10^{-5}$	$(1.1\pm0.1)\times10^{-2}$
Mg	$(8.7\pm1.1)\times10^{-6}$	$(4.5\pm0.1)\times10^{-3}$
Sr	$(3.0\pm0.3)\times10^{-7}$	$(5.5\pm0.1)\times10^{-5}$
Ba	$(2.5\pm2.2)\times10^{-6}$	$(2.0\pm0.4)\times10^{-5}$
S	$(1.7\pm0.6)\times10^{-5}$	$(4.6\pm0.1)\times10^{-3}$

Table 3: Cement content [g] for a total weight of 150 g grains of mortar M1.

Element	Cement content [g]
Al	10.87 ± 0.33
Ca	12.93 ± 0.09
Fe	11.80 ± 0.25
Mg	15.02 ± 0.45

In Table 3 the fraction of cement in mortar M1 grains is given in grams for a total weight of 150 g grains. The average cement content of mortar M1 grains is estimated to be 8.6±1.9 wt.-% (95% confidence level, n = 4) indicating some loss of HCP during sample preparation (original content 20 wt.-%). Note that HCP may not be dissolved completely in 1 M HNO_3 (leaching), which was used instead of a HF/HNO_3 solution required for total dissolution.

Thus, the value reported above only gives a lower bound on the cement content. However, it clearly indicates the presence of HCP in the crushed material. Note also that the dissolution of cement had been completed under the given experimental conditions within the equilibration period of 18 days. This was confirmed by additional measurements after one month of equilibration.

2.1.2 Mortar Material used for the Column Experiments

The COLEX (COLumn EXperiments) project was a large-scale flow experiment with the goal of studying coupled gas and water transport processes in the backfill mortar M1 (MAYER et al. 1998). The study was carried out at the Institute for Building Materials (ETH Zürich) within the frame of the Swiss radioactive waste disposal programme. Measurements of colloid concentrations were carried out on pore water samples collected from a column, which was filled with mortar M1. MAYER et al. (1998) has described preparation and filling of the column elements. The mortar filling had an average bulk density of 1827 kg m^{-3}. HCP contributed to about 20 wt.-% of the mortar material. MAYER et al. (1998) determined the free water porosity and permeability of the mortar to be 27 % and 10^{-10} m^2, respectively, which is in good agreement with values previously reported by JACOBS et al. (1994) (ε = 24 %; k = (4±3)$\times 10^{-10}$ m^2).

Table 4: Characteristic parameters of HCP (JACOBS et al. 1994; MAYER 1998).

Parameter	HCP
Median pore diameter (volume) [µm]	0.075
ε [Vol.%]	8.2±0.6
Estimated total pore area [$m^2 g^{-1}$]	5.8±1.0

The pore size distribution of mortar M1 (w/c = 0.4) after 90 days storage in water was determined by mercury intrusion porosimetry (MIP) and image analyses (IA) (JACOBS et al. 1994). The investigations showed a dual pore size distribution for mortar M1. Pore diameters of the HCP were typically smaller than 1 µm (Table 4), whereas the porous structure of the mortar shows pores with diameters in the range of 1 to 5 mm. The free water porosity of the HCP was determined to be 8.2±0.6 % using MIP measurements (range 8.2 to 9.1 %; JACOBS et al. 1994). This value is consistent with an estimated pore area of about 5.8±1.0 $m^2 g^{-1}$ (Appendix A; MAYER 1998).

Assuming a porosity of 8.2 % for the HCP and a total porosity of 27 % for mortar M1, the porosity of the mortar structure was estimated to be about 19 %. Thus, the porosity of mortar M1 is attributable to the large volume of the macro pores. The pore volume of the backfill mortar significantly contributes to the total pore space of a repository. NEALL (1994) estimates that the mortar M1 pore volume contributes to more than 50 % of the total pore volume of the planned L/ILW repository and to about 10 % of total repository volume. Thus, we anticipate that a large fraction of the near-field pore water is stored in the backfill matrix and, therefore, investigations addressing the fate of colloids in the mortar backfill are representative for near-field conditions.

2.2 Chemical Composition of the Backfill Pore Water

Cement and concrete (i.e. cement plus aggregate material) are the main constituents of the near-field in the planned L/ILW repository. Modelling and experimental studies show that alteration of the near-field with time is due to the interaction of the cementitious materials with groundwater of the surrounding host rock. The driving force for cement degradation is an inherent disequilibrium between cement and groundwater infiltrating into the near-field. Leaching of

hydrated cement occurs to adjust the chemical composition of the groundwater to a level in equilibrium with respect to the cement matrix. As indicated from experimental and modelling studies, three distinct stages of the cement degradation can be distinguished:

Stage I:

The pore water composition is dominated by alkali hydroxides (NaOH and KOH) resulting in a pH of about 13.3. In this study, the alkali-rich pore water is denoted as “young” cement fluid. The chemical composition is approximately given by $[K]_{tot}$ = 0.18 M, $[Na]_{tot}$ = 0.14 M, and is saturated with respect to portlandite ($[Ca]_{tot}$ ~2×10^{-3} M). In contact with groundwater, (Na,K)OH phases are depleted from the cement matrix giving rise to a gradual drop in pH to 12.5.

Stage II:

The chemical composition of the alkali-depleted pore water is controlled by the solubility of portlandite ($[Ca]_{tot}$ ~2×10^{-2} M, pH ~12.5). The term “evolved” fluid is used for the calcium-rich pore water throughout this study. The near-field is continuously depleted from portlandite by the groundwater flow. However, since the quantity of portlandite is large, pH of the pore water is buffered over long periods of time, i.e., up to 1000 exchange cycles of the pore volume.

Stage III:

As the buffering capacity of the portlandite is exhausted, pH falls continuously to pH ~11 and, hereafter, even to lower values as soon as dissolution of CSH gels and other cement phases (ettringite, hydrogarnet, hydrotalcite) starts.

Models of the cement degradation have been developed and used for predicting the evolution of the pore water composition and the cement composition in the near-field of the planned Swiss L/ILW repository (BERNER 1990; NEALL 1994; PFINGSTEN & SHIOTSUKI 1998). NEALL (1994) used a mixing tank model to predict the evolution of the cementitious near-field in contact with infiltrating groundwater of different compositions: 1) a Wellenberg (WLB) $NaHCO_3$ groundwater (pH = 8.3), and 2) a Wellenberg (WLB) NaCl pore water (pH =

7.5). The results of the modelling study indicate that high pH conditions are maintained in the near-field of the planned repository for hundreds of exchange cycles of percolating groundwater (one cycle is taken to correspond to more than 1000 years). The pore water composition in the near-field and, consequently, in the backfill material is governed by the interaction of the percolating groundwater with hydrated cement. NEALL (1994) predicts a pH > 12.5 for the CPW in the beginning of the near-field degradation due to the release of alkali hydroxides from the cement matrix. After about 10 exchange cycles, pH is buffered at 12.5 controlled by portlandite solubility (stage II of the cement degradation). In this study the chemical conditions employed in the experiments correspond to either stage I or II of the cement degradation in line with a diffusion-dominated system. The batch-type studies were performed using an artificial cement pore water (ACW) with pH = 13.3 (stage I CPW). In the COLEX study the composition of the pore water was controlled by portlandite solubility as in stage II of the cement degradation.

2.3 Driving Force for Colloid Generation in the Backfill

Quartz is unstable in contact with high pH, silica under-saturated solutions. Thus, when mortar M1 is immersed in alkaline CPW (pH > 11), and quartz grains are accessible to alkali attack, dissolution of quartz will occur. The dissolution of quartz and precipitation of secondary minerals is considered to be the driving force for colloid generation in cement materials (RAMSAY et al. 1991).

Numerous studies have been performed to investigate the dissolution of quartz in aqueous solution on cleaned and well-characterised quartz samples (e.g., BRADY & WALTER 1990 and references therein). It has been found that the dissolution of quartz is fast and promoted by OH^- in basic aqueous solutions. Speciation of Si in solution comprises monomeric and presumably polymeric silicic species (STUMM & MORGAN 1995). In this study a few experiments with non-pretreated quartz grains as starting material were carried out to assess the dissolution behaviour of the aggregate material at high pH (Fig. 1). In the experiments quartz grains were exposed to 1 M NaOH or an ACW ($[Na]_{tot}$ = 0.11 M, $[K]_{tot}$ = 0.18 M, $[Ca]_{tot}$ = 1.2×10^{-3} M), respectively, at a solid to liquid ratio of 0.1 kg L^{-1}. An aliquot of the supernatant solution (30 mL) was sampled and replaced by fresh solution. The aliquot was centrifuged (60 min at 95000×g)

and analysed for total Si and Ca. Monomeric Si was analysed using the standard colorimetric method (silico-molybdate determination) reported by PAGE et al. (1982).

Fig. 1a shows increasing Si concentrations with time in 1 M NaOH indicating quartz dissolution. The concentrations of total and monomeric Si agree within the experimental uncertainties (estimate ±5 %). Thus, the concentration of polymeric Si species is low at total Si concentrations in the mmolar range. Note that Si concentrations were always well below the solubility of amorphous silica and quartz (STUMM & MORGAN 1995). The Ca concentration was found to remain constant with time indicating the presence of small amounts of rapidly dissolving Ca-containing impurities associated with quartz. The dissolution behaviour of quartz shows markedly different features in Ca-rich ACW (Fig. 1b). Compared to the 1 M NaOH solution, the Si concentrations are lower by almost one order of magnitude. Note again that the difference between total and monomeric Si is small and hardly significant. The concentration of Si in the systems is controlled by the solubility of calcium silicate hydrates (CSH phases) in the presence of Ca (GREENBERG & PRICE 1957; GREENBERG & CHANG 1965). At ambient temperatures, the formation of CSH phases can be expressed by (BERNER 1990):

$$p\ Ca(OH)_{2(aq)} + q\ SiO_{2\ (aq)} = xCaO{\cdot}SiO_2{\cdot}yH_2O_{(s)}. \qquad (10)$$

In ordinary Portland cement x ranges from about 1.4 to 1.8. The C:S ratio of CSH phases can be determined based on the chemical composition of the pore water and well-known relationships between the solid $CaO:SiO_2$ (C:S) ratio and the fluid composition (MACPHEE et al. 1989; TITS et al. 1998 and references therein).

For a (Na,K)OH CPW (pH = 13.3; $[Ca]_{tot}$ = 0.8 to 1.2×10^{-3} M), the C:S ratio of the CSH phase was estimated to be in the range 1.2 to 1.3. The corresponding equilibrium Si concentration was predicted to range from 0.8 to 1.6×10^{-4} M. Note the excellent agreement of predicted and measured Si concentrations, i.e., 0.8 to 1.6×10^{-4} M and 1.2 to 1.6×10^{-4} M (Fig. 1b), respectively.

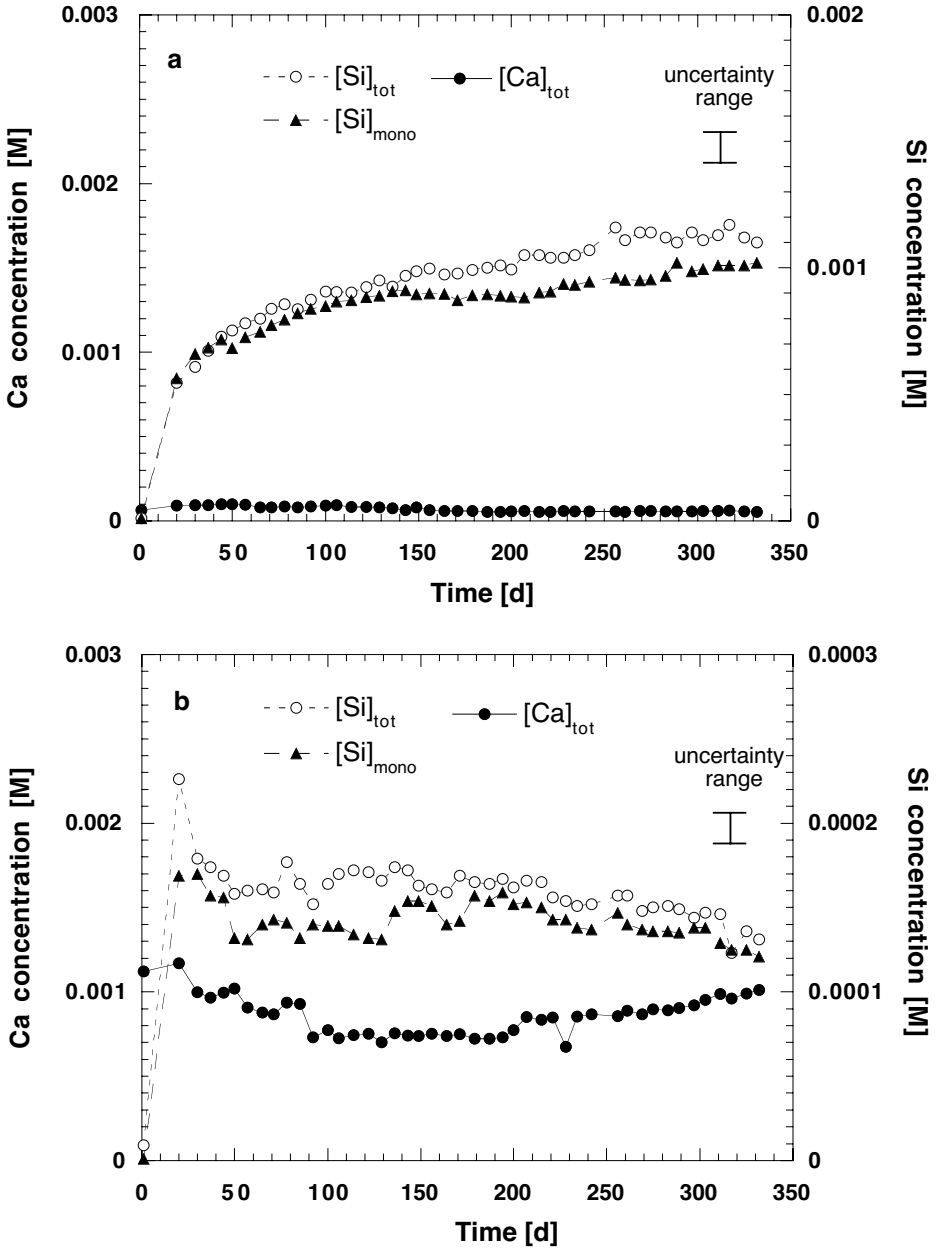

Fig. 1: Time dependence of the aqueous Ca and Si concentrations for two experimental systems a) quartz immersed in 1 M NaOH and b) quartz immersed in ACW ($[Na]_{tot}$ = 0.11 M, $[K]_{tot}$ = 0.18 M, $[Ca]_{tot}$ = 1.2×10^{-3} M). Measurements of total Si and monomeric Si species were carried out using ICP-OES and a colorimetric method (silico-molybdate determination).

The formation of CSH phases was further investigated by contacting mortar M1 with ACW. Equilibrium Ca and Si concentrations were in agreement with those given for the corresponding quartz system. Scanning electron microscopy coupled with energy dispersive spectrometry (SEM/EDS) was employed for a qualitative and semi-quantitative analysis of the CSH precipitates (Fig. 2). The C:S ratio of the CSH material was determined to be 1.24±0.28 (number of analysis = 6). This value is in good agreement with the ratio given above, which was estimated based on the studies by MACPHEE et al. (1989) and TITS et al. (1998). The results confirm that CSH-type colloidal matter with a C:S ratio of ~1.2 may be formed in the backfill mortar M1. Note that RAMSAY et al. (1991) identified colloidal material with similar compositions in cement leachates.

BATEMAN et al. (1995) report the presence of CSH phases in systems, which are similar to the ones investigated in this study. In their study, Bateman and co-workers percolated a “young” (Na-K-Ca-OH) fluid through a column packed with quartz. Although the experiments were conducted at temperatures of 70°C, the results are still informative for the present study.

BATEMAN et al. (1995) identified a succession of CSH and C(A)SH phases with varying Ca:Si ratios. The precipitates were representative of both the CSH(I) and CSH(II) groups of minerals. Moreover, the authors concluded that the availability of Ca and Si in the reacting fluid, i.e., mainly the supply of Si due to quartz dissolution, controlled the fluid chemistry and the compositions of the solid phases.

From the above results and discussion we infer that CSH phases, in principle, are generated when mortar M1 is immersed in CPW. CSH formation requires sources of Ca (CPW, cement) and Si (quartz aggregate material). The CSH material formed can be colloidal (size ≤ 1000 nm) as well as particulate (size > 1000 nm).

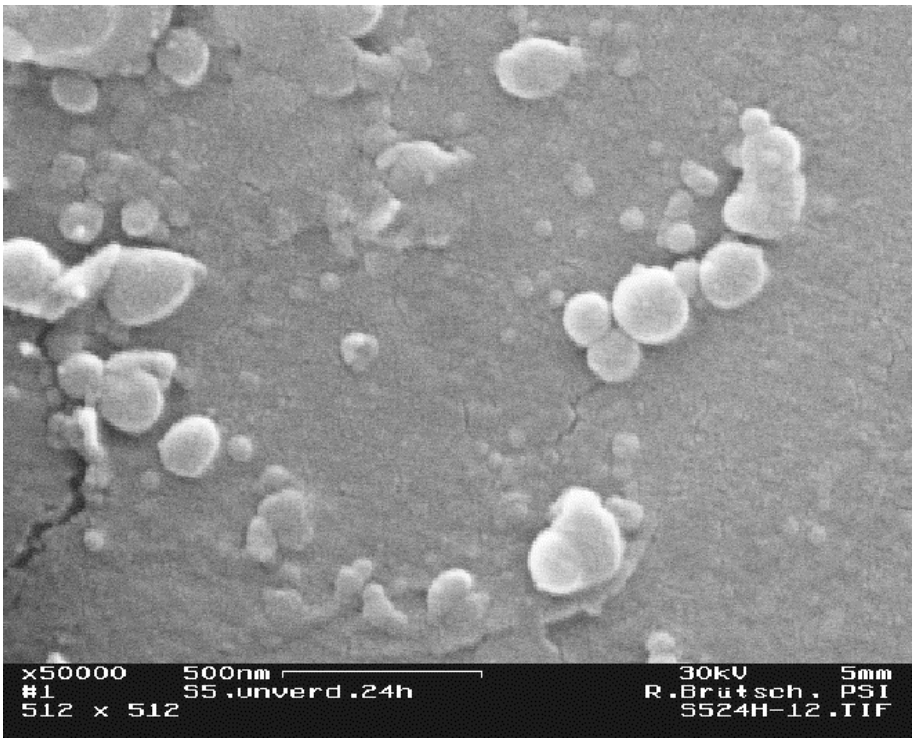

Fig. 2: SEM images of cementitious material collected after exposition of crushed mortar M1 to a “young” cement fluid.

3 CHEMICAL ASPECTS OF COLLOID STABILITY

3.1 Colloid Removal Processes in Backfill Mortar

In a general sense, colloid removal in the pore water of mortar M1 may be due to coagulation or colloid deposition on the backfill. Both processes include a series of consecutive transport and surface chemical processes. In the case of colloid deposition, both theoretical and experimental studies on colloid transport in porous media show that fluid velocity and the chemical composition of the fluid affect colloid mobility and the inventory of dispersed colloids (e.g., ELIMELECH et al. 1995). Note that fluid velocity determines the transport to the collector surface, that is, the probability of inter-particle contact. The studies by ELIMELECH et al. (1995) and KRETSCHMAR et al. (1997) indicate that the dependence of the colloid deposition rate on the fluid velocity is weak at low to moderate flow velocities, i.e., less than a few cm h^{-1}. Theoretical analysis of colloid mobility shows that the deposition rate increases with flow velocity by a power of zero to one third at low to moderate flow velocities (SONG & ELIMELECH 1995). In colloid migration studies on natural porous media (sandy soil and aquifer material) it was found that increasing the water flow from 1 cm h^{-1} to 100 cm h^{-1} enhances the deposition rate of colloids on the collector only by a factor of 5 (KRETSCHMAR et al. 1997). The studies demonstrate that fluid velocity exerts only a minor effect on colloid mobility. For the COLEX experiments presented in chapter 6, the fluid velocity in the backfill mortar was estimated to be ~5 cm h^{-1} (MAYER et al. 1998). We infer that, under these conditions, physico-chemical aspects of the solid-liquid interface of colloids and collector rather than fluid velocity control colloid deposition in the porous backfill and, consequently, the concentration of dispersed colloids. The characteristics of the interfacial regions of colloids and collector surfaces are strongly affected by the chemical composition of the fluid (see next section).

Filtration is the controlling colloid removal process in fractured systems and aquifer systems with low water flow rates and microscopic channels in the µm size range. The specific feature of the mortar M1, however, implies that filtration may not be the dominating removal process in the backfill. The high porosity of the macrostructure (~19 %) and the large pore diameters pores (pore diameters range between 1 to 5 mm) indicate that an additional process may be effective

in controlling the colloid inventory, e.g., colloid removal by a coagulation-sedimentation process.

Characteristic reaction times were estimated to assess the importance of the two processes, i.e., filtration and coagulation in the backfill mortar. The characteristic reaction time of the filtration process is approximated by the characteristic time of a diffusive transport to the collector surface. The characteristic distance for dispersal of material by diffusion is approximately given by:

$$\Delta x \approx 2\sqrt{D\ \Delta t} \qquad [m]. \tag{11}$$

The diffusion coefficient for the molecular diffusion of spheres (ø = 100 nm) is estimated to be D ~2.2×10^{-10} m^2 s^{-1} using the Stokes-Einstein relationship (LERMAN 1979). In the pore volume of the backfill, the characteristic distance between colloid and the backfill material (collector), Δx, is approximately 2.2×10^{-3} m. With Eq. (11), the characteristic reaction time for diffusive transport, Δt, is then estimated to be about 1.5 hours. Note that we assume a collision efficiency of 100 % implying that that each colloid-collector interaction results in attachment (collision efficiency factor = 1). On this assumption, the deposition rate is only limited by the frequency of colloid-backfill interactions and, thus, controlled by diffusive transport.

The characteristic reaction time of the coagulation process was estimated based on the half-life ($t_{1/2}$) of a monodisperse population of spherical particles. For a monodisperse colloid population in a batch-type system, a second-order reaction kinetics can describe colloid removal (ELIMELECH et al. 1995; DEGUELDRE et al. 1996b). Time dependence of the total colloid concentration can be written as:

$$\frac{dC}{dt} = -\alpha \frac{4k_B T}{3\eta}[C]^2 . \tag{12}$$

The half-life ($t_{1/2}$) is the time at which the colloid concentration in the pore water is one half of its initial value. The half-life of the colloid population is given by:

$$t_{1/2} = \frac{3\eta}{4\alpha k_B T C_0} \quad [s], \qquad (13)$$

α: attachment (sticking) factor [-],

k_B: Boltzman constant 1.38×10^{-23} m^2 kg s^{-2} K^{-1},

T: absolute temperature [K] ,

η: viscosity of the fluid (H_2O, 25°C: 8.904×10^{-4} kg m^{-1} s^{-1}) ,

C_0: total colloid concentration [coll m^{-3}].

Note that the collision rate expressed with Eq. (12) is independent of colloid size, which only holds for colloids of approximately equal size (monodisperse size distribution).

Estimates for the half-lives of colloid populations with various initial colloid concentrations and α values are listed in Table 5. Colloid concentrations in the range 0.2 to 20×10^{13} coll m^{-3} as well as α values in the range 0.1 to 1 can be taken as being representative for a cementitious environment. In the next section it will be shown that the attachment factor α is expected to be close to unity due to the chemical conditions prevailing in cementitious systems. Note that, according to Eq. (13), the half-life of a colloid population is reduced or enhanced in proportion to the initial colloid concentration.

The characteristic reaction times of the diffusive transport (Eq. (11)) and coagulation/aggregation (Eq. (13)) were compared for an overall assessment of the importance of the two colloid removal processes in the mortar backfill.

Table 5: Calculated colloid population half-lives ($t_{1/2}$).

C_0 [coll m^{-3}]	α	$t_{1/2}$ [h]
0.2×10^{13}	0.1	230
2.0×10^{13}	0.1	23
20×10^{13}	0.1	2.3
0.2×10^{13}	1	23
2.0×10^{13}	1	2.3
20×10^{13}	1	0.23

The characteristic reaction times for both processes were found to be in the range of a few hours at colloid concentrations above 10^{13} coll m^{-3}. Taking into account the uncertainties in both calculations, the reaction times are considered to be similar under these conditions indicating that, in principle, both removal processes may be operative in the backfill.

It also emerges from these considerations that, at very low colloid concentrations, diffusive transport and attachment onto the near-field material rather than colloid-colloid interactions control colloid removal. Conversely, coagulation-aggregation processes are more effective at high colloid concentrations.

3.2 Physico-Chemical Aspects of Colloidal Stability

The term “colloidal (or colloid) stability” is used to denote the state of colloid dispersion over the period of observation. A system containing colloids is said to be stable if the state of dispersion (or the colloid concentration) is only slowly changing over time. Otherwise, colloid suspensions are said to be unstable.

Physical and chemical aspects affect colloid stability. Three physical processes lead to inter-particle contact: Brownian diffusion, fluid shear and gravity. These processes can readily be integrated in theories of particle coagulation and deposition processes (sections 3.3 and 3.4). Chemical aspects of colloid stability arise from inter-surface forces, which depend on the properties of the interfacial regions. The inter-surface forces include double layer interactions, London-van der Waals attraction, and poorly characterised short-range forces such as hydration and steric repulsion. The DLVO theory (DLVO Derjaguin-Landau-Verwey-Overbeek) for colloidal stability considers London-van der Waals attraction and diffuse double-layer repulsion as the sole operative factors. Numerous studies and reviews have demonstrated that the DLVO theory can be applied successfully to predict some characteristics of particle-particle interactions, namely the collision efficiency factor α under “favourable” chemical conditions. However, the theory fails in predicting the collision efficiency factor α under “unfavourable” chemical conditions, that is when specific chemical binding reactions are involved (for detailed reviews see LYKLEMA 1978; O’MELIA 1987; GRAUER 1990; ELIMELECH et al. 1995).

Particles are electrostatically destabilised when attractive forces dominate particle-particle interactions. The conditions are considered to be favourable for coagulation or deposition of colloids. For example, favourable conditions are established when oppositely charged particles approach each other. Unfavourable conditions occur when electrostatic repulsion dominates during particle-particle interactions, for example, when similarly charged particles approach each other. In this case, particles are said to be electrostatically stabilised. Characteristics of the colloid surface have to be taken into account, i.e, surface charge and surface reactions such as protonation/deprotonation of surface hydroxyl groups, adsorption of organic ligands etc. to interpret colloid stability under unfavourable chemical conditions.

The charge on colloid surfaces gives rise to surface potentials and diffuse double layers that extend into the bulk solution. The surface charge of colloids is strongly dependent on solution pH as surface hydroxyl groups can undergo protolysis reactions. Repulsive forces between colloids increase with increasing surface charge, and surface potentials, between like-charged surfaces. On the other hand, a reduction in the surface charge of like-charged surfaces enhances attractive forces. The ionic strength of the solution controls the extent to which double layers extend from the surface into the bulk solution. The surface charge is counterbalanced within a small double layer at high ionic strength. Under these conditions, the double layers of approaching surfaces will overlap only at small separation distances reducing the double layer repulsion between the surfaces. Low ionic strength will produce large double layers giving rise to enhanced double layer repulsion. In general it is observed that high ionic strength enhances coagulation and deposition (favourable conditions). By contrast, low ionic strength promotes colloid dispersion in suspension (unfavourable conditions). Therefore, the collision efficiency factor, α, strongly depends on ionic strength (ELIMELECH et al. 1995; O'MELIA 1980; 1985).

Besides ionic strength divalent metals occurring in natural water, in particular, Ca can exert destabilising effects on colloids and particles in lakes and aquifer systems (e.g., O'MELIA 1987 and references therein; DEGUELDRE et al. 1996b). In addition it was found that Ca affects the transport and deposition of colloids in heterogeneous, porous media (e.g., ELIMELECH et al. 1995; KRETSCHMAR et al. 1997). The studies indicate that Ca exerts a pronounced effect on colloidal stability even at low concentrations (mmolar range).

Colloidal stability of particles is also affected by naturally occurring organic matter (NOM) dissolved in the water (e.g., LIANG & MORGAN 1990; O'MELIA & TILLER 1993). The presence of natural organic matter changes the interfacial potential and charge, and, hence, electrostatic interactions between particles are altered. In many natural systems the predominant fraction of NOM is comprised of humic or fulvic substances that, after adsorption, confer a stabilising negative charge to the particle surface. Thus, naturally occurring organic matter and, moreover, low-molecular weight organic ligands which sorb on solid surfaces tend to stabilise the colloid fraction in the fluid.

From the above review of colloid stability in natural systems it emerges that ionic strength, Ca concentration as well as the concentration of organics exert a strong effect on colloidal stability. Coagulation and filtration/deposition of colloids are promoted by high ionic strength, increasing Ca concentrations and decreasing concentrations of organic ligands.

3.3 Coagulation of Colloids

The removal of colloids from solution can be described by consecutive coagulation and sedimentation processes, which are schematically given by:

$$\text{colloid} \xrightarrow{\text{coagulation}} \text{aggregates} \xrightarrow{\text{sedimentation}} \text{settled aggregates}$$

The removal of colloids is controlled by the rate-determining step of the sequence, i.e., either coagulation or sedimentation. The rate law for sedimentation can be written as (O'MELIA 1980):

$$\frac{V\,dn_k}{dt} = -\left(\frac{v_k}{z}\right) V\,n_k \qquad [s^{-1}]. \qquad (14)$$

V is the volume of the system [m^3], z is a representative sedimentation distance [m], v_k is the settling velocity [m s^{-1}] and n_k is the number concentration of k-size particles [pt m^{-3}]. The settling velocity of a spherical particle can be described in terms of Stokes law assuming laminar flow conditions (LERMAN 1979):

$$v = \frac{z}{t} = \left(\frac{d_p^2 (\rho_p - \rho_l)}{18\eta} \right) \times g \qquad [m\ s^{-1}], \qquad (15)$$

z: distance of particle movement [m],

t: settling time [s],

d_p: diameter of the spherical particle [m],

g: gravitational acceleration (9.81 m s^{-2}),

ρ_p: density of the solid (cement: 2000 kg m^{-3}),

ρ_l: density of the fluid (H_2O, 25°C: 997.07 kg m^{-3}),

η: viscosity of the fluid (H_2O, 25°C: 8.904×10^{-4} kg m^{-1} s^{-1}).

Besides sedimentation, coagulation of colloids is the second process that controls the number concentration of the k-size particles. The present understanding of interaction frequency in coagulation is based on the work by VON SMOLUCHOWSKI (1917). In his classical analysis of both perikinetic (Brownian motion) and orthokinetic (shear) flocculation, particle encounters are treated as binary collisions between rigid spheres. Particles approach each other on a rectilinear path behaving as though no other particles were present. Long-range attractive forces are assumed to be zero for all but interacting particles. Differential settling refers to the sweeping of small particles by larger ones overtaking them during their fall through the water column. The same approach developed for aerosols by FRIEDLANDER (1960) was adopted for hydrosols by O'MELIA (1980). The coagulation reaction for the k-size particles in a system with volume V is described by:

$$\frac{V dn_k}{dt} = V \left(\frac{1}{2} \right) \sum_{i+j=k} \alpha\beta(i,j) n_i n_j - V n_k \sum_{i=1}^{\infty} \alpha\beta(i,k) n_i \qquad [s^{-1}], \qquad (16)$$

with n_i, n_j and n_k as the number concentrations of the i-size, j-size and k-size particles [m^{-3}]. α denotes the collision efficiency factor. β (i,j) and β (i,k) are the collision frequency functions between particles of the size classes indicated. The two terms in Eq. (16) account for the rate of formation of k-size particles from particles (i+j$\rightarrow$k) and the loss of k-size particles due to coagulation and growth. When two particles (i+j$\rightarrow$k) are aggregated, it is useful to consider that

their volume is conserved and a new particle of size k having a volume V_k is formed (coalesced sphere assumption). The factor 1/2 is needed because collisions are counted twice in this summation. The collision frequency function β depends on the mode of inter-particle contact. Inter-particle contacts in water can occur by several different physical mechanisms, three of which are of specific interest to this study (FRIEDLANDER 1977):

1) Brownian motion or diffusion: $$\beta_{bd}(i,j) = \frac{2k_B T}{3\eta} \times \frac{(d_i + d_j)^2}{d_i d_j}, \quad (17a)$$

2) Velocity gradient of shear: $$\beta_{vg}(i,j) = \frac{1}{6}(d_i + d_j)^3 G, \quad (17b)$$

3) Differential settling: $$\beta_{ds}(i,j) = \frac{\pi g}{72\eta}(\rho_p - \rho_l)(d_i + d_j)\left|d_i - d_j\right|, \quad (17c)$$

d is the diameter of the particle class indicated [m]. G denotes the shearing rate of the fluid [s^{-1}] (for k_b, T, η, g, ρ_p, ρ_l see Eqs. (13) and (15)).

When modelling the particle distribution in natural systems, the overall collision frequency is assumed to be the sum of the three separate contributory mechanisms given by Eqs. (17a) - (17c) (O'MELIA 1985). The modes of particle interactions are operative for specific ranges of the particle spectrum (FRIEDLANDER 1977). For the lower range of the particle spectrum, i.e., particles with diameter ≤ 1 µm, Brownian motion controls the collision velocity. Interparticle contacts are dominated by Brownian motion and shear in the size range 1 µm to 10 µm. If larger particles are present in solution, differential settling and velocity gradients account for the mode of inter-particle contacts. In the present study we consider the behaviour of colloids at the smaller end of the size spectrum, that is for colloids with diameter ≤ 1 µm (Brownian motion).

The attachment or collision efficiency factor α, respectively, accounts for the chemical aspects of particle stability in the system. The collision efficiency is given by

$$\alpha = \frac{\text{rate at which particles attach}}{\text{rate at which particles collide}}, \quad (18)$$

which is the ratio of particle attachment (successful contacts) to the particle contact rate (total number of contacts). The stability factor varies from zero to one, meaning that either none of the collisions results in coagulation (α = 0) or all particle contacts are successful (α = 1). The stability coefficient is operationally defined but originates from theoretical models for particle transport (e.g., O'MELIA 1980; 1985). To date, no theoretical approaches are sufficiently advanced to predict collision efficiency factors. Thus, they have to be determined experimentally for any system under investigation (GRAUER 1990; ELIMELECH et al. 1995). Batch-type flocculation is a common technique employed for the determination of collision efficiency factors in model systems (LAWLER et al. 1983).

3.4 Deposition of Colloids

Deposition or filtration involves collisions between suspended particles and stationary collectors in the porous medium. Theoretical prediction of the kinetic of colloid deposition requires detailed knowledge of colloidal forces, flow field and hydrodynamic influences within the colloidal system. A review on quantitative descriptions and modelling approaches of deposition phenomena is given in ELIMELECH et al. (1995). Transport and deposition of colloidal particles during flow through porous media have been studied extensively using well-characterised model systems. For a monodisperse colloid population, the rate of colloid capture in porous media with respect to the depth, x, of a clean filter bed can be described by the following equation (O'MELIA & TILLER 1993):

$$\frac{\partial n}{\partial x} = -\frac{3}{2}\alpha_d \eta_0(p,c)\frac{(1-\varepsilon)}{d_c} n, \qquad (19)$$

where n is the particle concentration, x denotes the distance along the length or depth of the filter medium, α_d is the collision efficiency factor for deposition, $\eta_0(p,c)$ denotes the particle transport or collision frequency function for contacts between particles and media grains under favourable chemical conditions, d_c is the diameter of the grains comprising the porous media (the grains are assumed to be homogeneous with a fixed porosity), and ε is the porosity of the filter. Eq. (19) has been used to estimate colloid travel distances in saturated porous media and verified in numerous column experiments with various colloids, porous media and solution chemistry (ELIMELECH et al. 1995).

For an isolated spherical collector, the collision frequency function $\eta_0(p,c)$ is the sum of three transport mechanisms:

$$\eta_0 = \eta_D + \eta_I + \eta_G , \tag{20}$$

η_D as transport by diffusion:

$$\eta_D = 4.0 A_s^{1/3} \left(\frac{D_\infty}{U d_c} \right)^{2/3} \tag{21a}$$

η_I as transport by interception:

$$\eta_I = \frac{3}{2} A_s \left(\frac{d_p}{d_c} \right)^2 \tag{21b}$$

η_G as transport by gravity:

$$\eta_G = \frac{(\rho_p - \rho_l)}{18 \eta U} g d_p^2 \tag{21c}$$

Here A_s is a flow parameter accounting for the effect of neighbouring collectors (grains) in the filter on the flow field around a single collector. D_∞ is the bulk particle diffusion coefficient calculated from the Stokes-Einstein equation. U is the approach velocity to the filter, whereas d_p and d_c are the particle and collector diameters, respectively. The densities of the particles and the fluid are given by ρ_p and ρ_l, g is the gravitational acceleration, and η is the viscosity of the fluid (see Eq. (15)).

Comparing Eqs. (16) and (21) reveals that, for both particle coagulation and filtration, the same principal processes, i.e., mass transport and collision efficiency, control inter-particle reactions. As for coagulation, the empirical collision efficiency factor describes the fraction of colloid collisions with the collector surface, which results in attachment (Eq. (18)). Modelling calculations and experimental studies have demonstrated the importance of the collision efficiency factor α for deposition, and colloid transport is highly dependent on the collision efficiency factor α. When chemical conditions are favourable for deposition, i.e., α = 1, the transport of colloids and particles of all sizes is extremely small. Under unfavourable chemical conditions, that is, at very low α values, colloids and particles are very mobile. It has been shown that colloids with sizes ≤ 100 nm can travel several meters in groundwater aquifers, when chemical conditions are unfavourable for deposition. As for colloid-colloid interaction processes, no adequate theories are available for predicting the collision efficiency α in colloid deposition. Therefore, α is determined experimentally

using packed-bed column techniques. To date, a very limited number of studies have been published focussing on the determination of the collision efficiency factor α in natural porous media, e.g., soil and aquifer sediments. To the best of our knowledge no experimental studies have been performed in cementitious systems.

An important constraint for experimental deposition studies is the fact that, to date, theories of particle deposition can only be tested in deposition experiments carried out with model particles and/or collectors under strictly controlled chemical-physical conditions (ELIMELECH et al. 1995). Therefore, a great number of studies dealing with the deposition of colloids in granular porous media under unfavourable conditions have been performed using negatively charged latex colloids of a well-defined size penetrating through columns packed with glass beads. The studies on model systems have led to an improved understanding of the influence of specific chemical parameters such as ionic strength, the concentration of Ca and organic ligands dissolved in the fluid on the deposition rate of colloids.

In Fig. 3 collision efficiency factors measured on model systems are displayed to illustrate the influence of ionic strength, e.g., NaCl and KCl electrolytes, and the Ca concentration on colloid stability. The collision efficiency factor depends on ionic strength for I < 0.1 M (Fig. 3a). In this range, colloid efficiencies predicted by the DVLO theory are many orders of magnitude smaller than those observed experimentally (RYAN & ELIMELECH 1996). Maximum collision efficiency is reached at I > 0.1 M developing favourable chemical conditions for coagulation and colloid deposition regardless of the dynamic conditions of the experimental systems. Under these conditions a fair agreement was found between theoretical predictions based on the DVLO theory and experimental observations. Fig. 3b reveals a strong effect of Ca on colloid deposition even at low concentrations. The results, which illustrate the influence of Ca on colloid deposition in different experimental systems, appear to be less consistent among the different studies. However, it clearly emerges from Fig. 3b that chemical conditions are favourable for colloid deposition at Ca concentrations $> 10^{-3}$ M ($\alpha > 0.1$).

3.5 Colloid Stability in Cement Pore Water

Colloidal suspensions are destabilised when the net particle charge vanishes. Thus, the point of zero charge (PZC) of particles, i.e., the pH at which the net total particle charge is zero, is an important surface parameter used to assess the coagulation behaviour of colloidal suspensions. Note that the PZC is not affected by the concentration of the background electrolyte. The surface characteristics of the colloidal matter have not been addressed experimentally in this study. However, knowing the chemical composition of cement-derived colloids, the surface characteristics of the cement-derived colloids can be assessed on the basis of available literature data. As outlined above, colloidal matter formed in the mortar M1/ACW systems has a chemical composition similar to CSH phases (see section 2.3; RAMSAY et al. 1988; 1991). The CSH structure consists of alternating CaO sheets and SiO_4 tetrahedral chains. Therefore, the surface characteristics of CSH-type colloids can be predicted based on the surface potentials and the acid-base behaviour of CaOH and SiOH sites (STEIN 1968; HEATH et al. 1996; IWAIDA et al. 2000). A discussion of the surface characteristics of CSH phases then allows qualitative predictions of the stability of CSH-type colloids in highly alkaline CPW.

For modelling the surface chemical behaviour of CSH phases, HEATH et al. (1996) assumed that the surface hydroxyl groups undergo protolysis reactions, which are schematically given by:

$$\equiv CaOH_2^+ \Leftrightarrow \equiv CaOH + H^+$$
$$\equiv CaOH \Leftrightarrow \equiv CaO^- + H^+$$
$$\equiv SiOH_2^+ \Leftrightarrow \equiv SiOH + H^+$$
$$\equiv SiOH \Leftrightarrow \equiv SiO^- + H^+.$$

The PZC (point of zero charge) of calcium sites on hydrous CaO is reported to be approximately 12.9 (PARKS 1967). In the same work, the PZC of silicon sites was given as 2.4. Thus, all SiOH surface sites are deprotonated under conditions relevant to CPW and, consequently, negatively charged. Note that deprotonated OH groups pre-dominate above the PZC, and protonated OH groups below the PZC. Therefore, the negative surface charge on SiOH sites tends to stabilise suspensions containing CSH-type colloids. At pH 12.5 and higher, the sign of the charge carried by the surface CaOH groups is pH

dependent. Positively charged and neutral sites are expected to be the dominating surface species in the pH range 12.5 to 12.9. Above pH ~13, neutral and negatively charged sites may predominate due to deprotonation of the CaOH groups. Thus, due to the high PZC, CaOH sites tend to destabilise suspensions with CSH-type colloids.

Sorption model predictions show a negative surface potential for low Ca/Si ratios of CSH phases (C/S < 1), attributable to the larger proportion of negatively charged SiOH groups (HEATH et al. 1996). A positive surface potential is predicted with increasing Ca/Si ratio (C/S > 1), i.e., when the proportion of CaOH sites is increased. It appears that the model predictions are in good agreement with measured zeta potentials (HEATH et al. 1996). Models and measurements indicate that, in the pH range of CPW, i.e., pH ≥ 12, the surface potential and charge of CSH-type minerals is very small (either positive or negative) or even zero (STEIN 1968; IWAIDA et al. 2000). This further indicates that the surface properties of cement-derived colloids are favourable for coagulation and colloid deposition in this pH range.

Based on the above discussion of colloidal stability and the surface properties of cement-derived colloids we anticipate that the chemical conditions in the near-field of a repository are favourable for both colloid deposition and colloid coagulation. To summarise, the following characteristics of cement systems support our conclusion: 1) The surface properties of the cement-derived colloids are strongly influenced by the proportion of CaOH sites (PZC ~ 12.9), 2) the high ionic strength (0.07 M ≤ I ≤ 0.3 M), and 3) Ca concentrations in the range 1.6 to 20×10^{-3} M in CPW. Therefore, it is justified to assign values in the range of 0.1 to 1 to the collision efficiency factor α under CPW conditions. Values in this range were previously used to estimate the characteristic coagulation time of colloids present in the backfill mortar (section 3.1). As a consequence of the high α values, colloid removal due to colloid-colloid and colloid-collector interactions is anticipated to be very effective in the mortar backfill and, hence, low colloid inventories are expected in CPW.

Measurements of low colloid concentrations require a sensitive analytical instrumentation and careful sampling procedures. The analytical methods applied in this study will be presented in the next section.

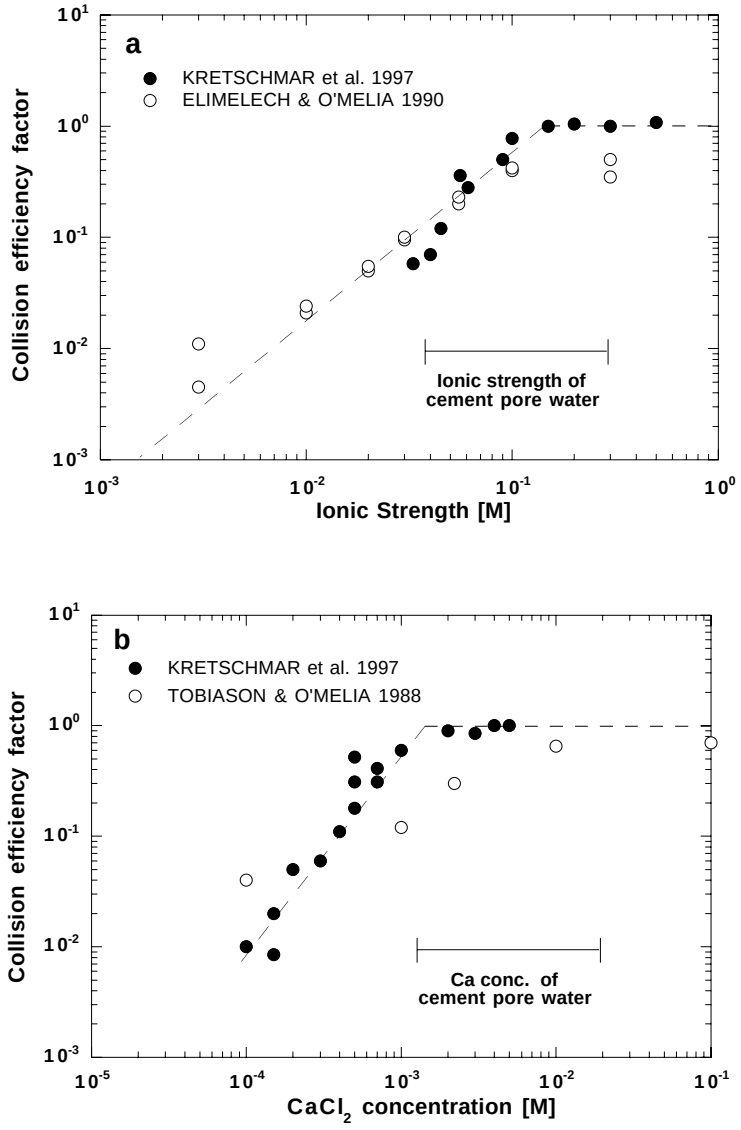

Fig. 3: Dependence of the collision efficiency factor α on the electrolyte concentration in model systems (latex particles and columns packed with glass beads). a) Effect of ionic strength in model systems. The following electrolytes were used: NaCl (pH 9.5) by KRETSCHMAR et al. (1997) and KCl (pH 7±0.2) by ELIMELECH & O'MELIA (1990). b) Effect of $CaCl_2$ on the following systems: TOBIASON & O'MELIA (1988) used latex particles and columns packed with glass beads, fluid at pH ~ 7; KRETSCHMAR et al. (1997) used latex colloids in columns packed with sandy soil material, fluid at pH 5.8.

4 ANALYTICAL METHOD

4.1 Single Particle Counting

Colloid concentrations were determined by in-situ particle counting. In this context “in-situ” means that colloids were directly detected in the fluid without further pre-treatment of the water samples. The method has been successfully applied for single particle analysis in environmental samples (DEGUELDRE 1994). A schematic view of the particle counting system is given in Fig. 4. A high volume carrier flow of de-ionised water is generated in the water purification system to establish a flow rate of 500 mL min^{-1}. The samples are injected into the carrier flow using a HPLC pump at an injection rate between 200 and 2200 mL h^{-1}. The injection rate is adjusted according to the colloid concentrations of the samples. Three sensors are employed in combination: a Horiba sensor (PLCA-311; Horiba Ltd., Kyoto, Japan) arranged in series with two PMS sensors (HVLIS-C200-Cor and HSLIS-M50; Particle Measuring Systems Ltd., Boulder, USA). After passing the sample cell of the PLCA-311 sensor, the carrier flow is split into two branches of different flow rates, 100 mL min^{-1} and 400 mL min^{-1}, as recommended for operation of the in-parallel arranged PMS sensors. Regulators control the carrier flow.

The sensors operate on the principle that light scattered by a liquid borne particle (or colloid), resident in a laser beam, is directly proportional to its size. Particles of a given size scatter light through a given angle, which increases with decreasing particle size. Therefore, colloids of the same size transiting the laser beam produce pulses of the same amplitude and finite width. Particle concentrations are sufficiently low to ensure detection of single particles. The pulses of radiant energy are recorded by photodiode detectors, which are oriented at 90° to the laser beam. A rectangular orientation greatly improves the signal-to-noise ratio. The pulses are amplified and their maximum amplitude stored with a conventional pulse height analyser (peak detection). Optical sensors are calibrated with standard size particles to establish the pulse vs. size interval curves.

Although operating on the same principle, the sensors differ with respect to the optical systems, data acquisition as well as the properties of the lasers and sample cells. The PLCA-311 counter operates with a Gaussian TEM_{∞} mode

laser (10 mW, 480 nm). Despite the high resolution, it only incorporates three size channels with size thresholds ≥ 100 nm, ≥ 200 nm and ≥ 500 nm at standard sensitivity. Output data represent colloid concentrations above the threshold settings. The PMS sensors operate with Gaussian TEM_{∞} mode lasers (30 mW, 780 nm). The HSLIS-M50 is a 0.05 µm threshold monitor unit incorporating 4 size channels. The sensor is connected to a PDS-PB data system.

This instrument has been designed for fast and continuous real-time detection of colloids. The HVLIS-C200-Cor operates in the spectrometer mode incorporating a total of 8 size channels in the size range 200 nm to 5000 nm. The sensor is controlled by a MicroLPS data system. The instrument has been designed for applications where high flow rates are appropriate. The particle counting system is controlled by an in-house developed PC compatible software based on DELPHI (Borland). Moreover, the programme allows data acquisition and data compilation. For data analysis and data treatment, however, commercially available programmes are employed.

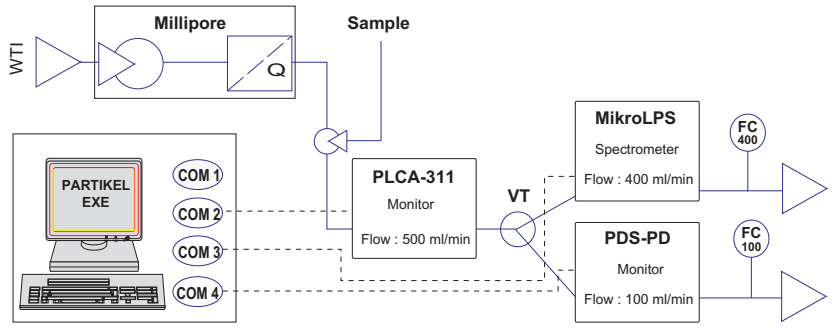

Fig. 4: Schematic representation of the particle counting system. The system consists of the following components: Millipore Milli-Q Plus water purification system (Millipore); HPLC pump for sample injection (Sample); a combination of three particle counters: Horiba PLCA-311 counter (PLCA-311), PMS HSLIS-M50/PDS-PB monitor (PDS-PB) and PMS HVLIS-C200-Cor/MicroLPS monitor (MikroLPS); flow splitting unit (VT); flow regulators (FC); PC for instrument control and data acquisition.

The particle counting system was designed for measuring colloid concentrations and size distributions of natural samples. The specifications of the counter (PLCA-311), monitor (HSLIS-M50) and spectrometer (HVLIS-C200-Cor) differ with respect to sensitivity (smallest detectable colloid size), resolution (number of channels) and the flow rate (carrier flow). Spectrometers operate with high resolution and relatively low sensitivity. Monitors are a relatively new class of instruments with a high sensitivity, high sampling rates but relatively poor resolution. Optical counters have higher intrinsic resolutions, however, incorporating only a very limited number of size channels. A combination of sensors enables us to determine particle size distributions over the size range 50 nm to 5000 nm at relatively high resolution (maximum 13 size channels) and at very low concentration levels (10^5 to 10^8 coll mL^{-1}).

The dynamic ranges of the sensors as given below were deduced from measurements of certified standard size particles (WIELAND et al. 1998b):

PMS-M50/PDS-PB: $(3\pm1)\times10^4$ coll mL^{-1} - $(1\pm0.5)\times10^7$ coll mL^{-1}

Horiba/PLCA-311: $(7\pm2)\times10^3$ coll mL^{-1} - $(5\pm1)\times10^7$ coll mL^{-1}

PMS-Cor200/MikroLPS: $(2\pm1)\times10^3$ coll mL^{-1} - $(3\pm1)\times10^7$ coll mL^{-1}

The lower concentration limit is determined by the background level of colloids in Milli-Q water. The background was found to range from ~10^6 - ~5×10^7 coll L^{-1} depending on the size range detected by the sensors (Fig. 5). The limit was determined by injecting purified water (Milli-Q water) via injection pump (injection rates: 200 mL h^{-1} and 2200 mL h^{-1}) into the carrier flow (Fig. 4). This mode of operation was employed for sample analysis. The background is caused by particulate impurities present in Milli-Q water, tubing and the injection system. Note that even intensive flushing of the injection system with Milli-Q water did not reduce the background below the concentration levels shown in Fig. 5. The upper concentration limit is due to coincidence errors occurring at particle concentrations larger than about 10^7 coll mL^{-1}.

4.2 The Power-law Size Distribution (Pareto)

The classification of particles or colloids is based either on size (radius or diameter), volume or mass. When laser scattering is applied for sorting particles into size fractions, the characteristic dimension is expressed in terms of an

equivalent spherical-cross-sectional area diameter ø. The general equation for a particle-number distribution, or a particle-number spectrum, relates the number of particles (N) of a size between ø and ø+dø (dN) to the particle size ø according to (FRIEDLANDER 1977):

$$dN = f(ø)dø \qquad \text{(particles)}, \qquad (22)$$

where ø is some characteristic linear dimension, e.g., spherical-cross-sectional-area diameter, and f(ø) is a mathematical relationship describing the particle-number distribution.

Note that “particle-size distribution” and “particle-number distribution” are used as interchangeable expressions. The particle-volume distribution is expressed as:

$$dV = v(ø)dN \qquad \text{(length}^3\text{)}, \qquad (23)$$

with dV as the volume of dN particles of size between ø and ø + dø, and v(ø) as the volume of an individual particle of size ø.

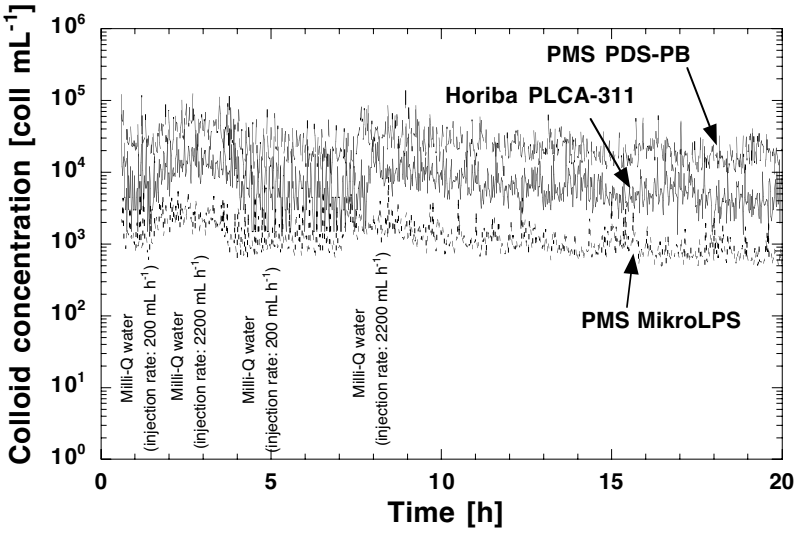

Fig. 5: Determination of the colloidal background in Milli-Q water. The colloid concentrations determined by the sensors are shown as a function of time. Purified water (Milli-Q water) was injected either directly into the carrier flow or added via HPLC pump (injection rates: 200 mL h^{-1} and 2200 mL h^{-1}).

The corresponding particle mass spectrum is given by:

$$dM = \rho(ø)dV \qquad \text{(weight)}, \tag{24}$$

with $\rho(ø)$ as the particle density [g cm^{-3}], which may be taken as constant or dependent on particle size ø.

Three frequency distributions have been extensively used to describe particle-number spectra (or particle-volume and mass spectra) with pronounced asymmetric shapes: the lognormal distribution, the Weibull or Rosin-Rammler distribution, and the Pareto or power-law distribution (LERMAN 1979). Each of the three distributions has been applied to characterise the particle-size spectra in natural systems. The lognormal and the Weibull or Rosin-Rammler distributions are unimodal asymmetric distributions. A size spectrum with continuously decreasing particle concentrations at increasing particle size can be displayed in terms of a hyperbolic distribution (power-law or Pareto distribution). It has been applied to display size distributions of atmospheric and stratospheric aerosol particles (micron and sub-micron size range) as well as sedimentary particles and suspended matter in the ocean (sub-millimeter size range) (LERMAN 1979). Numerous examples have demonstrated its wide applicability for representing size spectra of particles (or colloids) in natural systems.

The power-law distribution is given by:

$$dN(ø) = Aø^{-b}dø. \tag{25}$$

Integration between boundaries $ø_1$ and $ø_2$ leads to:

$$N = \int_{ø_1}^{ø_2} dN = \frac{A}{(1-b)}\left(ø_2^{1-b} - ø_1^{1-b}\right) \quad (b\neq 1), \tag{26}$$

with N as the colloid number, ø as the size of the particles and A and b as empirical constants. For a graphical presentation of the analytical data, the continuous size distribution is approximated by a discrete differential size distribution with dN(ø)/dø given by the concentration of colloids per unit of size $N(ø_p)/\Delta ø$:

$$\frac{dN(ø)}{dø} \approx \frac{N(ø)}{\Delta ø} = Aø^{-b} \qquad [mL^{-1}\,nm^{-1}]. \tag{27}$$

Here N(ø) denotes the cumulative concentration of colloids in the size range $ø_p$ to $ø_{p+1}$ or the bar height of the histogram, respectively, and $\Delta ø$ corresponds to the size interval for that bar (= $ø_{p+1}$ - $ø_p$). In this study, colloid concentrations are given in number of colloids per volume [coll mL^{-1} or coll L^{-1}], whereas the colloid size is given in nm units [nm]. As concentration and size can vary over several orders of magnitude, the logarithmic form of Eq. (27) is generally used to display colloid concentrations as a function of linear colloid dimension:

$$\log\frac{N(ø)}{\Delta ø} = \log A - b \times \log ø. \tag{28}$$

A and b are characteristic parameters of the colloid size distribution. Particle populations of natural samples show size distributions with a slope -b typically ranging from about -1.8 to -4.5 (LERMAN 1979). Size distributions of groundwater colloids show slopes ranging between -2.6 and -4 (DEGUELDRE 1994; DEGUELDRE et al. 1996a). Assuming spherical geometry of the particles, the differential equation for the colloid-number distribution can be converted into the corresponding expression for the colloid-volume distribution:

$$dV = \left(\frac{\pi}{6}\right) A ø^{3-b} dø \quad [cm^3]. \tag{29}$$

Assuming constant colloid density, the corresponding expression for the colloid-mass distribution results to:

$$dM = \rho\left(\frac{\pi}{6}\right) A ø^{3-b} dø \qquad [g]. \tag{30}$$

The logarithmic forms of the colloid-volume and colloid-mass distributions are:

$$\log\frac{dV}{dø} = \log[(\pi/6)A] - (b-3)\log ø, \tag{31}$$

$$\log\frac{dM}{dø} = \log[(\pi/6)\rho A] - (b-3)\log ø. \tag{32}$$

The cumulative volume of colloids with size between $ø_1$ and $ø_2$ is calculated by integrating Eq. (29):

$$V = \int_{ø_1}^{ø_2} dV = \frac{A\pi}{6(4-b)}\left(ø_2^{4-b} - ø_1^{4-b}\right) \ (b \neq 4). \tag{33}$$

The total mass of colloids is obtained by multiplying Eq. (33) with the density for cementitious materials (ρ = 2 g cm^{-3}).

An alternative way of estimating the total volume and mass of colloidal material is based on a direct evaluation of colloid-volume and colloid-mass distributions. The distributions can be deduced by calculating the volume and mass of individual size classes $N(ø_p)$:

$$V_{ø_p} = N(ø_p) \times ø_p^3 \times \frac{\pi}{6}, \tag{34}$$

$$M_{ø_p} = N(ø_p) \times ø_p^3 \times \frac{\rho\pi}{6}. \tag{35}$$

In these calculations colloids are assumed to be ideal spheres with diameter $ø_p$, and the density ρ, used for cementitious materials. Volume and mass distributions result from displaying the volume or mass of individual size classes as a function of size ø. The total volume or mass of a colloid population is obtained by integrating the equations for the volume and mass distributions between size $ø_1$ and $ø_2$ of the colloid population.

The two ways of estimating the total volume and mass of colloidal material are expected to yield consistent values. In this study the two procedures were applied and compared for the COLEX samples (see chapter 6).

Description of size distributions in terms of the power-law approach allows an evaluation of the specific (geometric) surface area of colloidal matter. In this study the specific surface area of a colloid population is estimated by calculating an average colloid diameter based on number and volume concentrations. The average colloid diameter of a colloid population can be written as:

$$\bar{d}_p = \sqrt[3]{\frac{6V_t}{N_t \pi}}, \tag{36}$$

with V_t and N_t as the number and volume concentrations of the colloid population. Note that spherical shape of the colloids is implicitly assumed. The specific (geometric) surface area can be written as:

$$S_t = \frac{N_t \bar{d}_p^2 \pi}{M_t} = \frac{3.3 N_t^{1/3} \pi^{1/3}}{\rho V_t^{1/3}}, \qquad [\text{cm}^2\ \text{g}^{-1}]. \tag{37}$$

From the above presentation it is evident that size distributions of colloids may be represented in different ways depending on whether colloid number, colloid mass, colloid volume is considered as the important variable for a specific problem. Size distributions on the basis of colloid mass are preferentially applied for studying colloid fluxes. For example, the colloid mass is an input parameter in the transport models used to predict colloid-facilitated radionuclide migration. By contrast, processes affecting the colloid number, e.g., coagulation processes, are better related to the corresponding size distributions.

4.3 Size Distributions of Synthetic Colloid Systems

The performance of the particle counting system was tested using synthetic colloid systems (WIELAND et al. 1998b). Synthetic colloid suspensions were prepared from certified Nanosphere^{TM} size standards with well-defined diameters (Duke Scientific Corp., Palo Alto, CA, USA). Two series of tests were performed: First, the dynamic (working) ranges of the individual sensors were evaluated using suspensions prepared from a single size standard, and, second, measurements were carried out using mixtures of size standards to evaluate reproducibility and accuracy of the analytical method.
A linear response of the particle counting system was obtained in the concentration range from about 5×10^4 coll mL^{-1} to 1×10^7 coll mL^{-1} irrespective of the size standards used in the tests. The concentration range corresponds to the dynamic (working) range of the instrument. Mixtures of size standards with well-defined size distribution in the range 50 to 5000 nm were employed to test accuracy and reproducibility of the particle counting method. The size distributions of the mixtures were prepared in such a way that slopes (-b) were approximately -3 and -4 (expected values given in Table 6).

In Fig. 6 measurements (symbols) and expected size distributions (lines) are displayed in accordance with the notation given in Eq. (28). The characteristic parameters log A and -b of the power-law distribution were calculated on the basis of known and measured colloid concentrations. The tests show that expected and measured parameters, i.e., intercept (log A) and slope (-b), agree well, indicating that size distributions of synthetic colloid suspensions can be determined accurately with the particle counting system.

Table 6: Expected and determined values of the characteristic parameters (log A, -b) for two model systems. “Expected” values were calculated based on known colloid concentrations in suspension. “Determined” values were evaluated from measured colloid concentrations [coll mL^{-1}].

Slope (-b) expected	Slope (-b) determined	logA expected	logA determined	Correlation coeff. R
- (3.00 $\pm$ 0.03)	- (3.25 $\pm$ 0.21)	10.93 $\pm$ 0.09	11.44 $\pm$ 0.55	0.99/0.98
- (3.99 $\pm$ 0.07)	- (3.99 $\pm$ 0.23)	13.24 $\pm$ 0.19	13.09 $\pm$ 0.62	0.99/0.98

For natural samples, however, some uncertainties remain due to the non-spherical shape and differences in the chemical composition of the colloids. Thus, the following assumptions have to be made for natural samples: 1) natural particles scatter laser light in the same way as ideal spheres, and 2) the index of refraction of natural particles (e.g., quartz: n_D = 1.544 at 589 nm) and reference particles (e.g., polystyrene: n_D = 1.59 at 589 nm) are not sufficiently different to cause any distortion of the size distribution. An inter-laboratory comparison exercise in which different techniques were applied to enumerate colloid samples showed that these assumptions are justified (DEGUELDRE 1994). Measurements based on laser light scattering agree with other sizing and counting techniques. Thus, it is anticipated that the single particle counting technique allows accurate measurements of colloid concentrations and size distributions in natural samples.

4.4 Sampling

Prior to measurements colloid-containing CPWs were stored in pre-washed 250 mL Teflon bottles in a glove box under a controlled N_2 atmosphere (O_2, CO_2 < 2 ppm). Sampling and colloid analysis were carried out without exposing the high pH solutions to air. To avoid artefacts during analysis, sampling bottles were designed in such a way to allow injection of the samples into the particle counting system under a nitrogen atmosphere.

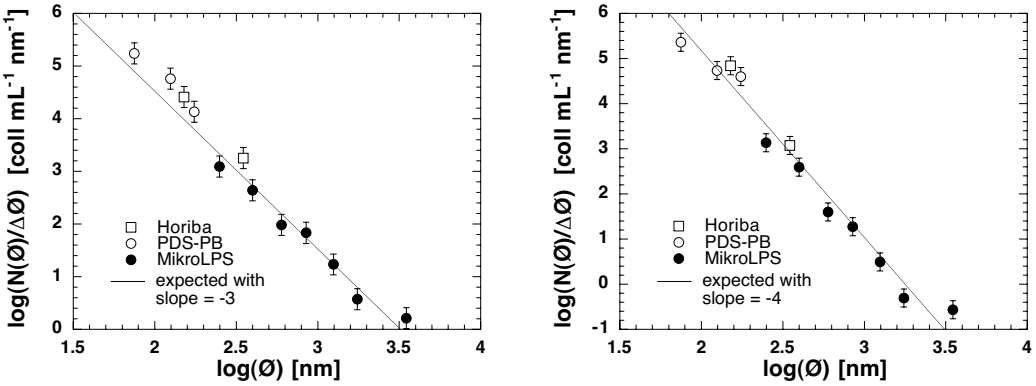

Fig. 6: Tests measurements with colloid suspensions prepared from certified Nanosphere^{TM} size standards. The model systems were prepared in such a manner to give colloid size distributions with a) slope = -3 and b) slope = -4 (power-law distribution). Lines represent the expected decrease in the colloid concentrations with increasing diameter (ø). Symbols indicate measurements of colloid concentrations.

Prior to colloid counting, samples were diluted with Milli-Q water to give colloid concentrations lower than 4×10^7 coll mL^{-1} to 5×10^7 coll mL^{-1}. To minimise the effect of disaggregation of larger colloids, samples were diluted immediately before the analysis. For the batch experiments reported in chapter 5, sampling and dilution of the samples were performed in the glove box. The Teflon bottles were tightly closed and transferred from the glove box to the particle counter. For the COLEX studies reported in chapter 6, 100 mL volumes of CPW were collected directly into pre-cleaned Teflon bottles flushed with N_2. No additional dilution was required due to the low colloid concentrations of the samples.

In this study a specific procedure was applied to minimise systematic errors in colloid concentration measurements caused by wall sorption onto the sampling containers: After injecting the fluid into the carrier flow of the particle counting system, the remaining solution was discarded, and the sampling containers rinsed with Milli-Q water. After adding a volume of 100 mL Milli-Q water, they were placed in an ultrasonic bath and treated for 2 min. The aqueous solution was again analysed for colloids. Replacement of the solution with fresh Milli-Q water and ultrasonic treatment were repeated until the measured colloid concentration was within the uncertainty of the analytical method (≤ 10 %). Tests with suspensions prepared from standard size colloids showed that the loss of

colloids caused by wall sorption was less than approximately 10 % after three treatments. As a consequence the colloid concentration of a sample is given as the total after three treatments.

4.5 Particle Counting in High pH Solutions

Colloid concentrations measurements in high pH solutions are subject to a series of possible artefacts: 1) Colloid concentrations of high pH solutions are expected to be very low due to colloidal instability under these conditions. Consequently, background colloid concentrations resulting from colloidal impurities present in the sampling containers and the counting system have to be reduced to extremely low levels. In this study sampling containers were carefully cleaned by ultrasonic treatment and repeated washings with Milli-Q water. 2) Contact of high pH solutions with air has to be avoided due to an instantaneous uptake of CO_2 and the formation of calcium carbonate under these conditions. Thus, sampling and colloid analysis were carried out without exposing high pH solutions to air. 3) As previously mentioned, systematic errors may result from a reduction of the colloid concentration in solution caused by wall sorption. The specific procedure applied in this study is expected to minimise the error and to allow the determination of total colloid inventories. 4) Systematic errors may also result when high pH solutions are diluted, e.g., by injecting the samples into the sampling flow of purified Milli-Q water. Dilution of cement pore waters with purified water lowers the salt concentration and, thus, reduces ionic strength. In principle, changes in electrolyte concentrations can exert an effect on the colloid stability and, therefore, on colloid concentration measurements. Thus, the following tests were performed to assess uncertainties in colloid concentrations associated with sample dilution.

The test were carried out using colloid suspensions prepared by immersing mortar M1 grains in ACW (pH=13.3). (Note that the SEM image displayed in Fig. 2 shows colloidal matter collected from the same type of suspensions). 300 mL aliquots of the suspensions (two identical series) were sampled in pre-cleaned Teflon bottles and analysed at injection rates of 200 mL h^{-1} and 2000 mL h^{-1}. An increase in the injection rate corresponds to a reduction in the dilution factor from 150 to 15 at a given carrier flow of 500 mL min^{-1}, which is equivalent to changes in ionic strength from about 0.3 M to 2×10^{-2} M or 2×10^{-3} M, respectively. According to Fig. 3, changes in electrolyte concentra-

tions by one to two orders of magnitude should exert an effect on the collision efficiency factor and, consequently, on colloid stability. Therefore, the assumption that colloid concentrations measurements may depend on sample dilution is justified. Note, however, that the residence time of the colloidal material in the carrier flow prior to detection is short, i.e., less than 1 s (volume ~5 mL, carrier flow = 500 mL min^{-1}). Under these conditions, the effect of colloidal destabilisation on the measurements is expected to be markedly reduced.

The colloid size distributions emerging from these tests are displayed in Fig. 7. The characteristic parameters of the size distributions together with calculated number and mass concentrations are listed in Table 7. Fig. 7 shows a trend to systematically higher colloid concentrations at the lower injection rate. However, the results indicate clearly that the number and mass concentrations deduced from the size distributions differ at a maximum by a factor of about two in spite of an order of magnitude difference in electrolyte concentrations (Table 7).

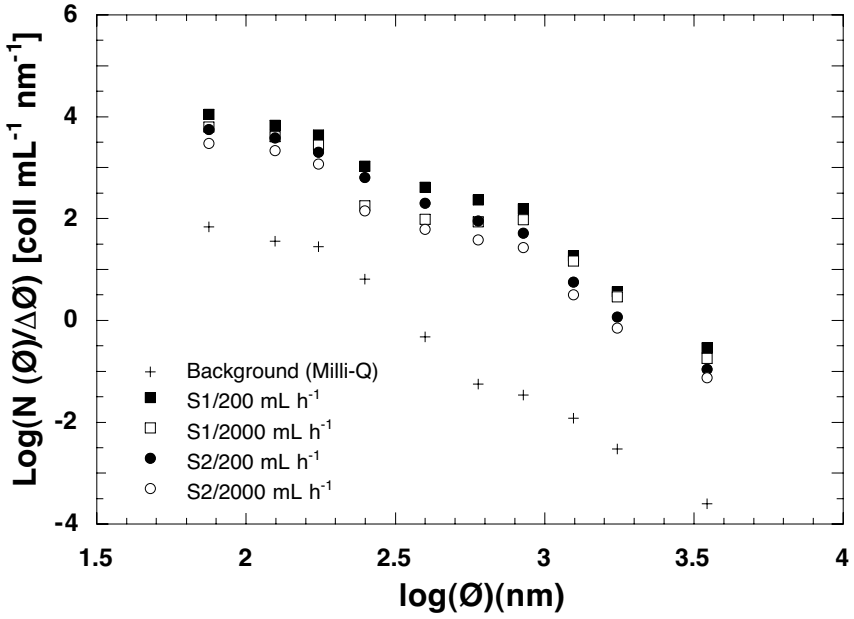

Fig. 7: Tests measurements with high pH colloid suspensions (mortar M1 immersed in ACW of pH=13.3). Colloid size distributions are given for two identical runs (S1 and S2) and injection rates of 200 mL h^{-1} (filled symbols) and 2000 mL h^{-1} (open symbols).

Table 7: Characteristic parameters (logA, -b) of the size distributions as well as number and mass concentrations of the colloid populations (size

range 50 nm - 1000 nm) for two runs (S1 and S2) and different injection rates (200 mL h^{-1}, 2000 mL h^{-1}). Definition and use of the uncertainty factor are given in Appendix B.

Sample	Slope -b	logA	Number conc. [coll L^{-1}]	Mass conc. [μg L^{-1}]	Uncert. factor
S1/200	-(2.73±0.22)	9.61±0.59	2.7×10^{9}	21	6.8
S1/2000	-(2.60±0.24)	8.97±0.66	1.1×10^{9}	11	8.7
S2/200	-(2.88±0.20)	9.65±0.56	1.5×10^{9}	9	6.0
S2/2000	-(2.80±0.19)	9.11±0.52	6.2×10^{9}	4	5.4

Note that both number and mass concentrations are associated with uncertainties attributable to uncertainties on slope (-b) and intercept (log A) of the size distribution (see Appendix B). The tests demonstrate that, in principle, systematic errors are inherently associated with colloid concentration measurements at high pH due to a reduction in the electrolyte concentration after dilution. However, the results clearly indicate that uncertainties in the method, which are associated with statistical uncertainties on slope (-b) and intercept (logA), exceed the systematic error caused by sample dilution.

5 COLLOID STABILITY IN A "YOUNG" CEMENT FLUID

The experimental work on colloid stability was designed to assess coagulation of colloids under the chemical conditions encountered in the near-field of a repository. Flocculation tests were performed to investigate the stability of colloidal suspension in a "young" cement fluid, that is, a (Na,K)OH CPW at pH = 13.3. Batch flocculation tests are well established for assessing the stability of colloidal suspensions (LAWLER et al. 1983; FARLEY & MOREL, 1986; DEGUELDRE et al. 1996b).

The tests allow the determination of colloid concentrations as a function of time for the perikinetic regime, that is, when colloid collisions are brought about by Brownian motion. A perikinetic regime is appropriate under stagnant flow conditions when colloid collision due to fluid shear or differential settling are negligible (ELIMELECH et al. 1995). Such conditions are considered to correspond to those likely existing in the near-field of a repository.

5.1 Experimental Method

80 g of quartz material or mortar M1 grains were added to 800 mL of alkaline fluid and stored in 1 L Teflon containers (diameter 7 cm; height 13.7 cm). By adding quartz or mortar M1 to this fluid, the generation of colloidal material was induced. The mixtures were shaken periodically (2 times a day) end-over-end for 2 min to ensure complete mixing of the solution. Sampling for colloid concentration measurements was performed weekly. Prior to sampling a 5 mL aliquot for colloid analysis, the suspensions were completely mixed and left standing for 1 min to allow sedimentation of quartz and mortar grains. The batch systems were then allowed to stand for at least 24 h. After 24 h, or longer time periods, additional 60 mL aliquots were sampled from the centre of the containers at a height of 6.8 cm and analysed for colloids. The total volume withdrawn during sampling (65 mL) was replaced by a fresh aliquot of the same composition as the initial solution in order to retain a constant volume of 800 mL throughout the experiments. All manipulations were performed in a glove box under a controlled N_2 atmosphere (O_2, CO_2 < 2 ppm, T = 25±3° C). An overview of the systems prepared for this study is given in Table 8.

The alkaline fluids listed in Table 8 were prepared from chemicals of analytical grade quality in de-ionised water as follows:

ACW: The ACW contains 11.61 g KOH, 4.56 g NaOH and 88.8 mg $Ca(OH)_2$ in 1 L of de-ionised water and was equilibrated for at least 2 weeks with 2 g L^{-1} $CaCO_3$ and 2 g L^{-1} $Ca(OH)_2$, left standing over night and filtered through 100 nm polyethersulfone membrane filters (Criticap-M^{TM}, GelmanSciences, USA). $CaCO_3$ was added to reduce the CO_3^{2-} concentration in solution caused by impurities of Na_2CO_3 and K_2CO_3 present in the NaOH and KOH pellets to a level of saturation with respect to $CaCO_3$. A few experiments were carried out in ACW solutions, which had not been equilibrated with $CaCO_3$ prior to use. The different methods used for ACW preparation had no measurable effect on colloid inventories and colloidal stability.

The chemical composition of ACW corresponds to a pore water in stage I of cement degradation ($[Na]_{tot}$ = 0.11 M, $[K]_{tot}$ = 0.18 M, $[Ca]_{tot}$ = 1. 2×10^{-3} M, pH = 13.3).

In two experiments, isosaccharinic acid (ISA) in the Na-form (Na(α-ISA)) was added to simulate the effect of cellulose degradation products on colloid stability ($[ISA]_{tot}$= 5×10^{-3} M).

NaOH/KOH solution: The solution was prepared by dissolving 11.61 g KOH and 4.56 g NaOH in 1 L of de-ionised water and filtered through a 100 nm Criticap-M^{TM} filter before being used in the experiments.

Table 8: Overview of the experimental systems.

Solid	Fluid	Figure
Quartz	ACW	9 a
Quartz	0.11 M NaOH/0.18 M KOH	9 b
Mortar M1	ACW	10 a / b
Quartz	ACW/$[ISA]_{tot}$ = 5×10^{-3} M	11 a
Mortar M1	ACW/$[ISA]_{tot}$ = 5×10^{-3} M	11 b

1) The colloid concentration observed immediately after end-over-end mixing of the batch-type systems: This concentration accounts for the total number of colloids present in solution with diameters ≥ 100 nm. The lower cut-off of 100 nm corresponds to the detection limit of the particle counter (Horiba PCLA-311) used for determining colloid concentrations in these studies.

2) The colloid concentration observed after leaving the batch-type system undisturbed for 24 h: One day is the time required for particles ≥ 1000 nm to settle in the batch systems (Fig. 8). Thus, the colloid concentration determined after a standing time of 24 h corresponds to the number of colloids with diameters ranging between 100 nm to 1000 nm. The upper cut-off of the colloidal size is 1000 nm assuming that colloids with diameters larger than 1000 nm are completely removed from solution after a sedimentation period of 24 h. Fig. 8 indicates that this assumption holds. It shows that, in the initial stage of the experiments ($t \leq 50$ h), the evolution of the colloid number concentration in solution with time can be predicted correctly assuming sedimentation as the only inventory-controlling process. Calculations of particle settling are based on Stokes law (Eq. 15). Solid densities of 2.0 g cm^{-3} and 2.5 g cm^{-3} and a vertical settling distance of 6.8 cm (half of the total settling distance) were assumed for the calculations.

3) The colloid concentration in undisturbed batch-type systems accounts for the long-term colloid concentration. “Undisturbed” means that end-over-end mixing was not applied between the weekly sampling. In this stage of the investigations, the standing periods were extended up to 150 days. The colloid concentrations obtained under these experimental conditions are a measure of the total number of colloids with size between 100 nm and 1000 nm which will be dispersed in solution over longer time scales. On a long term, the colloid inventory is controlled either by sedimentation or a coupled process of coagulation/sedimentation of the colloids, respectively. Thus, the colloid inventory observed in undisturbed batch-type systems is considered to be representative for conditions of low or stagnant water flow in the near-field of a repository.

To summarise, colloid stability was investigated in batch-type systems by measuring colloid concentrations in samples taken after complete mixing of the

solutions, after leaving the solutions undisturbed for 24 h or longer, according to the sampling protocol.

5.2 Background Colloid Concentrations

A series of tests were carried out to determine the background colloid concentrations in these systems. Measurements of colloid concentrations in de-ionised water, filtered and non-filtered ACW are listed in Table 9.

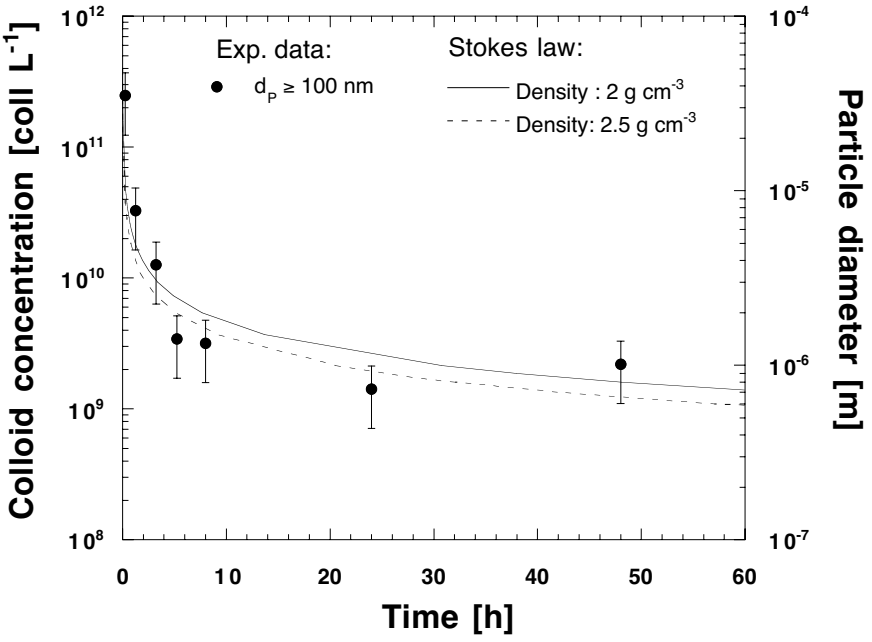

Fig. 8: Time-dependent particle concentrations determined in solution for the system quartz in contact with ACW. The experimental data correspond to the total particle inventory (colloid size 100 nm - 1000 nm plus particles with size ≥ 1000 nm) measured in the system. The lines indicate the time required by particles of size ≥ 1000 nm (right hand scale) to settle over a distance of 6.8 cm as estimated with Stokes equation (Eq. (15)) assuming two different particle densities. A vertical distance of 6.8 cm has to be covered by the particles ≥ 1000 nm to be depleted from the sampling volume.

Table 9: Background colloid concentrations in de-ionised water and ACW.

Solution	Size class 100 - 200 nm [coll L^{-1}]	Size class 200 - 500 nm [coll L^{-1}]	Size class > 500 nm [coll L^{-1}]
De-ionised water	$(4.4\pm0.6)\times10^{7}$	$(3.5\pm1.2)\times10^{6}$	$(3.2\pm1.7)\times10^{6}$
De-ionised water	$(6.9\pm0.7)\times10^{7}$	$(4.0\pm1.9)\times10^{6}$	$(1.5\pm1.2)\times10^{6}$
ACW non-filtered	$(4.6\pm0.1)\times10^{9}$	$(1.7\pm0.4)\times10^{9}$	$(2.3\pm0.1)\times10^{9}$
ACW non-filtered	$(2.5\pm0.1)\times10^{10}$	$(1.8\pm0.2)\times10^{9}$	$(1.1\pm0.2)\times10^{9}$
ACW filtered (0.1 µm)	$(4.2\pm0.4)\times10^{8}$	$(8.2\pm0.3)\times10^{7}$	$(5.9\pm2.1)\times10^{6}$
ACW filtered (0.1 µm)	$(1.5\pm0.1)\times10^{8}$	$(0.9\pm0.2)\times10^{7}$	$(2.7\pm0.7)\times10^{6}$
ACW filtered (0.1 µm)	$(1.2\pm0.1)\times10^{8}$	$(4.4\pm4.8)\times10^{6}$	$(1.1\pm2.0)\times10^{6}$

Total colloid concentrations between 5×10^{7} coll L^{-1} and 7.5×10^{7} coll L^{-1} were observed in de-ionised water, which was stored in Teflon bottles. Total concentrations up to about 3×10^{10} coll L^{-1} were determined in non-filtered, but freshly prepared ACW made up from chemicals of analytical grade quality. Colloid concentrations in ACW could be reduced by about two orders of magnitude by filtering the solution through 100 nm Criticap-M™ filters. Additional tests were carried out with a tangential filtration device and a benchtop hollow filter system (ultrafiltration technique) with the aim to further reduce colloidal impurities. However, a reduction of the concentrations of colloidal impurities to levels significantly below the ones given in Table 9 was not achieved even with improved filtration techniques.

The preliminary tests show that filtration of the alkaline solutions was important to attain a reduction in the concentration of colloidal impurities in laboratory systems to analytically acceptable levels of about 10^{8} coll L^{-1} to 10^{9} coll L^{-1}. The tests further indicate that colloid concentrations below 10^{7} coll L^{-1} are difficult to achieve and, consequently, to quantify accurately in laboratory systems.

The problem of background colloidal levels was further checked in reference systems that contained 800 mL ACW stored in Teflon bottles. They were treated according to the experimental procedure outlined for the mortar- and quartz-containing systems. In these systems, the concentrations of colloidal impurities were found to be constant with time in the range 1×10^{8} coll L^{-1} to

5×10^{8} coll L^{-1}. Note that the values fall within the range of levels observed in freshly prepared and filtered alkaline solutions (Table 9).

5.3 Results and Discussion

5.3.1 Time Dependence of Colloid Concentrations

The results obtained for the experimental systems listed in Table 8 are shown in Figs. 9 - 11. Irrespective of the experimental set-up, the general behaviour of the colloidal suspensions is similar which allows us to discuss the results together. In Figs. 9 - 11, colloid concentrations in solution are displayed as a function of the contact time between the backfill material and the fluid.

Reproducibility of the experimental protocol was tested by conducting a few experiments in duplicates, e.g., the experiments mortar M1 in contact with ACW (Fig. 10). In general, reproducibility of the results was good within the uncertainty range of the method. The results show the presence of colloids in the hyper-alkaline fluids, which were either released during the initial contact of quartz or mortar M1 grains, respectively, with the fluids or formed subsequently as secondary CSH-type colloidal material.

In keeping with the sampling protocol, three distinct concentration levels appear in the plots: Colloid concentrations measured after end-over-end mixing of the batch systems (open circles) as well as after a 24 h or longer standing of the samples (filled circles). Mean values are indicated in the plots in cases where constant concentrations with time are anticipated given the experimental uncertainties on the data. In a few experiments, the colloid concentrations tended to increase with time, and the concentrations indicated in the plots (arrows) represent maximum colloid concentrations measured in solution before changing the experimental protocol.

The total colloid concentrations measured after end-over-end mixing of the batch systems range from about 6.7×10^{10} coll L^{-1} (Fig. 9 a) to about 3.4×10^{11} coll L^{-1} (Fig. 11 a). The data indicate total colloid concentrations in the well-mixed systems with size ≥ 100 nm and, therefore, includes particles larger than 1000 nm. After a standing time of 24 h, colloid concentrations typically ranged from about 1.8×10^{9} coll L^{-1} (Fig. 9 a) to about 6.2×10^{10} coll L^{-1} (Fig. 11 b). Therefore, leaving the batch systems undisturbed for 24 h, which allows

particles larger than 1000 nm to be depleted from the sampling volume, lowers the colloid concentration level between a factor of about 3 and about 70.

Note the fluctuations in the colloid concentrations measured after 24 h during the initial phase of a few experiments (e.g., Fig. 10 b). The fluctuations may be due to experimental artefacts (e.g., increased colloid concentrations resulting from the disintegration of larger aggregates into sub-micron colloids during the end-over-end mixing of the samples) or due to changes in the colloid stability. However, there is no conclusive explanation for the large scatter in the data.

In the last stage of the investigations, periodic end-over-end mixing of the batch systems was stopped, and sampling of the undisturbed systems was extended over a time period of up to 200 days. This last stage started after the samples had been mixed end-over-end over a time period of 180 days (Fig. 10a), 200 days (Figs. 11 a/b), 220 days (Figs. 9 a/b) and 330 days (Figs. 10 b). The colloid concentrations measured in the last stage of the experiments correspond to the lowest concentration levels given in Figs. 9 - 11. The plots show that, in the undisturbed systems where the batch systems had stood for 10 days and longer, colloid concentrations were at least two orders of magnitude lower than in the completely mixed systems. Irrespective of the solutions in contact with quartz and mortar M1 grains, leaving the systems undisturbed significantly reduced the colloid concentration to levels of ~2×10^{8} coll L^{-1} to ~8×10^{8} coll L^{-1}. These concentrations are close to the background colloidal levels determined for the systems. It will be shown that the low colloid concentrations are the consequence of removal by a process controlled by colloid-colloid interactions (see section 5.3.3).

5.3.2 The Effect of Isosaccharinic Acid (ISA)

The effect of isosaccharinic acid (ISA) on the stability of colloidal suspensions was investigated for quartz and mortar M1 immersed in ACW (Figs. 11 a/b). ISA is the main degradation product of cellulose under alkaline conditions (VAN LOON & GLAUS 1998).

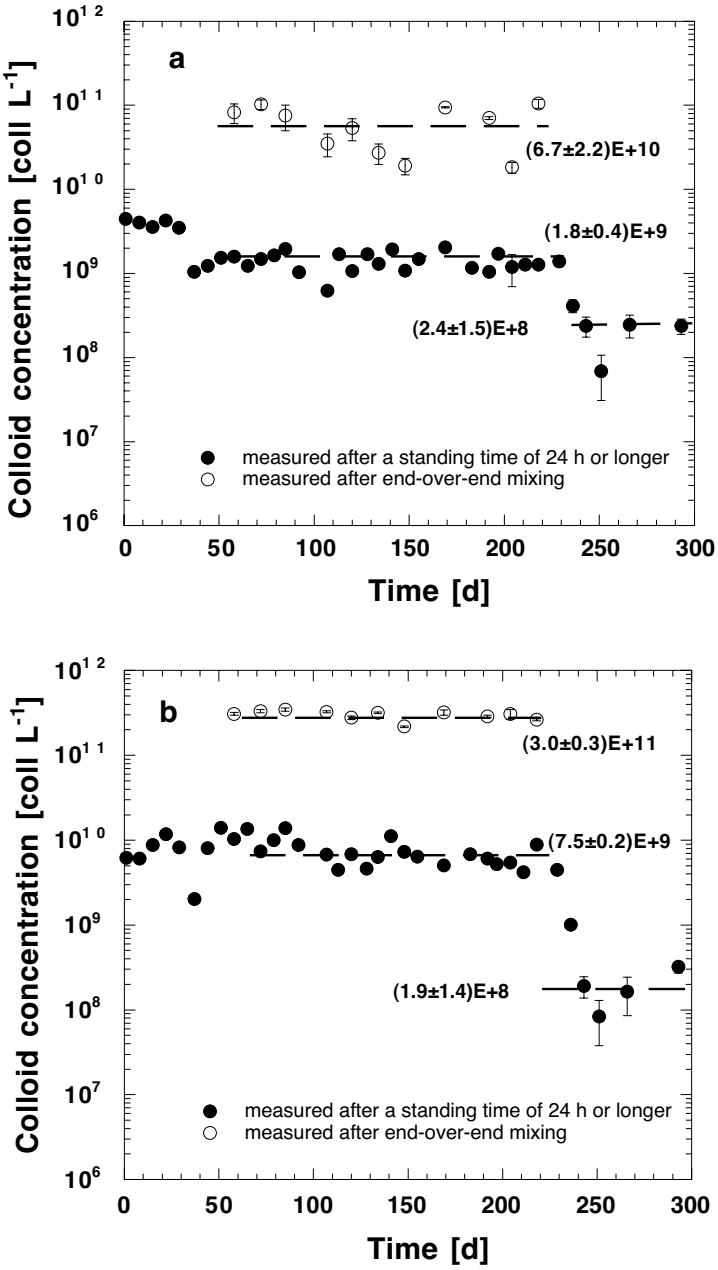

Fig. 9: Colloid concentrations in the systems a) Quartz in ACW (pH=13.3) and b) Quartz in 0.11 M NaOH/0.18 M KOH solution (pH=13.3). Colloid concentrations were determined in samples taken immediately after end-over-end mixing (open symbols) and after a 24 h standing of the samples (filled symbols). After 220 days, mixing was stopped leading to longer than 24 h standing time.

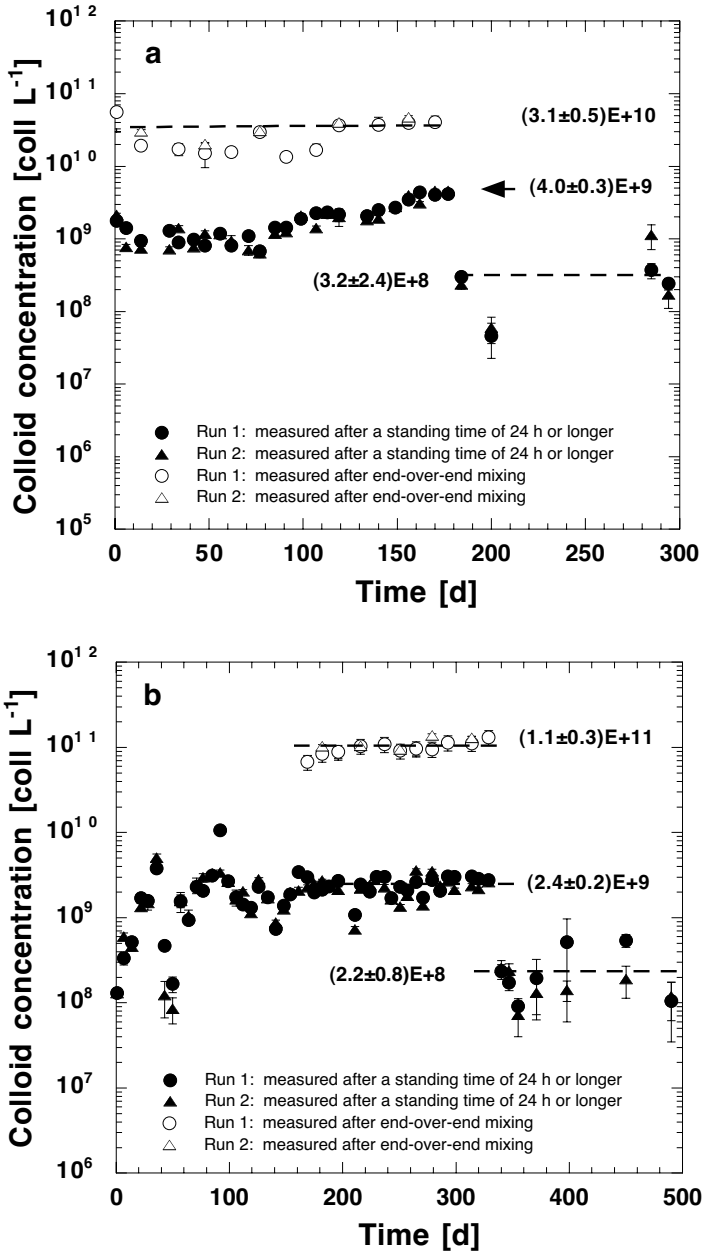

Fig. 10: Colloid concentrations in systems containing mortar M1 in contact with ACW (pH=13.3). The data given in a) and b) correspond to identical systems. The experiments were carried out in duplicates (run 1 and 2). Colloid concentrations were determined in samples taken immediately after end-over-end mixing (open symbols) and after a 24 h standing of the samples (filled symbols). After 320 days, mixing was stopped leading to longer than 24 h standing time.

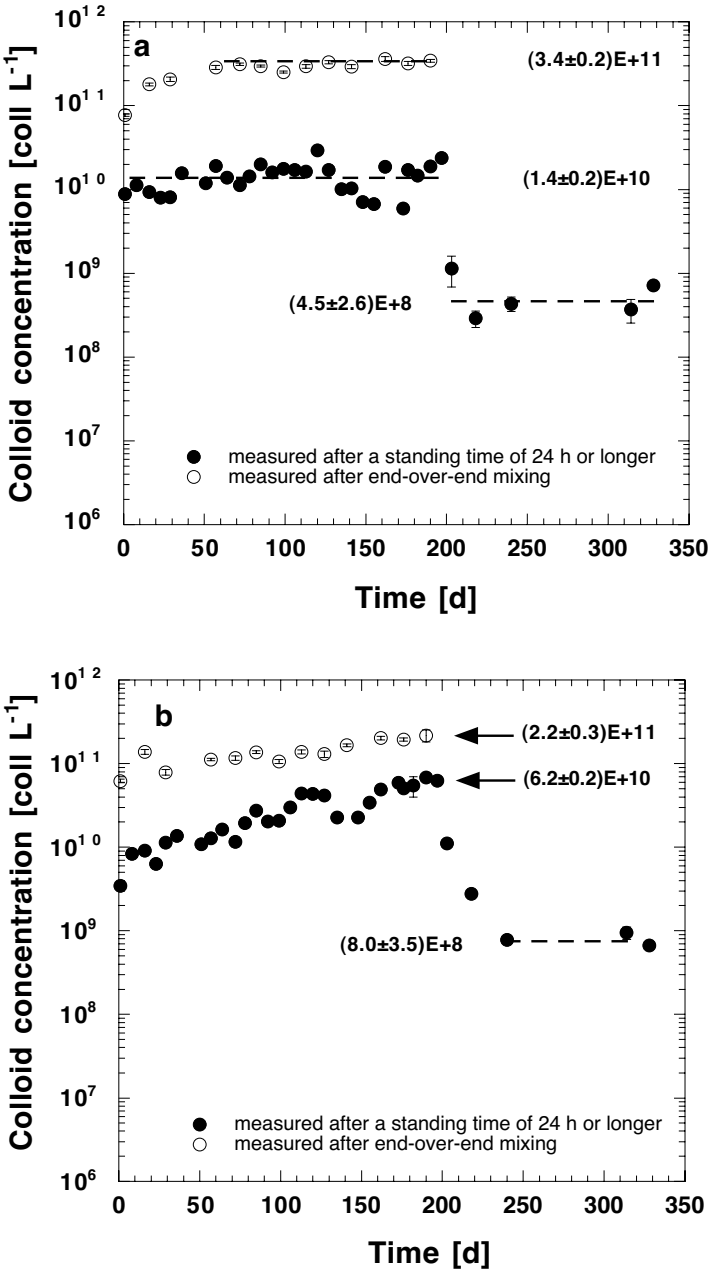

Fig. 11: Colloid concentrations in the systems a) Quartz/ACW/ISA ($[ISA]_{tot}$= 5×10^{-3} M; pH=13.3), and b) mortar M1/ACW/ISA ($[ISA]_{tot}$ = 5×10^{-3} M; pH=13.3). Colloid concentrations were determined in samples taken immediately after end-over-end mixing (open symbols) and after a 24 h standing of the samples (filled symbols). After 200 days, mixing was stopped leading to longer than 24 h standing time.

It was observed that ISA strongly sorbs on cement and C(A)SH phases in alkaline solutions (VAN LOON & GLAUS 1997). Assuming a Langmuir type of isotherm for ISA sorption on cement as reported by VAN LOON & GLAUS (1997), the equilibrium ISA concentration for the mortar M1 containing systems was estimated to be 4.2×10^{-3} M (cement: water ratio = 8.6×10^{-3} kg L^{-1}, $[ISA]_{tot}$ = 5×10^{-3} M). No measurements of ISA sorption on quartz are available.

In the quartz/ACW/ISA system the colloid concentrations were determined to be $(3.4\pm0.2)\times10^{11}$ coll L^{-1} after end-over-end mixing, $(1.4\pm0.2)\times10^{10}$ coll L^{-1} after standing for 24 h and $(4.5\pm2.6)\times10^{8}$ coll L^{-1} for the undisturbed batch system (Fig. 11 a). In the mortar/ACW/ISA system (Fig. 11 b) the corresponding concentrations were found to be $(2.2\pm0.3)\times10^{11}$ coll L^{-1}, $(6.2\pm0.2)\times10^{10}$ coll L^{-1} and $(8.0\pm3.5)\times10^{8}$ coll L^{-1} (Fig. 11b).

Note that colloid concentrations agree within the experimental errors in the undisturbed quartz and mortar M1 containing systems. However, the time required to reach the final colloid concentration is affected by the presence of ISA as indicated by the slightly enhanced colloid concentration in the mortar M1 system after a standing time of 24 h. In addition, the results show that the long-term colloid concentration levels are comparable in ISA free and ISA containing solutions for both quartz/ACW and mortar M1/ACW systems (compare Figs. 9a and 10 a/b with Figs. 11 a/b). Thus, it is concluded that the presence of ISA exerts no significant effect on the long-term stabilisation of the backfill-derived colloids.

5.3.3 Colloid Generation and Colloid Stability

The distribution of particles in a system is governed by a sequence of processes, which control production and removal of colloids (e.g., FILELLA & BUFFLE 1993; DEGUELDRE 1994). The time dependence of the number concentration ($n_k = N_k/\Delta ø_k$) of a colloid size class k (size range ø to ø + dø) depends on contributions from generation (P) and removal (R) processes and can be written as:

$$\frac{V dn_k}{dt} = P_E + P_F + P_D - R_C - R_S - R_A \qquad [\text{coll d}^{-1}]. \qquad (38)$$

V is the volume of the system. P denotes production rates, 1) due to erosion of colloidal material from the bulk material (E), 2) due to chemical formation (nucleation/precipitation) (F), and 3) due to disaggregation of larger colloids or suspended particles to form colloids of size class k (D). R denotes removal rates, 1) due to coagulation (C) of colloids of the size class i to form larger colloids, 2) due to sedimentation of colloids (S), and 3) due to attachment of colloids to the bulk material (A). The rates can be assessed according to their relevance.

For the batch systems investigated in this study, the total colloid concentrations at the beginning of the experiments lie in the range ~10^{10} coll L^{-1} to ~10^{12} coll L^{1} (Figs. 9 - 11). Initial concentrations may be due to instantaneous formation of secondary colloids or due to detachment of colloids from the bulk surface during the initial contact of the solids with the fluid. We suspect that release of colloids attached to the surface of the bulk material accounts for the initial colloid inventory. However, colloid generation due to erosion can be excluded as an important process in the subsequent phases of the experiments (P_E ~ 0).

In principle, end-over-end mixing of the batch systems may contribute to colloid production due to disaggregation of large aggregates to give colloids of size class k (P_D). Note however that if disaggregation was an input term for colloids of size class k, the contribution would be constant as mixing was repeated regularly prior to colloid analysis (P_D ~ constant). To some extent, disaggregation of colloids may account for the scatter in the data as observed in the mortar M1/ACW system (Fig. 10 b).

The formation of secondary CSH-type colloidal material is considered to be an input term for k- size colloids (P_F). The results indicate that the total colloid concentrations were either constant (Fig. 9 a/b and Fig. 11 a) or slightly increasing with time (Fig. 10 a/b and Fig. 11 b). Mass balance calculations for the colloidal material allow us to estimate the total number of colloids generated in the batch systems. The calculations are based on measured colloid concentrations and the aliquot volumes exchanged, that is, 5 mL aliquot for the determination of the colloid concentration after end-over-end mixing and 60 mL aliquot for colloid analysis after standing for 24 h or longer of the samples. Mass balance calculations showed that the rates expressed in terms of number of colloids

generated per gram of bulk material were small for all systems (rate < 10^7 colloids g^{-1} d^{-1}; WIELAND 1997).

An important finding from these studies is that, on a long time scale, i.e., after a standing time of 10 days or longer, no measurable differences in the colloid concentrations appear irrespective of the initial colloid concentrations, the bulk materials involved or the presence or absence of ISA. In addition, it was found that the colloid concentrations in the systems after standing for 24 h are constant except for one batch (mortar M1/ACW/ISA). These findings can be explained taking into account the chemical composition of ACW, i.e., the high ionic strength and Ca concentrations in the mmolar range. Ionic strength and Ca concentration are the main parameters affecting colloid inventories in cement systems. The results imply that colloid removal rather than colloid production processes control the concentration of colloids dispersed in solution. Attachment of colloids on the bulk material (R_A), sedimentation (R_S) or a coagulation process (R_C) controls colloid removal. Due to the small surface area of the quartz and mortar M1 grains (7.8 cm^2 g^{-1}), colloid removal caused by the interaction with quartz and mortar M1 grains (filtration), however, is assumed to be negligibly small ($R_A \sim 0$) in the batch-type systems.

The influence of sedimentation (R_S) and coagulation (R_C) on colloid inventories was further elaborated. Some of the data displayed in Figs. 9 a/b, Figs. 10 a/b and Figs. 11 a/b were used to demonstrate changes in the colloid concentrations on the short time scale, i.e., a period of up to 40 days. The experimental data shown in Fig. 12 represent time-dependent colloid concentrations in solution, i.e., C(t) normalised to the initial colloid concentrations determined for the respective systems after complete mixing (C_0). The colloid concentrations C_0 and C(t) correspond to measurements made in the last stage of the flocculation studies, when the batch systems were completely mixed for the last time and left standing for up to 150 days. As shown in Figs. 9 - 11, this setting led to a sharp decrease in the concentration levels within less than 40 days. The data collected in this phase of the study were used to construct Fig. 12.

Fig. 12 shows that, for all experimental systems, colloid removal was enhanced compared to a situation only controlled by sedimentation. The solid line indicates predicted changes in the colloid concentrations with time if sedimentation was the only controlling removal process. The prediction is based, 1) on

measurements of the colloid size distribution in the samples taken after 24 h (size distribution approximated by the power law), and 2) on the assumption that Stokes law (Eq. 15) can be applied to describe time-dependent changes in the colloid concentrations of a given size class in the undisturbed systems. Thus, the solid line corresponds to sedimentation of a colloid population with an initial size distribution corresponding to the measured size distribution after 24 h standing of the samples. Note that Stokes law was applied successfully to describe the removal of particles ≥ 1 µm in the initial phase (t ≤ 24 h) of the experiments (Fig. 8). These predictions are not shown in Fig. 12 due to the different time scales involved.

Fig. 12 shows that if sedimentation were the only rate-controlling process in the long term, the colloid inventories would decrease steadily with time controlled by slow sedimentation of colloids with diameter below 1000 nm. Note that the settling time is significantly prolonged with decreasing colloid size according to the settling velocity, which decreases proportional to the square of the particle diameter (Eq. 15). Therefore, changes in the colloid inventory cannot be explained solely by sedimentation for a longer standing of the samples. However, the results displayed in Fig. 12 can be explained based on a coupled coagulation-sedimentation process: coagulation of small colloids promotes the formation of larger aggregates, which are then depleted from solution by sedimentation. The overall decrease in the colloid inventories can tentatively be quantified in terms of a first-order reaction (STEINFELD et al. 1989).

For the ISA free system, the half-life of the colloid population, i.e., the time required to reduce the colloid inventory to one half of its initial value, was estimated to be about 120±15 h. This value is consistent with half-lives calculated for monodispersed suspensions of spherical particles and similar initial colloid concentrations ($C = 0.2 \times 10^{13}$ coll m^{-3}), i.e., $t_{1/2} = 230$ h for $\alpha = 0.1$ and $t_{1/2} = 23$ h for $\alpha = 1$ (Table 5).

It should be noted that the experimentally determined value corresponds to the half-life of a colloid population with multimodal size distribution, whereas the calculated value accounts for the coagulation time of a colloid population with monodisperse size distribution. However, a comparison of the half-lives is justified if the following features of colloid populations are taken into account: 1) Eq. (13) allows us to reasonably approximate the coagulation time of colloid

populations, which differ in size by a factor of about 2 or less. It shows that the half-lives of monodispersed suspensions do not depend on size, but are inversely proportional to α and C_0. Thus, the initial number concentration is important, not the size. 2) For multimodal size distributions described by the parameters logA and -b given in Table 10, the number concentration of colloids markedly increases with decreasing size. For example, for the systems under consideration, an order of magnitude difference in size corresponds to a difference in the concentration by a factor of about 5 to 10. Therefore, the probability of the small colloids to interact with colloids of equal (or similar) size is greater than the probability of an interaction with colloids of markedly different size. Thus, on the assumption that the coagulation process is dominated by colloids of equal (or similar) size, the coagulation time estimated for monodispersed suspensions can be taken as a first approximation of the characteristic reaction times of multimodal suspensions.

Coagulation was retarded in the mortar M1/ISA system. No retardation was observed in the quartz/ISA system compared to the ISA free set-up. The final colloid concentration of $(8.0\pm3.5)\times10^8$ coll L^{-1} was reached within a period of about 40 days in the mortar M1/ISA system. The corresponding half-life of the colloid population was estimated to be 170±30 h. Thus, the specific interaction of ISA with the surface of cement-derived colloids tends to slightly retard coagulation as indicated by the longer half-life of the colloid population. However, the study shows clearly that the effect of ISA on colloid stability is too small to significantly affect the colloid inventory in the long term. We thus conclude that the presence of ISA should exert no adverse effect on the colloid inventory of a cementitious near-field.

The results of this study show that, in the long term and for the situation in which attachment to the backfill mortar is negligible, coagulation is an important process controlling the colloid inventory in CPW. The strongly alkaline solutions used in this study show an ionic strength of about 0.3 M. Ca concentrations range from 3×10^{-4} M in the quartz/NaOH/KOH system to 2×10^{-3} M in ACW containing systems. Thus, the flocculation experiments were carried out with fluids of the same ionic strength but different Ca concentrations.

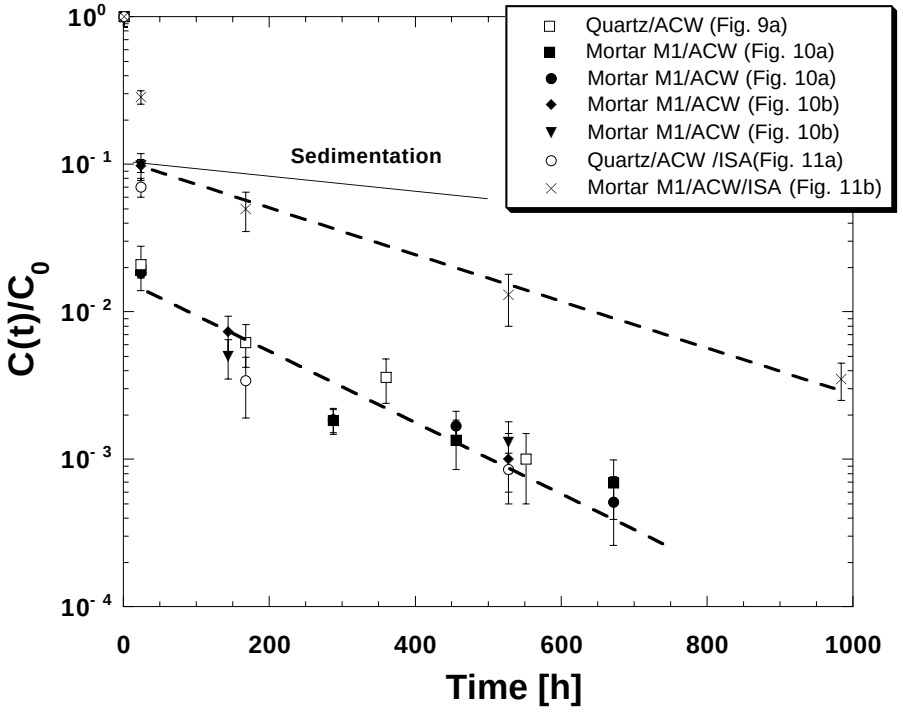

Fig. 12: Colloid stability in ACW solutions. Experimental data show changes in the normalised colloid concentrations with time (broken lines are drawn to guide the eye). C_0 denotes the initial colloid concentration, i.e., the total colloid concentration in the mixed systems. C(t) denotes colloid concentrations measured in the undisturbed systems as a function of time. The solid line indicates removal due to sedimentation predicted based on Stokes law.

Fig. 12 shows that, despite an order of magnitude difference in the Ca concentrations of the various systems, normalised colloid concentrations agree well within the uncertainties of the data. Thus, Ca exhibits no significant effect on colloid stability at high ionic strength indicating that ionic strength rather than the Ca concentration is the controlling parameter under CPW conditions. The high ionic strength causes a compression of the electric double layer at the colloid surface. As a consequence, attractive forces exceed electrostatic repulsion, which leads to a destabilisation of the colloid suspensions.

5.3.4 Size Distributions and Colloid Mass Concentrations

The colloid mass was deduced from measured colloid concentrations applying the power-law approach. The colloid mass concentration was obtained by multiplying the total volume of the colloid population with the particle density (ρ = 2 g cm^{-3} for cement-derived colloids). The total volume of a colloid population was estimated with Eq. (33). Thus, determination of the empirical parameters (intercept logA and slope -b) of size distributions was required prior to calculating total volumes.

The empirical parameters of the size distributions were determined for the samples taken immediately after end-over-end mixing (open circles in Figs. 9 -11) and after a standing of the samples for 24 h (filled circles in Figs. 9 - 11). The parameters could not be determined for the samples taken after extending the standing time (t > 24 h). In this case the colloid concentrations determined in the systems were comparable to the background colloid concentrations. The very low colloid concentrations led to large uncertainties in the measured size distributions, which did not allow well-constraint Pareto parameters to be deduced.

Slope (-b) characterises the particle size spectrum. It ranges from about -2.3 to about -3.1 for the colloid populations generated under the given experimental conditions (Table 10). Slopes (-b) of the particle size distributions range from about -2.3 to about -2.6 after a standing of 24 h. According to FRIEDLANDER (1960), a value of -2.5 is characteristic for a size spectrum dominated by coagulation. Note that, in general, the size spectra of the completely mixed systems tend to be steeper than those after 24 h standing (note the range of uncertainties given in Table 10). A shift of slope (-b) to more negative values indicates a shift of the size spectrum towards smaller colloids.

The total volume of a colloid population was calculated with Eq. (33) for appropriate size ranges. For the completely mixed systems, the limits were assumed to be $ø_1$ = 1 nm and $ø_2$ = 1500 nm. The upper limit is set arbitrarily but accounts for rapid sedimentation of particles with diameter > 1500 nm. For the samples taken after a standing of 24 h, the limits are given by the experimental protocol ($ø_1$= 1 nm and $ø_2$ = 1000 nm). The cumulative volume of the colloids at the lowest concentration level (undisturbed systems) was estimated based on the colloid volume calculated for the samples taken after a standing of 24 h.

The colloid volumes of the two series were assumed to be proportional to their number concentrations.

Average, minimum and maximum colloid mass concentrations are given in Table 11. Uncertainties in the colloid mass concentrations are caused by uncertainties on the parameters logA and -b (Table 10). The colloid mass concentrations of the samples taken from the mixed systems range from 1 mg L^{-1} to 19 mg L^{-1} (averaged value). The colloid mass concentration was significantly reduced after the large particles had been depleted from solution. The mass concentrations decreased to less than about 1 mg L^{-1} (range 52 µg L^{-1} to 1100 µg L^{-1}) after the samples have stood for 24 h. Leaving the batch systems undisturbed for more than 24 h further reduced colloid inventories and, consequently, mass concentrations.

Table 10: Power-law parameters logA and slope (-b) for the systems listed in Table 8 (Resultant number concentrations in coll mL^{-1}).

Experiment	Mixed system		24 h Standing time	
	slope (-b)	logA	slope (-b)	logA
Q/ACW (Fig. 9 a)	-(2.76±0.21)	11.52±0.55	-(2.50±0.07)	9.35±0.18
Q/NaOH/KOH (Fig. 9 b)	-(2.50±0.08)	11.68±0.21	-(2.30±0.08)	9.61±0.20
M1/ACW (Run 1 Fig. 10 a)	-(2.83±0.16)	11.35±0.41	-(2.53±0.13)	9.67±0.33
M1/ACW (Run 2 Fig. 10 a)	-(2.88±0.16)	11.52±0.41	-(2.63±0.14)	9.73±0.35
M1/ACW (Run 1 Fig. 10 b)	-(3.05±0.10)	12.46±0.25	-(2.45±0.20)	9.33±0.53
M1/ACW (Run 2 Fig. 10 b)	-(3.02±0.11)	12.43±0.28	-(2.53±0.09)	9.65±0.23
Q/ACW/ISA (Fig. 11 a)	-(2.63±0.08)	12.01±0.20	-(2.30±0.09)	9.93±0.22
M1/ACW/ISA (Fig. 11 b)	-(2.63±0.11)	11.66±0.27	-(2.48±0.11)	10.64±0.27

Table 11: Colloid mass concentrations (average (Av), minimum (Min) and maximum (Max) values).

Experiment	Mixed system [mg L^{-1}]			24 h Standing [µg L^{-1}]			Standing t > 24 h [µg L^{-1}]		
	Av	Min	Max	Av	Min	Max	Av	Min	Max
Q/ACW	2	0.2	34	52	22	120	5	2	13
Q/(Na,K)OH	19	7	54	310	120	830	8	3	21
M1/ACW	1	0.2	8	82	16	400	5	1	22
M1/ACW	1	0.2	8	54	11	280	4	1	22
M1/ACW	3	1	9	62	6	790	6	1	71
M1/ACW	4	1	14	85	32	240	7	3	23
Q/ACW/ISA	18	6	47	650	230	1940	20	7	62
M1/ACW/ISA	8	2	30	1100	360	4050	14	5	52

For the undisturbed systems, colloid mass concentrations are estimated to be in the range of a few micrograms per litre (range 4 - 20 µg L^{-1}). Note that mass concentrations were slightly enhanced in the presence of ISA (Table 11). The results show that the mass concentrations of cement-derived colloids are typically lower than 20 µg L^{-1} (= 0.02 ppm) in the undisturbed batch systems. The upper bound is estimated to be 100 µg L^{-1} (= 0.1 ppm) taking into account the uncertainties on the data. These values are considered to be representative for stagnant water flow conditions in the backfill mortar and, thus, relevant under repository conditions in the long term.

5.4 SUMMARY

Colloid concentrations were measured in batch systems with backfill mortar M1 (cementitious backfill of the L/ILW repository) or quartz (potential aggregate material of the backfill) in contact with ACW or alkaline solutions (0.114 M NaOH/0.18 M KOH). The laboratory systems are considered to address conditions encountered in the cementitious backfill of a repository during the first stage of the cement degradation.

Time dependence of the colloid concentrations, the effect of colloid removal as well as the effect of ISA on colloid concentrations was investigated. ISA is the

most important degradation product formed during the alkaline degradation of cellulose material.

Three colloid concentration levels were distinguished in the flocculation studies:

1) The total colloid concentration measured after end-over-end mixing of the batch-type systems: This is a measure of the total number of colloids present in the systems with size ≥ 100 nm. Colloid concentrations range from about 0.7×10^{11} coll L^{-1} to about 3×10^{11} coll L^{-1}. The main contribution to the total colloid inventory in solution is caused by a rapid release of colloids in the initial phase of the experiments. It is believed that the colloids were attached to the surface of the bulk material. The generation of colloids due to in-situ formation of CSH-type phases was slow. Colloid production rates are estimated to be below 10^7 coll d^{-1} per gram of solid. Note that the rates are hardly representative for field conditions due to the large contribution of quartz surface exposed to solution in the laboratory systems.

2) The colloid concentration measured after leaving the batch-type systems undisturbed for 24 h: One day is the time required for colloids ≥ 1000 nm to settle in the batch-type systems. The colloid concentrations measured after a standing time of 24 h correspond to the number of colloids with diameters ranging from 100 nm to 1000 nm. Leaving the batch undisturbed for 24 h reduces the colloid inventories by a factor between 3 and 70. Colloid concentrations typically range from about 1.5×10^9 coll L^{-1} to about 8.5×10^9 coll L^{-1}. In the ISA containing quartz/ACW and mortar M1/ACW systems, the concentrations were slightly enhanced, i.e., $(1.4\pm0.2)\times10^{10}$ coll L^{-1} and $(6.2\pm0.2)\times10^{10}$ coll L^{-1}, respectively. The higher colloid concentrations in solutions found in the presence of ISA are due to ISA sorption onto the colloidal material, which exhibits a retarding effect on colloid removal.

3) Colloid concentration measured after leaving the batch systems undisturbed for more than 24 h. The colloid concentrations determined in the undisturbed batch-type systems are considered to be a measure for the number of colloids suspended in CPW in the long term. Thus, they are believed to represent the long-term colloid inventory in the backfill mortar M1. The concentrations range from about 2.0×10^8 coll L^{-1} to about 5×10^8 coll L^{-1}. The colloid concentrations are

extremely low and, actually, within the range of the background colloid concentrations determined for the experimental systems.

Conversion of colloid number concentrations into mass concentrations is based on the evaluation of volume distributions. The mass concentrations of colloids in samples taken from completely mixed systems range from about 1 mg L^{-1} to about 19 mg L^{-1} (average values). Leaving the systems undisturbed for 24 h reduces the colloid mass to a level between about 50 µg L^{-1} and 1100 µg L^{-1} (average values). Colloid mass concentrations are further reduced leaving the systems undisturbed for more than 24 h, resulting in a concentration level of a few micrograms per L^{-1} (range 4 µg L^{-1} to 20 µg L^{-1}). The lowest colloid concentrations are considered to be representative for stagnant water flow conditions in the backfill mortar and, thus, relevant under repository conditions in the long term.

We infer that a coagulation-sedimentation process controls colloid removal in the batch-type flocculation studies. Coagulation promotes the formation of larger aggregates, which are depleted from solution by sedimentation. The kinetics of the removal process is fast, and long-term colloid concentrations are established within about 20 days. Colloid removal is slightly retarded in ISA containing systems, and the time required to reach the background colloid concentration is extended to about 40 days.

The specific features of the mortar M1, i.e., high porosity and the large pores of the macrostructure (pore size ranging from 1 mm to 5 mm) allow, in principle, colloids to be dispersed in the pore water of the backfill material. The coupling of coagulation/sedimentation, however, is expected to cause a reduction in the colloid inventory of the pore water mainly at high initial colloid concentrations. However, we cannot preclude that colloid removal due to attachment may also occur in the backfill. Thus, the colloid number and mass concentrations determined in the flocculation studies are expected to represent upper limits of the actual colloid concentrations in stagnant pore water of the backfill mortar M1.

6 COLLOID INVENTORY OF AN "EVOLVED" SYSTEM

The flocculation studies reported in the previous chapter were conducted to assess colloid concentrations for cementitious systems, which are preserved in the initial stage of the cement degradation. High alkali concentrations are characteristic during the stage I of cement degradation ($[Na]_{tot}$ ~0.11 M, $[K]_{tot}$ ~0.18 M, $[Ca]_{tot}$ ~1.2×10^{-3} M, pH ~13.3, I ~0.3 M). The chemical conditions established under strongly alkaline conditions can be termed favourable with regards to colloidal stability. Progressive ageing of the cementitious material due to interaction with infiltrating groundwater occurs in a repository environment. This process causes the release of Na and K from the cement matrix. Tentative predictions can be made regarding the colloid inventories in pore waters in stage II of the cement degradation. In this stage Na and K concentrations are significantly lower than in stage I (BERNER 1992; NEALL 1994). The composition of the CPW, i.e., namely pH and Ca concentration, is controlled by the solubility of portlandite ($[Ca]_{tot}$ ~20×10^{-3} M, I ~0.07 M). A comparison of the chemical conditions of the two subsequent stages reveals a reduction in the ionic strength by a factor of 4 in stage II but an increase in the Ca concentration by one order of magnitude. Thus, the following counter-effect on colloidal stability is envisaged to be operative: Decreasing ionic strength tends to stabilise colloids in solution, whereas an increase in the Ca concentration enhances the collision efficiency of particle-particle interactions. Therefore, due to this counteracting effect on colloid stability, chemical conditions are also expected to be favourable for colloid removal in stage II of the cement degradation.

This chapter reports colloid concentration measurements in an evolved backfill mortar system (stage II of cement degradation). The study was carried out within the frame of the COLEX project. COLEX (COLumn EXperiments) was a large-scale flow experiment with the goal of studying coupled gas and water transport processes in the backfill mortar M1 (MAYER et al. 1998). Colloid concentration measurements were performed on a few pore water samples. Sampling occurred before and after migration experiments with NaCl, uranine and ^{3}He tracers (phase II of COLEX project; MAYER 1998).

6.1 Set-Up of COLEX

A schematic view of the experimental set-up is given in Fig. 13. The column was made of two elements each of which were filled with mortar M1 (total length = 2.69 m, inner diameter = 0.274 m, total volume = 158.8 L). Average bulk density and porosity of the filling as well as porosity of HCP and the mortar structure were given in section 2.1.2. During operation, a constant flow of 10 mL min^{-1} of pre-conditioned CPW was maintained using a peristaltic pump. The injected cement water was prepared by mixing tap water with Portland cement (water/cement ratio = 20). We infer that the pore water volume of each element was replaced after about 36 h based on a pore volume of 21.4 L (porosity = 27 %) and the flow rate given above. Each steel tube was equipped with four drill-holes, which were used to connect pressure and water saturation sensors. Pore water samples were collected through the top and bottom drill-holes. The inlet was connected at the bottom of the column inducing a bottom-up water flow.

In the first phase of the COLEX project, the columns had been used for gas transport studies (MAYER et al. 1998). In these experiments, the column was prepared by filling the pore volume of the mortar M1 with tap (drinking) water, which implicitly induced cement degradation (Na and K release from HCP into the pore water). A comparison of the free water porosity of HCP (~8 %) and the macro-porosity (~19 %) indicates that each filling of the column with tap water was equivalent to approximately 2 to 3 water exchange cycles in HCP. Since the column was completely refilled with tap water at least 3 times, which is equivalent to about 6 to 9 pore water exchanges, it is likely that HCP was already degraded to stage II at the end of the preparation phase.

In the second phase of the COLEX project, tracer migration studies were performed (MAYER 1998). Prior to migration studies, the mortar material was treated for 10 days as follows: The mortar M1 material was contacted with pre-conditioned cement water (w/c = 20). The cement water was pumped through the column and back into the reservoir in a closed cycle (flow rate of about 0.5 L min^{-1}). Note that the colloid concentrations of the so prepared CPW were found to be close to the analytical detection limit (< 2 µg L^{-1}).

6.2 Sampling and Colloid Concentration Measurements

Three sampling campaigns were carried out within a time period of three months (week 1, week 4, week 12) and analysed for colloids and the concentrations of cement-derived elements (total of 12 samples). Samples were taken in duplicates through the bottom and the top valves of the column (Fig. 13). The concentrations of Ca, Na and K were determined to be ~2.3×10^{-2} M, ~6×10^{-3} M and ~1.7×10^{-2} M, respectively, indicating that the Ca concentration of the cement water was controlled by portlandite solubility which fixes the pH at 12.5 (Table 12). Therefore, the chemical conditions established in the column during the experiments should be in accordance with a cement system evolved to stage II of the cement degradation. As a consequence of the use of pre-conditioned cement water, chemical equilibrium was maintained during tracer migration studies and, thus, when samples for colloid analyses were taken. In addition, it implies that continuous degradation of the cementitious materials was avoided with this set-up. Note that, within the time period of three months, the total volume of cement water passed through corresponded to about 180 pore volume exchanges.

Fig. 14 represents the power-law size distributions obtained for the first series of measurements. The results of the two other series of measurements (not shown) were consistent with those displayed below.

Table 12: Chemical analysis of the pore water of backfill mortar M1 (number of measurements = 6).

Element	Concentration [M]
Na	$(6.1\pm0.8)\times10^{-3}$
K	$(1.7\pm0.2)\times10^{-2}$
Ca	$(2.3\pm0.3)\times10^{-2}$
S	$(5.1\pm0.3)\times10^{-3}$
Si	$(6.6\pm0.9)\times10^{-6}$
Al	$(2.0\pm0.4)\times10^{-6}$
Mg	$(1.0\pm0.5)\times10^{-5}$

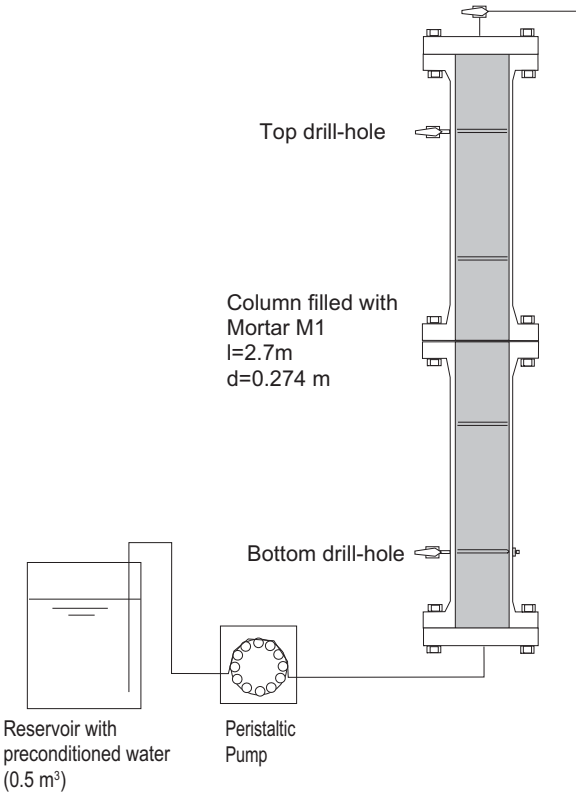

Fig. 13: Schematic view of the experimental set-up for the COLEX project (MAYER et al. 1998).

Fig. 14 shows a continuous increase in the colloid number concentration with decreasing colloid size in the range 50 nm to 5000 nm. The parameters of the power-law size distributions as given by Eq. (28) are summarised in Table 13. The slopes -b of the size distributions range from about -2.6 to -3.7. Slopes were typically in the range -3 to -3.7. Two outliners with slopes -b > -3 are presumably caused by sampling artefacts. Calcite precipitation due to the presence of air in the sample containers may have occurred during sampling, which would explain the shift of the size spectrum towards larger particles.

The finding of a continuous size distribution in the range 50 nm to 5000 nm (Fig. 14) implies the possibility of further extension of the regression line to the size range below 50 nm. Nevertheless, the measurements presented in Fig. 14 provide no unequivocal evidence whether or not an extrapolation of the size distribution to the lower end of the colloidal size spectrum is fully justified.

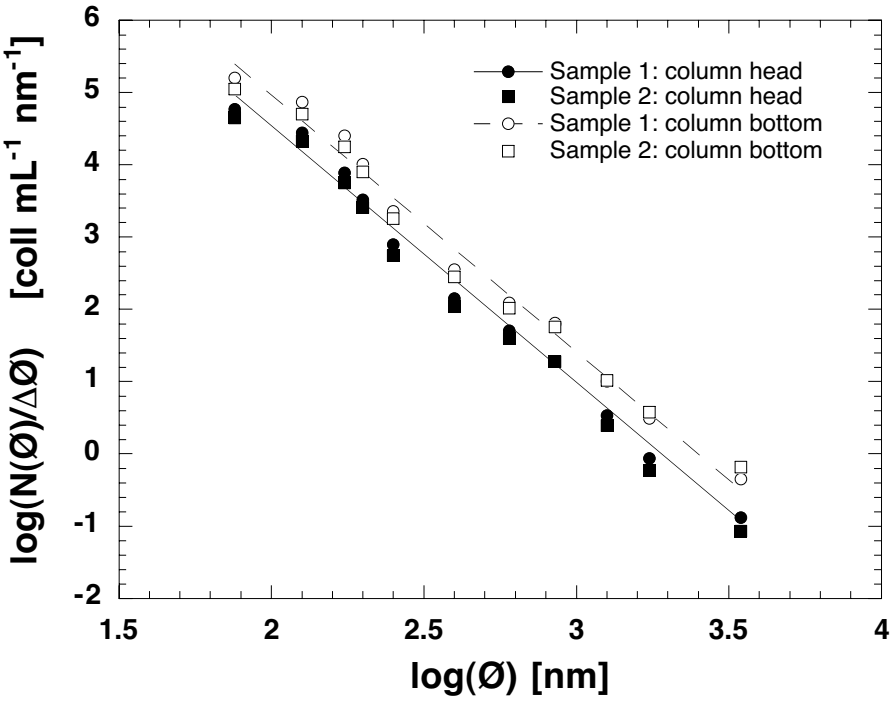

Fig. 14: Colloid size distributions measured in the pore water of mortar backfill. The concentrations of distinct classes ($\Delta N(ø)/\Delta ø$) are shown as a function of size (ø) (range 50 nm to 5000 nm) for the first series of measurements (Sampling 1).

Table 13: Power-law parameters logA and slope (-b) determined for the COLEX samples (Resultant number concentrations in coll mL^{-1}).

Sampling	Column bottom		Column head	
	slope (-b)	logA	slope (-b)	logA
Sampling 1				
Sample 1	-(3.55±0.13)	12.07±0.34	-(3.55±0.16)	11.64±0.43
Sample 2	-(3.35±0.13)	11.49±0.34	-(3.62±0.12)	11.67±0.32
Sampling 2				
Sample 1	-(3.25±0.17)	11.02±0.47	-(2.63±0.14)	9.59±0.38
Sample 2	-(3.43±0.11)	11.11±0.29	-(3.00±0.10)	10.37±0.26
Sampling 3				
Sample 1	-(3.56±0.13)	11.12±0.36	-(3.33±0.08)	10.58±0.21
Sample 2	-(3.70±0.11)	11.33±0.30	-(2.47±0.08)	9.16±0.23

In previous studies it was indicated that colloid concentrations expressed per size class may be constant in the size range below 100 nm in groundwater (e.g., DEGUELDRE 1994). In this study, however, linear extrapolation over the entire size range is considered to allow estimates of maximum colloid concentrations.

6.3 Number, Volume and Mass Concentrations

Colloid concentrations (number, volume and mass concentrations) were estimated based on the assumption that the parameters determined for the size range 50 nm to 5000 nm also hold for the colloid size distribution below 50 nm. In the following, the contributions of the different size ranges are proved by evaluating colloid quantities for both size ranges, i.e., 1 nm to 1000 nm and 50 nm to 1000 nm.

The colloid number concentrations listed in Table 14 were determined with Eq. (26). Uncertainties in the concentrations result from uncertainties on both the intercept and the slope (see Appendix B). Total colloid number concentrations were found to range from about 10^{12} coll L^{-1} to about 5×10^{14} coll L^{-1} for the size range 1 nm to 1000 nm.

Table 14: Colloid number concentrations calculated for the colloidal size ranges 1 nm to 1000 nm and 50 nm to 1000 nm. Definition and use of the uncertainty factor f are given in Appendix B.

Sampling	Column bottom			Column head		
	Coll. conc. [coll L^{-1}] 1-1000	Coll. conc. [coll L^{-1}] 50-1000	f	Coll. conc. [coll L^{-1}] 1-1000	Coll. conc. [coll L^{-1}] 50-1000	f
Sampling 1						
Sample 1	4.6×10^{14}	2.1×10^{10}	2.2	1.7×10^{14}	8.0×10^{9}	2.7
Sample 2	1.3×10^{14}	1.4×10^{10}	2.2	1.8×10^{14}	6.2×10^{9}	2.1
Sampling 2						
Sample 1	4.7×10^{13}	7.0×10^{9}	3.0	2.4×10^{12}	4.0×10^{9}	2.4
Sample 2	5.3×10^{13}	3.9×10^{9}	1.9	1.2×10^{13}	4.7×10^{9}	1.8
Sampling 3						
Sample 1	5.1×10^{13}	2.3×10^{9}	2.3	1.6×10^{13}	1.8×10^{9}	1.7
Sample 2	7.9×10^{13}	2.1×10^{9}	2.0	9.8×10^{11}	3.0×10^{9}	1.7

The concentration of colloids with size range 50 nm to 1000 nm is significantly lower ranging from about 2×10^{9} coll L^{-1} to about 2×10^{10} coll L^{-1}. Thus, the high colloid concentrations deduced for the size range 1 nm to 1000 nm are the consequence of a significant contribution of colloids smaller than 50 nm to the colloid inventory.

Total volumes of the colloid populations were evaluated with Eq. (33) for the two size ranges (Table 15). Size distributions allow us to estimate the contribution of the individual size classes to the total volume of the colloid population. Slope (-b) of a size distribution indicates the trend in the volume distribution. With slope (-b) > -3, the volume contribution increases with increasing colloid size. A size-independent distribution is observed with -b = -3. With -b < -3, the contribution of the small colloids to the total volume of the colloid population increases with decreasing colloid size.

For the COLEX samples, the volume distributions tend to increase with decreasing size corresponding to the slopes of the size distributions (range 3 to -3.7). The results listed in Tables 15 indicate that the contribution of the smaller colloids, i.e., size < 50 nm, to the total volume of colloids is at maximum about 20 %.

Table 15: Colloid volume concentrations calculated for the colloidal size ranges 1 nm to 1000 nm and 50 nm to 1000 nm. Definition and use of the uncertainty factor f are given in Appendix B.

Sampling	Column bottom			Column head		
	Vol. conc. [$cm^3\ L^{-1}$] 1-1000	Vol. conc. [$cm^3\ L^{-1}$] 50-1000	f	Vol. conc. [$cm^3\ L^{-1}$] 1-1000	Vol. conc. [$cm^3\ L^{-1}$] 50-1000	f
Sampling 1						
Sample 1	2.9×10^{-5}	2.3×10^{-5}	2.7	1.1×10^{-5}	8.5×10^{-6}	3.6
Sample 2	2.2×10^{-5}	1.9×10^{-5}	3.1	8.2×10^{-6}	5.9×10^{-6}	2.6
Sampling 2						
Sample 1	1.3×10^{-5}	1.2×10^{-5}	4.3	1.9×10^{-5}	1.9×10^{-5}	3.4
Sample 2	6.0×10^{-6}	5.0×10^{-6}	2.4	1.2×10^{-5}	1.2×10^{-5}	2.3
Sampling 3						
Sample 1	3.1×10^{-6}	2.4×10^{-6}	2.9	3.1×10^{-6}	2.7×10^{-6}	1.9
Sample 2	2.6×10^{-6}	1.8×10^{-6}	2.4	1.9×10^{-5}	1.9×10^{-5}	2.1

As previously outline, the total mass of a colloid population can be estimated based on number and mass distributions (section 4.2). Mass concentrations calculated with Eq.(33), and assuming a density of 2 g cm^{-3} for cementitious colloids, are listed in Table 16 (size ranges 1 nm to 1000 nm and 50 nm to 1000 nm). The mass concentrations calculated from mass distributions (Eq.(35) and Fig. 15) are given in Table 17 (size ranges 1 nm to 1000 nm and 50 nm to 1000 nm). Both ways of calculating the total mass of colloid populations lead to consistent results taking into account the uncertainty factors on the data. Colloid mass concentrations were determined to be in the ppb range (6 to 60 µg L^{-1}). An upper bound on the mass concentration of colloids is estimated to be 100 µg L^{-1}. Note that the mass contribution of the smaller colloids is equivalent to their volume contribution, i.e., their contribution is at maximum about 20 %.

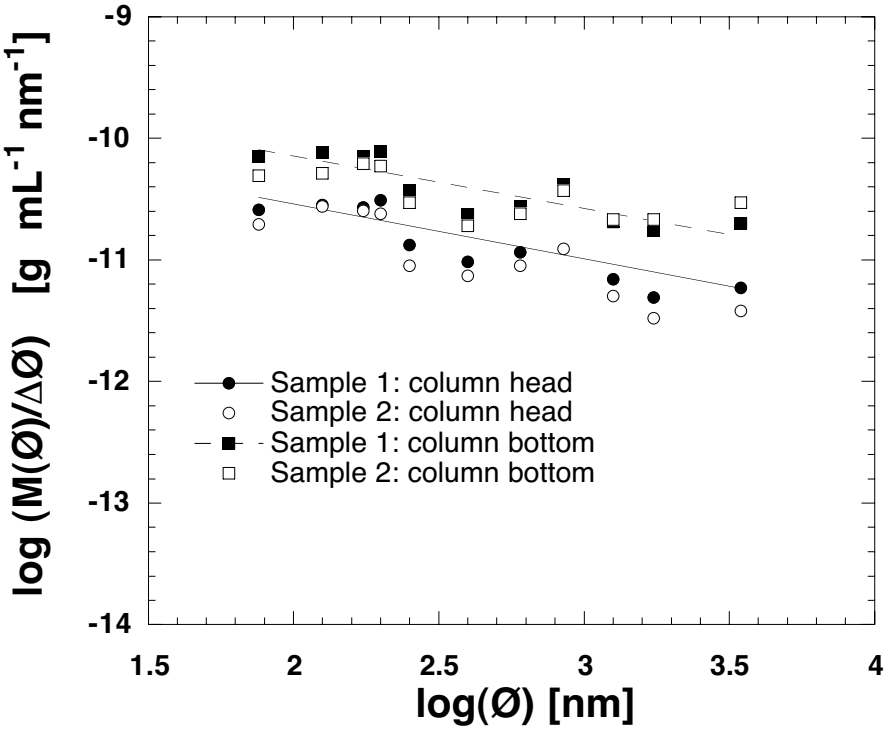

Fig. 15: Colloid mass distributions (Sampling 1). The mass of distinct classes ($\Delta M(ø)/\Delta ø$) are shown as a function of size (ø) (range 50 nm to 5000 nm).

6.4 Specific Surface Area

Size distributions also allow us to assess the contribution of individual size classes to the total surface area of the colloid population. Exponent b of the number distribution indicates the trend in the surface distribution. With -b > -2, the contribution of colloid classes to the surface area of the colloid population increases with colloid size. With -b = -2 an even distribution results, whereas slope -b < -2 indicates an increase in the contribution with decreasing size of the colloids. For the given particle number distributions, the contribution of the colloids to the surface area increases with decreasing size. It indicates the pertinent rôle of the smaller colloids for surface area-dominated processes, e.g., the transport of colloids sorbed on the colloid surfaces. The specific surface areas calculated with Eqs. (36) and (37) are listed in Table 18 (colloidal size range 1 nm to 1000 nm). The values range from 90 $m^2\ g^{-1}$ to 770 $m^2\ g^{-1}$. Low specific surface areas result for those samples with exponent b < 3, that is, for the samples with a relatively flat size distribution and, thus, a relatively high concentration of larger colloids. However, as noted above, contamination of the samples during sampling may explain the outliners. For the other samples, the specific surface areas were found to range from 240 $m^2\ g^{-1}$ to 770 $m^2\ g^{-1}$.

Table 16: Colloid mass concentrations calculated for the size ranges 1 nm to 1000 nm and 50 nm to 1000 nm based on number distributions. Definition and use of the uncertainty factor f are given in Appendix B.

Sampling	Column bottom			Column head		
	Mass conc. [µg L^{-1}] 1-1000	Mass conc. [µg L^{-1}] 50-1000	f	Mass conc. [µg L^{-1}] 1-1000	Mass conc. [µg L^{-1}] 50-1000	f
Sampling 1						
Sample 1	58	46	2.7	22	17	3.6
Sample 2	44	38	3.1	16	12	2.6
Sampling 2						
Sample 1	26	24	4.3	38	37	3.4
Sample 2	12	10	2.4	25	23	2.3
Sampling 3						
Sample 1	6	5	2.9	6	5	1.9
Sample 2	5	4	2.4	38	37	2.1

Table 17: Colloid mass concentrations calculated for the size ranges 1 nm to 1000 nm and 50 nm to 1000 nm based on mass distributions. Definition and use of the uncertainty factor f are given in Appendix B.

Sampling	Column bottom			Column head		
	Mass conc. [µg L^{-1}] 1-1000	Mass conc. [µg L^{-1}] 50-1000	f	Mass conc. [µg L^{-1}] 1-1000	Mass conc. [µg L^{-1}] 50-1000	f
Sampling 1						
Sample 1	45	38	2.8	19	15	3.7
Sample 2	37	33	3.2	15	11	2.6
Sampling 2						
Sample 1	27	24	4.3	38	37	3.5
Sample 2	13	11	2.5	33	31	2.5
Sampling 3						
Sample 1	6	5	2.9	6	5	2.2
Sample 2	4	3	2.6	36	36	2.3

Table 18: Specific surface area of cement-derived colloids (size range 1 nm to 1000 nm).

Sampling	Column bottom	Column head
	Surface area [m^2 g^{-1}]	Surface area [m^2 g^{-1}]
Sampling 1		
Sample 1	620±120	620±140
Sample 2	450± 80	700±130
Sampling 2		
Sample 1	380±120	120± 30
Sample 2	520±100	240± 50
Sampling 3		
Sample 1	640±130	440± 60
Sample 2	770±130	90± 15

It is noted here that specific surface areas are lower for the size range 50 nm to 1000 nm (~15 to ~26 m^2 g^{-1}) due to a significant contribution of colloids with size < 50 nm to the total surface area. However, we expect colloids with size < 50 nm to be present in CPW and, therefore, consider the higher specific surface areas to be representative for the system.

6.5 Summary

Pore water of mortar M1 backfill material was collected and analysed for colloids (colloid concentrations and size distributions). The chemical analyses of the pore water for cement-derived elements indicate that the backfill material was in stage II of the cement degradation. Colloid size distributions were presented according to the power-law approach (Pareto law). The characteristic parameters (logA, slope -b) of the colloid number distributions were determined for the size range 50 nm to 5000 nm. Calculations of number, volume and mass concentrations for the size range 1 nm to 1000 nm were based on the assumption that the continuous size distributions observed for the range 50 nm to 5000 nm can be extrapolated to the lower colloidal size range (1 nm to 50 nm). Number, volume and mass concentrations of the two size ranges were compared to assess the contribution of colloids with size between 1 nm to 50 nm.

The slopes (-b) of the size distributions typically range from -3 to -3.7. The number concentration of colloids with size < 50 nm is the dominant contribution to the colloid inventory. Colloid mass concentrations were determined to be in the ppb range. The upper bound value for the colloid mass concentration is estimated to be 100 µg L^{-1} (= 0.1 ppm) taking into account the uncertainties on the data. The contribution of the colloids with size < 50 nm to the total colloid mass is at a maximum about 20 % depending on the slope (-b) of the number distribution. However, the contribution of colloids with size < 50 nm to the total surface area is significant. The specific surface area of the colloidal matter sampled from the mortar backfill CPW was found to be typically in the range 240 m^2 g^{-1} to 770 m^2 g^{-1}.

7 IMPLICATIONS FOR PERFORMANCE ASSESSMENT

7.1 Colloid Concentrations in the Near-Field of a Repository

The chemical conditions prevailing in the near-field of a repository appear to be favourable for colloid-matrix and colloid-colloid interactions. In the following, expected colloid concentrations in a cementitious environment will be compared with colloid concentrations measured in the groundwaters of potential host rocks. Within the Swiss programme for the disposal of radioactive waste, colloid analysis campaigns were performed in alpine and pre-alpine subsurface systems (DEGUELDRE 1994; 1997; DEGUELDRE et al. 1996a/b). The hydrogeochemical settings, which were studied, include aquifer systems in Northern Switzerland (Leuggern (Leu), Zurzach (Zur)) and the Black Forest (Menzenschwand (Men), Bad Säckingen (BDS)), Germany, the Grimsel Test Site (GTS) and the Marl formation at the Wellenberg site (WLB). The groundwaters are of Na-Ca-HCO_3-type (GTS, Men), Na-SO_4-HCO_3-Cl-type (Zur, Leu) or Na-Cl-type (BDS) or Na-Ca-HCO_3-type (WLB), respectively, with pH varying between 6.5 and 9.6 (Fig. 16 a). The CPW, however, is of Na-K-Ca-OH-type with pH above 12.5. Colloid concentrations in natural systems were reported to be a function of pH, ionic strength, hydrothermal activity and flow rate in the granitic subsurface systems (DEGUELDRE et al. 1996a). In these systems the salt concentration was considered to be an important parameter affecting colloid concentrations. Consequently, ionic strength is used as master variable for data comparison (Fig. 16 b). It is in line with the notion that ionic strength exerts a strong effect on particle-particle interactions (chapter 3). Note that the concentrations given in Figs. 16 a/b were determined in quasi-stagnant flow regime, which is anticipated both for the groundwater aquifers as well as the laboratory settings (DEGUELDRE et al. 1996a).

Fig. 16 b shows a trend to lower colloid concentrations with increasing ionic strength which appears in spite of the large differences in pH and the chemical composition of the groundwaters and the CPWs. Assuming ionic strength to be the only parameter affecting colloid inventories, however, is a simplification of the systems as indicated by the scatter in the data. Other parameters than ionic strength may also be effective, e.g., temperature, mineralogy of the colloidal fraction etc. Thus, the comparison given in Fig. 16 b only allows a qualitative interpretation of the data.

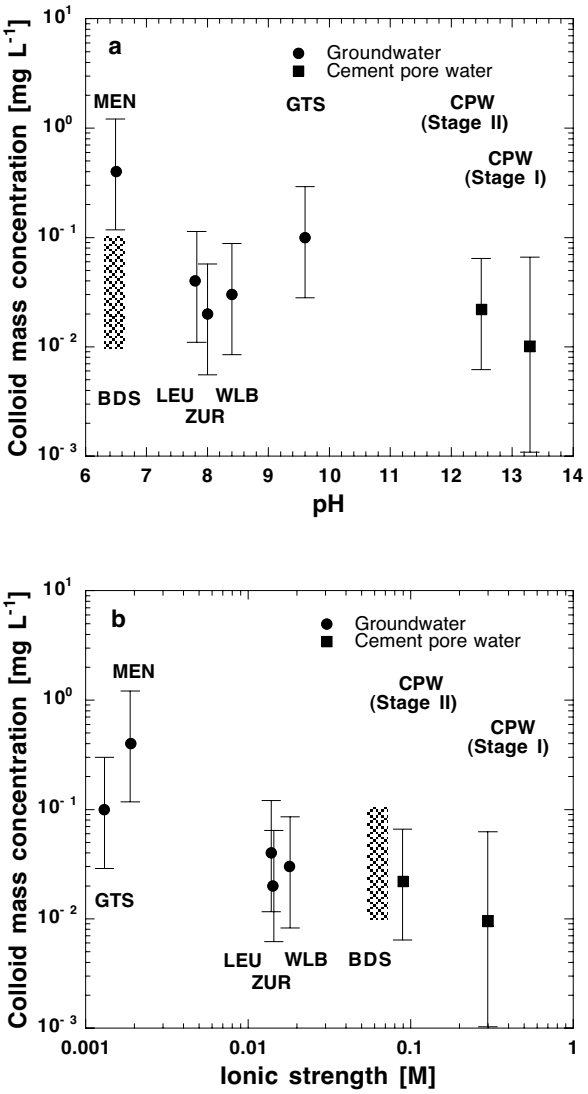

Fig. 16: Colloid mass concentrations of groundwater and CPW samples are shown as a function of a) pH and b) the ionic strength of the fluids. The values given for the aquifer systems with quasi-stagnant groundwaters (GW: BDS = Bad Säckingen, MEN = Menzenschwand, LEU = Leuggern, ZUR = Zurzach, GTS = Grimsel Test Site) were reported by DEGUELDRE et al. (1996a). Data for the Wellenberg site (WLB) were taken from DEGUELDRE (1997). The traced area (BDS) indicates an estimated colloid concentration range. CPW data are given in Tables 11 and 16. The uncertainties in the data are estimated to be one order of magnitude (corresponding to the uncertainties given in Table 16).

In stage I of the degradation of a cementitious near-field the ionic strength of the CPW was predicted to be I ~0.3 M ($[Ca]_{tot}$ ~2×10^{-3} M) (BERNER 1992; NEALL 1994). Consistently low colloid concentrations were observed in the batch flocculation studies. For the stage II of cement degradation the ionic strength was predicted to be lower than in stage I (I ~0.07 M). The reduction in ionic strength is compensated by a higher Ca concentration, which affects colloidal stability. Thus, low colloid concentrations were also found under these conditions as shown with the COLEX study.

The colloid mass concentrations reported in this study can be compared with values reported for the highly alkaline groundwater system at the Maqarin site. The composition of the Maqarin groundwater corresponds to a portlandite-buffered CPW in stage II of the cement degradation (pH=12.7, I ~0.07 M, $[Ca]_{tot}$ = 1.78×10^{-2} M). Thus, the Maqarin groundwater is considered to be a representative of a pore water discharging from the cementitious near-field of a repository at a late stage. Colloid mass concentrations for the Maqarin groundwater were reported to be in the range 0.07 to 0.2 ppm (WETTON et al. (1998) and references therein).

Thus, the data reported for the Maqarin groundwater and the values obtained from our laboratory systems are consistent indicating colloid mass concentrations well below 1 ppm under strongly alkaline conditions.

Based on the available data we can tentatively estimate a realistic value and an upper bound for the colloid mass concentration in the near-field (backfill pore water) of the planned L/ILW repository at the WLB site. In the low-permeability setting it is assumed that the residence time of groundwater infiltrating from the surrounding host rock through the cement liner of the cavern into the backfill will be sufficient to establish CPW conditions, i.e., pH > 12.5 (NEALL 1994). Under these conditions, a realistic value of the colloid mass concentration of the backfill pore water is given to be ~ 0.02 ppm, whereas the upper bound is estimated to be 0.1 ppm. Thus, the colloid mass concentrations are similar to the values reported for the Na-Ca-HCO_3-type groundwater at the WLB site (DEGUELDRE 1997). Note that the repository may be located in a Marl formation with a NaCl regime, i.e., a saline pore water of 0.2 M NaCl (NAGRA 1996). Nevertheless, low colloid mass concentrations are also expected under

these conditions (≤ 0.1 ppm) due to favourable chemical conditions for coagulation and filtration processes at high ionic strength.

Isosaccharinic acid (ISA) is produced in the near-field of a repository due to the degradation of cellulose material (VAN LOON & GLAUS 1998). From this study it is concluded that the effect of ISA on colloid stability and the long-term colloid concentration is negligible. Thus, we infer that ISA at concentrations below 10^{-3} M exerts no significant effect on the colloid inventory in the long term.

In addition to an in-situ production of organic ligands, infiltrating groundwater is a source of natural organic matter (NOM) in the near-field of a repository. LIANG & MORGAN (1990) report favourable conditions for particle-particle interactions if the concentration of fulvic and humic acids is in the range 0.1 ppm (coagulation of iron oxide particles, pH ~ 6.5 to 6.9). The influence of NOM on the colloid stability can tentatively be discussed for the high pH conditions. Assuming that NOM shows similar affinities for iron oxide (LIANG & MORGAN 1990) and cement-derived particles and, in addition, the fraction of NOM sorbed at pH ~ 7 and > 12.5 is identical (which most likely overestimates sorption under alkaline conditions), colloid stability is predicted to be enhanced at NOM concentrations larger than 0.1 ppm. Note, however, that the effect of NOM on colloid stability may be reduced due to the high Ca concentrations of CPW. The question concerning the actual concentration of dissolved humic substances in deep Swiss groundwater is not yet fully resolved. However, it is assumed that the maximum concentration of humics lies in the lower ppm range. The concentration is expected to be even lower for the WLB groundwater (ppb rather than ppm range) (GLAUS et al. 1997). Keeping in mind the uncertainties in both the available data and the prediction made above, one may speculate that the effect of NOM on colloid stability is presumably negligible due to the low NOM concentrations.

7.2 Assessment of the Effect of Near-Field Colloids on Radionuclide Migration

7.2.1 Sorption Values and Scaling Factors

The near-field of a repository mainly consists of cement and cementitious materials. Thus, radionuclide uptake by these solids represents one of the most important retardation mechanisms in the disposal cavern. In general, uptake is

described in terms of a distribution ratio, R_d, which accounts for the partitioning of a tracer between the cement (bulk) phase and the CPW (Eq. (2)). Sorption data (R_d values) have been compiled in sorption data bases for the cementitious near-field (e.g., BRADBURY & VAN LOON 1998). From the compilation of sorption values it emerges that R_d values of safety-relevant elements are typically in the range 0 to 100 m^3 kg^{-1} in cement systems. Low sorption values or no sorption, respectively, were reported for anions and alkali metals (e.g., BRADBURY & VAN LOON 1998), whereas high values were determined for the tri- and tetravalent metal cations, e.g., Eu(III) and Th(IV) (WIELAND et al. 1998a).

A scaling factor, S_c, was introduced to relate the uptake of a radioelement on hydrated cement (solid phase) to its affinity for the cementitious colloids (colloidal phase) (Eq. (9)). The proportionality expressed by S_c accounts for two aspects which, in principle, may affect the binding of a tracer onto the colloidal phase: 1) the high specific surface of the colloidal matter giving rise to a high sorption capacity, and 2) differences in the sorption affinities, i.e., binding constants on the bulk and the colloidal phases. The total number of surface sites per unit weight (sorption capacity) depends on the specific surface area of the material, whereas the stability of surface complexes is a direct consequence of the chemical nature of the surface sites and the characteristics of the radioelement.

The following considerations address the aspect of stability of surface complexes. We found clear evidence that the chemical composition of cement-derived near-field colloids is similar to the composition of hydrated cement. For example, it has been shown that CSH-type colloids appear to be formed in silica-rich CPW giving rise to an overall chemical composition of colloid population similar to CSH phases (section 2.3). Note that hydrated cement consists to approximately 50 wt.-% of CSH phases. Thus, we may conclude that the chemical nature of surface sites is similar on both cement-derived colloids and cement. This assumption is supported by sorption studies with the strongly sorbing radioelements Eu(III) and Th(IV). R_d values for Eu(III) and Th(IV) on C(A)SH phases of quite different compositions were reported to be in the range 100 m^3 kg^{-1} to 1000 m^3 kg^{-1} (TITS et al. 1998). Moreover, the sorption values were found to be similar to the ones reported for cement (WIELAND et al. 1998a). It indicates that the chemical nature of surface sites exhibits only a

minor effect on the uptake of the strongly sorbing radioelements. Thus, we anticipate that differences in the surface areas (or sorption capacities, respectively) of the colloidal fraction and the bulk cementitious material predominantly account for the respective differences in R_d values. We conclude that, for the strongly sorbing radionuclides, differences in the scaling factor can be attributed to differences in sorption capacities rather than sorption affinities.

Specific surface areas of bulk cement are required to deduce the scaling factor, S_c. N_2 sorption measurements (BET method) on a sulphate-resisting Portland cement with particle size < 70 µm yielded surface areas of approximately 50 $m^2 g^{-1}$ (WIELAND et al. 1997). ROWAN et al. (1988) determined the BET surface areas of HCP blends with different particle size distributions. The authors measured consistent surface areas independent of the particle size, i.e., 75±5 $m^2 g^{-1}$ for the 50 µm to 125 µm size range, 90±10 $m^2 g^{-1}$ for the 125 µm to 250 µm size range and 55±5 $m^2 g^{-1}$ for the 0.5 to 1.0 mm size range. It indicates that variations in particle size spectra of hydrated cement only cause minor changes in the accessible surface areas and, consequently, in the sorption capacities.

Surface areas of well-cured pastes have been determined using the BET method with N_2 and other non-polar sorbates (TAYLOR 1997). The results obtained by different investigators show considerable variations. The values were found to typically range from under 10 $m^2 g^{-1}$ to nearly 150 $m^2 g^{-1}$ arising from differences in the sorbate used and the characteristics of the HCP (e.g., w/c ratio, curing, treatment of the samples etc.). Note that even higher values, i.e., up to about 250 $m^2 g^{-1}$, were measured (TAYLOR 1997 and references therein). Mercury intrusion porosimetry (MIP) has been widely used in the study of cement pastes. For example, JACOBS et al. (1994) determined the total pore area of the HCP of the mortar backfill using MIP (Table 4). According to TAYLOR (1997), however, it is doubtful whether pore-size distributions and, consequently, surface areas deduced from MIP measurements are even approximately correct. For the present study, we thus rely on surface areas determined with the BET method using N_2 as sorbate. As a consequence representative values for the surface area of HCP are expected to be in the range 50 $m^2 g^{-1}$ to 90 $m^2 g^{-1}$ (ROWAN et al. 1988). For the following calculations a realistic value of 50 $m^2 g^{-1}$ and a lower limit of 10 $m^2 g^{-1}$ are taken into account.

Specific surface areas for cement-derived colloidal matter are given in Table 18. Surface areas were found to be in the range 240 m^2 g^{-1} to 770 m^2 g^{-1}. The scaling factor is estimated using the ratio of the surface areas of the colloidal and bulk materials. The representative value is

$$S_c = \frac{(240 \text{ to } 770)}{50} = \sim 5 \text{ to } \sim 16 . \qquad (42a)$$

The upper limit amounts to

$$S_c = \frac{(240 \text{ to } 770)}{10} = \sim 24 \text{ to } \sim 77 . \qquad (42b)$$

For further calculations, the scaling factor is set to S_c = 20, whereas S_c = 100 is considered to be an upper bound.

7.2.2 Sorption Reduction by Near-Field Colloids

The sorption reduction factor, F_{red}, given by Eq. (7) accounts for the potential effect of colloids on the retardation of radionuclides in the near-field. The dependence of F_{red} on the colloid mass concentration and the distribution ratio (R_d) is shown in Fig. 17. Note that the R_d value describes sorption on cement in the absence of colloids. Sorption reduction factors were calculated for sorption values ranging from 10^{-3} m^3 kg^{-1} (very weakly sorbing radionuclides) to 100 $m^3 kg^{-1}$ (very strongly sorbing radionuclides). Scaling factors of 20 or 100, respectively, were used to account for the proportionality between R_c and R_d (Eq. (9)).

Figs. 17 a and b show that the colloid-induced effects on the retardation of weakly to moderately sorbing radionuclides, i.e., $R_d \leq 1$ $m^3 kg^{-1}$, are expected to be negligible up to colloid concentrations of about 10^{-3} g L^{-1} (1 ppm). Sorption reduction is predicted to occur in the case of the strongly or very strongly sorbing radionuclides, respectively, with $R_d >> 1$ $m^3 kg^{-1}$. However, the effect is expected to be small up to a maximum concentration of 10^{-4} g L^{-1} (0.1 ppm), which is considered to be an upper bound for the colloid concentration in the mortar backfill of the planned L/ILW repository. For example, sorption reduction for Eu(III) and Th(IV) (R_d = 100 $m^3 kg^{-1}$), respectively, is negligible assuming a

colloid concentration of 10^{-4} g L^{-1} and S_c = 20. A conservative estimate (S_c = 100) results in a sorption reduction at a maximum by a factor of 2 ($R_{d,eff}$ = 50 $m^3\,kg^{-1}$).

The above assessment of the colloid effect indicates that no significant reduction of the radionuclide uptake by cement takes place in the presence of cement-derived colloids at colloid concentrations below about 1 ppm, except for the very strongly sorbing radionuclides, e.g., the lanthanides and actinides. However, at a colloid concentration of 0.1 ppm, which is considered to be an upper bound in CPW, the resultant effective distribution ratios of the strongly sorbing radionuclides are expected to be still high due to the strong retardation of tri- and tetravalent radioelements by cement.

It is re-emphasised that the above assessment of the effect of near-field colloids on radionuclide mobility is based on the following assumptions: First, the enhanced uptake of radionuclides by cement-derived colloids compared to cement is only caused by the higher sorption capacity of the colloidal matter. The scaling factor accounts for the difference in sorption capacities and, therefore, is attributed to the difference in the specific surface areas of the solid phase and the colloidal material. It was noted that, in principle, the scaling factor may depend on the chemical nature of the sites exposed on the surfaces. It was mentioned in the previous section that studies on radionuclide uptake by different near-field materials reveal similar chemical properties of the surface sites of cement and cement-derived colloids. Thus, the influence of the chemical properties of surface sites on radionuclide uptake is considered to be negligible.

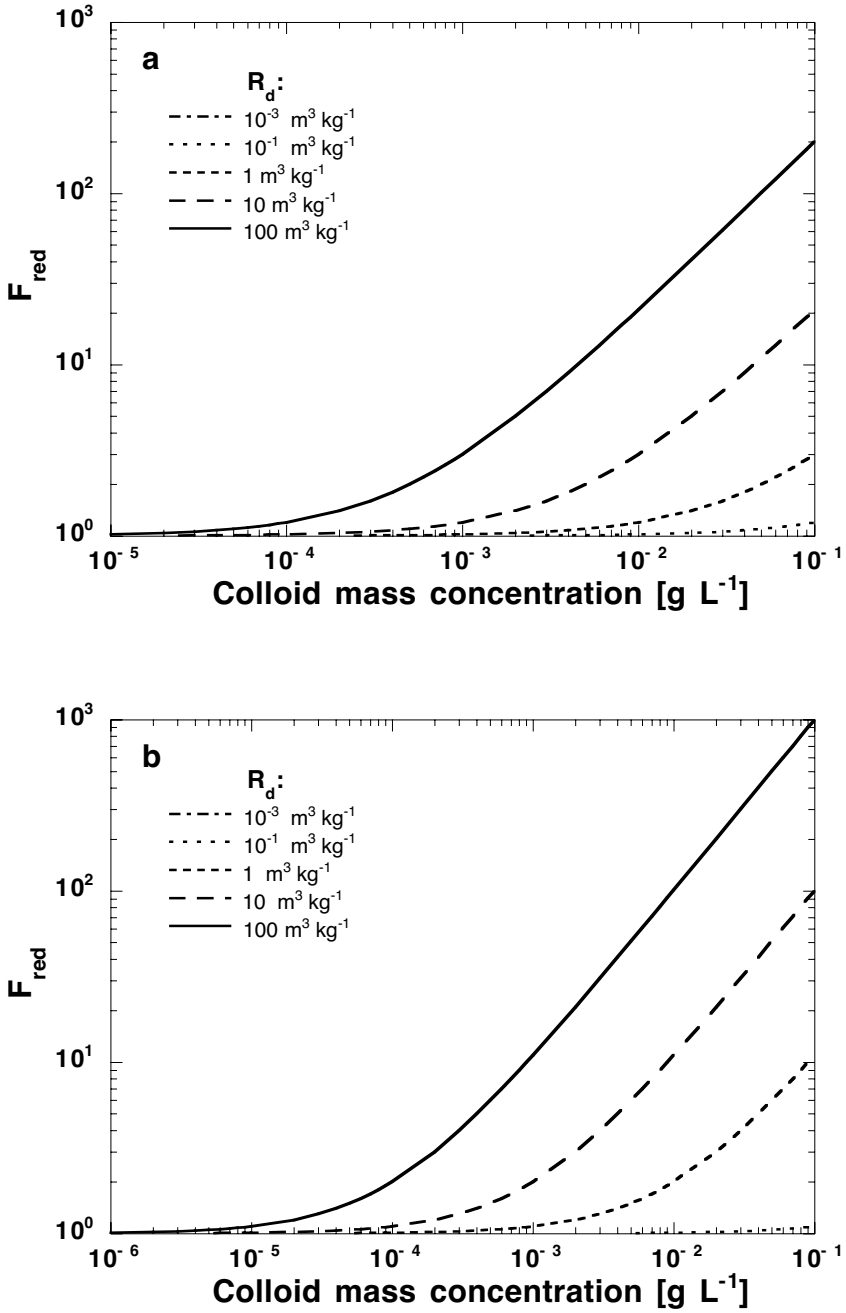

Fig. 17: Effect of colloids on the retardation of radionuclides in the cementitious near-field of a repository. F_{red} denotes the sorption reduction factor in the presence of colloids. F_{red} was calculated with Eq. (7) using scaling factors S_c = 20 (a) and S_C = 100 (b) (Eq. (9)). R_d denotes the sorption value on cement in the absence of colloids.

The second assumption concerns the mode of radionuclide-colloid interactions. In the above assessment reversibility of the uptake process is implicitly assumed. Nevertheless, irreversible uptake of radionuclides by cement-derived colloids is possible under certain conditions. For example, incorporation into the structure of cement-derived colloids may cause an irreversible binding of radionuclides. It requires that radionuclides are present in the pore water of the backfill mortar during colloid formation. To date, however, studies on co-precipitation/incorporation phenomena with cement-derived CSH-type materials are sparse, and, certainly, do not allow us to quantify irreversible uptake processes and to present final conclusions regarding their impact on radionuclide mobility. Note that the investigations presented in this work were started to characterise cement-derived colloidal matter and to quantify their concentration in the pore water of the backfill mortar rather than to elucidate mechanistic aspects of radionuclide binding onto CSH-type materials. It is also worth noting that an assessment of the relevance of irreversible uptake processes for radionuclide mobility actually requires a detailed discussion of the mechanisms governing radionuclide uptake by CSH phases, as well as considerations of the chemical stability of CSH-type materials in the near-field and the disturbed far-field of a repository. These considerations are certainly beyond the scope of the present study. Nevertheless, it is mentioned here that a research programme was started in our laboratory to elucidate sorption and co-precipitation processes with CSH phases under conditions relevant to the cementitious near-field of a repository. We expect that, with this information at hand, it should be possible to assess the effect of irreversible binding processes on radionuclide mobility and deduce consequences for performance assessment.

8 CONCLUSIONS

A porous mortar (Nagra designation: mortar M1) is foreseen to be used as backfill material in the planned Swiss L/ILW repository. Colloid generation and colloid dispersion may occur in the mortar due to the specific composition (cement covered quartz grains) and the high porosity (~27 %) of the material. Thus, it was considered that colloids might form in the pore water of backfill mortar M1 and facilitate radionuclide migration.

In this study colloid concentration measurements were carried out using an in-situ liquid particle counting system. The in-house developed counting system consists of three commercially available sensors for the detection of single particles and colloids at low concentrations in the size range 50 nm to 5000 nm. The counting system was tested using suspensions prepared from certified size standards. The tests show that the system allows fast and accurate measurements of colloid concentrations and size distributions. Moreover, statistically well-supported mass concentrations can be deduced based on measurements of colloid size distributions.

Colloid removal processes were investigated in batch-type flocculation studies. The studies were conducted to elucidate the effect of the cement pore water (CPW) composition, mainly the high ionic strength and Ca concentration, on colloid stability. In these experiments mortar M1 was immersed in a (Na,K)OH artificial cement pore water (ACW) to simulate the conditions during stage I of the cement degradation. In addition, control experiments with quartz immersed in ACW and an alkaline NaOH/KOH solution were carried out. Quartz was the aggregate material used to prepare the backfill mortar. In a few experiments isosaccharinic acid (ISA) was added to ACW to simulate the effect of cellulose degradation products on colloid stability. Initial colloid concentrations in well-mixed systems were found to be in the range 5×10^{10} coll L^{-1} to 5×10^{11} coll L^{-1}. It was observed that the initially high colloid concentrations decreased within a few days after leaving the mixed batch systems undisturbed (stagnant conditions). After a time period of 20 days the colloid concentrations were reduced to levels in the range 10^8 coll L^{-1} to 10^9 coll L^{-1}. The corresponding mass concentrations were in the range 4 to 20 µg L^{-1} (4 - 20 ppb). The upper bound is estimated to be 100 µg L^{-1} (0.1 ppm) taking into account the uncertainties on the data. It is shown that a coupled coagulation/sedimentation

process rather than sedimentation alone causes the reduction of the colloid concentration. ISA slightly retarded the coagulation/sedimentation process. However, the presence of ISA had no significant effect on the long-term colloid inventories in the laboratory systems.

Colloid concentrations were also determined in pore water, which was collected from a large column (total length = 2.69 m, inner diameter = 0.274 m, total volume = 158.8 L) filled with backfill mortar M1 (COLEX project). Analysis of the pore water was carried out to deduce in-situ colloid concentrations for the backfill. Chemical analysis of the pore water showed that it had the composition of a cement pore water characteristic for stage II of the cement degradation ("evolved" cement system). An upper bound value bound for the colloid mass concentration is estimated to be 100 µg L^{-1} (0.1 ppm) taking into account the uncertainties on the data. The specific surface area of the colloidal matter was estimated to be in the range 240 m^2 g^{-1} to 770 m^2 g^{-1} based on measurements of colloid size distributions.

From the above studies it emerges that colloid removal rather than colloid generation processes control the colloid inventory of the backfill pore water. Colloid removal is the consequence of colloid-colloid and colloid-solid phase interaction processes. Thus, in the long term, the resultant colloid concentration of the pore water is attributable to colloidal stability, which is strongly influenced by the chemical composition of the pore water. The specific conditions prevailing in a cementitious near-field, i.e., high ionic strength and Ca concentrations in the mmolar range, favour colloid coagulation and deposition processes, thus reducing the colloid inventories of the pore water. Favourable chemical conditions for colloid-colloid and colloid-solid phase interactions are retained in stage I and II of the cement degradation.

Colloid concentrations in the backfill mortar of the planned L/ILW repository can tentatively be assessed as follows: The concentration of cement-derived colloids in the pore water of the mortar backfill is estimated to be at maximum 100 µg L^{-1} (0.1 ppm). Note that this value is comparable to the colloid concentration determined for the Na-Ca-HCO_3-type groundwater of the Marl formation (WLB site). In addition, we anticipate that organic ligands, such as cellulose degradation products (i.e., ISA) at a mmolar concentration level and

humics at a ppb level, which are potentially present in the backfill pore water, exert no significant effect on colloid stability and, thus, colloid inventories.

A sorption reduction factor is introduced to assess the effect of cement-derived colloids on the retardation of radionuclides. The factor depends on the colloid mass concentration and the distribution ratio of a radionuclide between the pore water and the colloidal phase (R_c). A scaling factor (S_c) is introduced to account for the proportionality between R_c and R_d values, whereas R_d is the distribution ratio of a radionuclide between cement (solid phase) and cement pore water (liquid phase) in the absence of colloids. This approach holds for linear sorption and on the assumption that radionuclide partitioning is reversible. The scaling factor is deduced from the ratio of the specific surface areas of cement-derived colloidal matter and the bulk cement material. The representative scaling factor is estimated to be $S_c = 20$. In addition, an upper bound is given ($S_c = 100$). These values are used to calculate sorption reduction factors for increasing colloid concentrations and R_d values ranging between 10^{-3} m^3 kg^{-1} and 100 m^3 kg^{-1}. The effect of cement-derived colloids on radionuclide mobility is negligible for weakly to moderately sorbing radionuclides ($R_d \leq 1$ m^3 kg^{-1}) and colloid concentrations up to about 1 ppm. Uptake by cement may be reduced in the case of the strongly sorbing radionuclides ($R_d > 1$ m^3 kg^{-1}) and colloid mass concentrations exceeding 0.1 ppm. Nevertheless, under conditions relevant to a near-field situation, i.e., at a typical colloid concentration of 0.1 ppm and R_d = 100 m^3 kg^{-1}, no significant effect on radionuclide mobility is expected due to the strong interaction of radionuclides with cement in the absence of colloids.

9 REFERENCES

ABDEL-SALAM, A. & CHRYSIKOPOULOS, C.V. (1995). Modeling of colloid and colloid-facilitated contaminant transport in a two-dimensional fracture with spatially variable aperture. Trans. Por. Media. 20, 197 - 221.

BATEMAN, K., COOMBS, P., NOY, D.J., PEARCE, J.M. & WETTON, P. (1995). Nagra/Nirex/SKB column experiments: Results of experiments and modeling. Nagra unpublished internal report, Nagra, Wettingen, Switzerland.

BERNER, U. R. (1990). A thermodynamic description of the evolution of pore water chemistry and uranium speciation during the degradation of cement. PSI Bericht 90-62, Paul Scherrer Institut, Villigen, Switzerland, and Nagra Technical Report NTB 90-12, Wettingen, Switzerland.

BERNER, U.R. (1992). Evolution of pore water chemistry during degradation of cement in a radioactive waste repository environment. Waste Management 12, 201 - 219.

BONANO, E.J. & BEYELER, E. (1985). Transport and capture of colloidal particles in single fractures. Mat. Res. Soc. Symp. Proc. 44, 385 - 392.

BRADBURY, M.H. & VAN LOON, L.R. (1998): Cementitious near-field sorption data bases for performance assessment of a L/ILW repository in a Palfris marl host rock, CEM-94: UPDATE I, June 1997. PSI Bericht 98-01, Paul Scherrer Institut, Villigen, Switzerland, and Nagra Technical Report NTB 96-04, Wettingen, Switzerland.

BRADY, P.V. & WALTER, J.V. (1990). Kinetics of quartz dissolution at low temperature. Chem. Geol. 82, 253 - 264.

BUFFLE, J. & VAN LEEUWEN, H.P. (1992). Environmental particles, Vol 1, IUPAC environmental, analytical and physical chemistry series, Lewis Publishers, Boca Raton, FL, 1992.

COOK, R. A. (1991). Fundamentals of mercury intrusion porosimetry and its application to concrete materials science, Ph.D. thesis, Cornell University, NY, 1991.

DEGUELDRE, C. et al. (1989). Grimsel colloid exercise. PSI Bericht 89-39, Paul Scherrer Institut, Villigen, Switzerland, and Nagra Technical Report NTB 90-01, Wettingen, Switzerland.

DEGUELDRE, C. (1994). Colloid properties in groundwaters from crystalline formations. PSI Bericht 94-21, Paul Scherrer Institut, Villigen, Switzerland, and Nagra Technical Report NTB 92-05, Wettingen, Switzerland.

DEGUELDRE, C., PFEIFFER, H.-R., ALEXANDER, W., WERNLI, B. & BRUETSCH, R. (1996a). Colloid properties in granitic groundwater systems. I: Sampling and characterization. Appl. Geochem. 11, 677 - 695.

DEGUELDRE, C., GRAUER, R., LAUBE, A., OESS, A. & SILBY, H. (1996b). Colloid properties in granitic groundwater systems. II: Stability and transport study. Appl. Geochem. 11, 697 - 710.

DEGUELDRE, C. (1997). Groundwater colloid properties and their potential influence on radionuclide transport. Mat. Res. Soc. Symp. Proc. 465, 835 - 846.

ELIMELECH, M. & O'MELIA, C.R. (1990). Effect of particle size on collision efficiency in the deposition of Brownian particles with electrostatic energy barriers. Langmuir 6, 1153 - 1163.

ELIMELECH, M., GREGORY, J., JIA, X. & WILLIAMS, R. (1995). Particle deposition and aggregation. Butterworth-Heinemann Ltd., Oxford, GB.

FARLEY, K.J. & MOREL, F.M.M. (1986). Rôle of coagulation in the kinetics of sedimentation. Environ. Sci. Technol. 20, 187 - 195.

FILELLA, M & BUFFLE, J. (1993). Factors controlling the stability of sub-micron colloids in natural waters. Colloids Surf. 73, 255 - 273.

FRIEDLANDER, S.K. (1960). Similarity considerations for the particle-size spectrum of a coagulating, sedimenting aerosol. J. Meterology 17, 479 - 483.

FRIEDLANDER, S.K. (1977). Smoke, dust and haze. J. Wiley & Sons, N.Y.

GARDINER, M.P., SMITH, A.J. & WILLIAMS, S.J. (1990). Sorption on inactive repository components, DoE/HMIP/RP/90/084.

GLAUS, M.A., HUMMEL, W. & VAN LOON, L.R. (1997). Experimental determination and modelling of trace metal-humate interactions: A pragmatic approach for applications in groundwater. PSI Bericht 97-13, Paul Scherrer Institut, Villigen, Switzerland, and Nagra Technical Report NTB 97-03, Wettingen, Switzerland.

GRAUER, R. (1990). Zur Chemie von Kolloiden: Verfügbare Sorptionsmodelle und zur Frage der Kolloidhaftung. PSI Bericht 90-65, Paul Scherrer Institut, Villigen, Switzerland, and Nagra Technical Report NTB 90-37, Wettingen, Switzerland.

GREENBERG, S.A. & PRICE, E.W. (1957). The solubility of silica in solutions of electrolytes. J. Phys. Chem. 61, 960 - 965.

GREENBERG, S.A. & CHANG, T.N. (1965). Investigation of the hydrated calcium silicates. II. Solubility relationships in the calcium oxide-silica-water system at 25° C. J. Phys. Chem. 69, 1151 - 1173.

GRINDROD, P. (1990). An asymptotic spectral comparative approach to the derivation of one dimensional transport models for solutes and colloids in fractures. SKI (Swed. Nucl. Power Inspec.), Stockholm, Techn. Rep. TR 90-4.

HEATH, T.G., ILETT, D.J. & TWEED, C.J. (1996). Thermodynamic modelling of the sorption of radioelements onto cementitious materials. Mat. Res. Soc. Symp. Proc. 412, 443 - 449.

IRIYA, K., JACOBS, F., KNECHT, B. & WITTMANN, F.H. (1991). Cementitious backfill material for a L/ILW repository - Investigations of gas transport properties. Nucl. Eng. Design 129, 49 - 55.

IWAIDA, T., NAGASAKI, S. & TANAKA, S. (2000). Sorption study of strontium onto hydrated cement phases using a sequential desorption method. Radiochim. Acta 88, 483 - 486.

JACOBS, F. & WITTMANN, F.H. (1992). Long term behavior of concrete in nuclear waste repositories. Nucl. Eng. Design 138, 157 - 164.

JACOBS, F., MAYER, G. & WITTMANN, F.H. (1994). Hochpermeable, zementgebundene Verfüllmörtel für SMA Endlager. Nagra Technical Report NTB 92-11, Wettingen, Switzerland.

KRETSCHMAR, R., BARMETTLER, K., GROLIMUND, D., YAN, Y., BORKOVEC, M. & STICHER, H. (1997). Experimental determination of colloid deposition rates and collision efficiencies in natural porous media. Water Resour. Res. 33, 1129 - 1137.

LAWLER, D., IZURIETA, E. & KAO, C.-P. (1983). Changes in particle size distribution during Brownian coagulation. J. Colloid Interface Sci. 92, 315 - 325.

LERMAN, A. (1979). Geochemical processes. Water and sediment environments. J. Wiley & Sons, N.Y.

LIANG, L. & MORGAN, J.J. (1990). Coagulation of iron oxide particles in the presence of organic materials. In: Chemical modelling in aqueous systems. Melchior D.C. and Barlett R.L. (eds). ACS Symposium Series 416, Washington DC, 293 - 308.

LYKLEMA, J. (1978). Surface chemistry of colloids in connection with stability. In: The scientific basis of flocculation. Ives, K.J. (ed). Sijthoff and Noordhoff, The Netherlands, 3 - 36.

MACPHEE, D.E., LUKE, K., GLASSER, F.P. & LACHOWSKI, E.E. (1989). Solubility and ageing of calcium silicate hydrates in alkaline solutions at 25° C. J. Am. Ceram. Soc. 72(4), 646 - 654.

MAYER, G., MOETSCH H.A. & WITTMANN, F.H. (1998). Large scale experiment for water and gas transport in cementitious backfill materials (phase 1). Nagra Technical Report NTB 98-03, Nagra, Wettingen, Switzerland.

MAYER, G. (1998). Pers. Communication.

McCARTHY, J. & DEGUELDRE, C. (1993). Sampling and characterisation of colloids in groundwater for studying their rôle in the subsurface transport of contaminants. In: Environmental particles, Vol 2, Buffle J. and van Leeuwen H.P. (eds). IUPAC environmental, analytical and physical chemistry series, Lewis Publishers, Boca Raton, FL, 247 - 316.

NAGRA (1994a). Kristallin-1; Safety Assessment Report, Nagra Technical Report NTB 93 - 22, Wettingen, Switzerland.

NAGRA (1994b). Endlager für schwach- und mittelaktive Abfälle (Endlager SMA); Bericht zur Langzeitsicherheit des Endlagers SMA am Standort Wellenberg, NW, Nagra Technical Report NTB 94-06, Wettingen, Switzerland.

NAGRA (1996). Geosynthese Wellenberg 1996: Ergebnisse der Untersuchungsphasen I und II, Nagra Technical Report NTB 96-01, Wettingen, Switzerland.

NEALL, F. (1994). Modelling of the near-field chemistry of the SMA repository at the Wellenberg site. PSI Bericht 94-18, Paul Scherrer Institut, Villigen, Switzerland, and Nagra Technical Report NTB 94-03, Wettingen, Switzerland.

NUTALL, H.H., & LONG, R. (1993). Mobility of radioactive colloidal particles in groundwater. Rad. Waste Man. Nucl. Fuel Cycle 17, 237 - 251.

O'MELIA, C.R. (1980). Aquasols: the behaviour of small particles in aquatic systems. Environ. Sci. Technol. 14, 1052 - 1060.

O'MELIA, C.R. (1985). The influence of coagulation and sedimentation on the fate of particles, associated pollutants, and nutrients in lakes. In: Chemical processes in lakes. Stumm, W. (ed). J. Wiley & Sons, N.Y., 207 - 224.

O'MELIA, C.R. (1987). Particle-particle interactions. In: Aquatic surface chemistry: Chemical processes at the particle-water interface. Stumm, W. (ed). J. Wiley & Sons, N.Y., 385 - 403.

O'MELIA, C.R. & TILLER, C. (1993). Physicochemical aggregation and deposition in aquatic environment. In: Environmental particles, Vol 2, Buffle J. and van Leeuwen H.P. (eds). IUPAC environmental, analytical and physical chemistry series, Lewis Publishers, Boca Raton, FL, 353 - 386.

PAGE, A.L., MILLER, R.H. & KEENEY, D.R. (1982). Methods of soil analyses. Part 2: Chemical and microbiological properties. Am. Soc. Agr., 2nd Ed., Madison, Wisconsin, USA.

PARKS, G.A. (1967). Aqueous surface chemistry of oxides and complex oxide minerals. In: Equilibrium concepts in natural water systems. Advances in chemistry series, American Chemical Society, Washington, 121 - 160.

PFINGSTEN, W. & SHIOTSUKI, M. (1998). Modelling a cement degradation experiment by a hydraulic transport and chemical equilibrium coupled code. Mat. Res. Soc. Symp. Proc. 506, 805 - 812.

RAMSAY, J.D.F., AVERY, R.G. & RUSSELL, P.J. (1988). Physical characteristics and sorption behaviour of colloids generated from cementitious systems. Radiochim. Acta 44/45, 119 - 124.

RAMSAY, J.D.F., AVERY, R.G. & RUSSELL, P.J. (1991). Colloids related to low level and intermediate level waste. Final report, DoE/HMIP/RP/90/064.

ROWAN, S., DONALDSON, L. & WHITE, S. (1988). A comparative study of the pore structures and surfaces of hardened cement pastes of potential use in radioactive waste repositories. UK Nirex Ltd Report NSS/R108, Harwell UK.

RYAN, J.N. & ELIMELECH, M. (1996). Colloid mobilization and transport in groundwater. Colloids Surf. 107, 1 - 56.

SMITH, P. (1993). A model for colloid-facilitated radionuclide transport through fractured media. PSI Bericht 93-04, Paul Scherrer Institut, Villigen, Switzerland, and Nagra Technical Report NTB 93-32, Wettingen, Switzerland.

SMITH, P. & DEGUELDRE, C. (1993). Colloid-facilitated transport of radionuclides through fractured media. J. Contam. Hydrol. 13, 143 - 166.

SONG, L. & ELIMELECH, M. (1995). Calculation of particle deposition rate under unfavourable particle-surface interactions. J. Chem. Soc. Faraday Trans. 89, 3443 - 3452.

STEIN, H.N. (1968). Surface charges on calcium silicates and calcium silicate hydrates. J. Colloid Interface Sci. 28, 203 - 213.

STEINFELD, J.I., FRANCISCO, J.S. & HASE, W.L. (1989). Chemical kinetics and dynamics. Prentice Hall, N.J.

STUMM, W. & MORGAN, J.J. (1995). Aquatic chemistry. 3th ed, J. Wiley & Sons, N.Y.

SWANTON, S.W. (1995). Modelling colloid transport in groundwater; the prediction of colloid stability and retention behaviour. Adv. Colloid Interface Sci. 54, 129 - 208.

TAYLOR, H.F.W. (1997). Cement chemistry, 2nd ed., Thomas Telford Publ., London, UK.

TITS, J., BRADBURY, M.H., WIELAND, E. & MANTOVANI, M. (1998). The uptake of Cs, Sr, Ni, Eu and Th by CSH phases under high pH cement pore water conditions. PSI Interim Report TM-44-98-01, Paul Scherrer Institut, Villigen, Switzerland.

TOBIASON, J.E. & O'MELIA, C.R. (1988). Physico-chemical aspects of particle removal in depth filtration. J. Am. Water Works Assoc. 80, 54 - 64.

TRAVIS, B.J. & NUTALL, H.E. (1985). A transport code for radio-colloid migration: With an assessment of an actual low-level waste site. Mat. Res. Soc. Symp. Proc. 44, 969 - 976.

VAN LOON, L.R. & GLAUS, M.A (1997). Sorption of isosaccharinic acid, a cellulose degradation product, on cement. Environ. Sci. Technol. 31, 1243 - 1245.

VAN LOON, L.R. & GLAUS, M.A (1998). Experimental and theoretical studies on alkaline degradation of cellulose and its impact on the sorption of radionuclides. PSI Bericht 98-07, Paul Scherrer Institut, Villigen, Switzerland, and Nagra Technical Report NTB 97-04, Wettingen, Switzerland.

VILKS, P. & BACHINSKI, D.B. (1994). Colloid and suspended particle migration experiments in a granite fracture. Radiochim. Acta 66/67, 229 - 234.

VILKS, P., CARON, F. & HAAS, M.K. (1998). Potential for the formation and migration of colloidal material from a near-surface waste disposal site. Appl. Geochem. 13, 31 - 42.

VON SMOLUCHOWSKI, M. (1917). Versuch einer mathematischen Theorie der Koagulationskinetik kolloidaler Lösungen. Zeitschrift f. physik. Chemie 92, 129 - 168.

WETTON, P.D., PEARCE, J.M., ALEXANDER, W.R., MILODOWSKI, A.E., REEDER, S., WRAGG, J. & SALAMEH, E. (1998). The production of colloids at the cement/host rock interface. Maqarin natural analogue study: Phase III. Smellie, J.A.T. (ed.), Technical Report TR-98-04, Swedish Nuclear Fuel and Waste Management Co (SKB), Stockholm, Sweden.

WIELAND, E. (1997). Colloid generation in cementitious backfill material: Preliminary investigations in the systems quartz/cement pore water and "monokorn" mortar/cement pore water. PSI Interim Report TM-44-97-01, Paul Scherrer Institut, Villigen, Switzerland.

WIELAND, E., DOBLER, J.P. & SPIELER, P. (1997). Sorption measurements of ^{152}Eu and ^{234}Th on HTS cement. PSI Interim Report TM-44-97-04, Paul Scherrer Institut, Villigen, Switzerland.

WIELAND, E., TITS, J., SPIELER, P. & DOBLER, J.P. (1998a). Interaction of Eu(III) and Th(IV) with sulphate-resisting Portland cement. Mat. Res. Soc. Symp. Proc. 506, 573 - 578.

WIELAND, E., SPIELER, P. & WERNER, D. (1998b). Aufbau und Inbetriebnahme eines Partikelzählsystems zur Bestimmung von Partikel- und Kolloidkonzentrationen in Flüssigkeiten. PSI Interim Report TM-44-98-11, Paul Scherrer Institut, Villigen, Switzerland.

10 ACKNOWLEDGEMENTS

The author wishes to thank P. Seiler, P. Spieler and D. Werner for their assistance with the experimental work. Special thanks are due to Dr. G. Mayer (ETH Zürich), who allowed me to use some unpublished data, for his assistance with pore water sampling and a drawing of the COLEX column. Thanks are extended to R. Brütsch (PSI) for performing SEM/EDS analyses, Dr. M. Lauber for a translation of the abstract and B. Gschwend for the final layout work. The careful reviews by Drs. M. Bradbury (PSI), C. Degueldre (PSI), J. Hadermann (PSI), I. Hagenlocher (Nagra), P. Zuidema (Nagra) and H. Geckeis (external review, FZK, Germany) are gratefully acknowledged.

The work was partially financed by the National Cooperative for the Disposal of Radioactive Waste (Nagra).

APPENDIX A

MIP data for mortar M1 (MAYER 1998)

Characteristic MIP (mercury intrusion porosimetry) data for the mortar M1 HCP are summarised in Table A1. Preparation of the mortar material and MIP measurements were carried out as reported by JACOBS et al. (1994). COOK (1991) reported fundamentals of MIP and its application to concrete materials science.

Table A1: MIP data of a mortar M1 sample (Sample: Mortar M1 2/3, 3.2.92).

Parameter	HCP
Bulk density ρ_b [g cm^{-3}]	2.26
Apparent (skeletal) density ρ_a [g cm^{-3}]	2.42
Porosity ε [Vol.%] [1]	6.61
Median pore diameter (volume) [µm]	0.085
Total pore area [m^2 g^{-1}]	4.16

[1] Porosity was estimated using the following expression:

$$\varepsilon\ [\%] = \left(1 - \frac{\rho_b}{\rho_a}\right) 100$$

The total pore area of the mortar material described by JACOBS et al. (1994) (Table 4) was estimated based on the MIP data given in Table A1 and on the assumption that the total pore area increases linearly with the porosity.

APPENDIX B

Estimate of the uncertainties imposed on the particle number and particle volume concentrations

Applying the theory of error propagation gives the standard derivation, σ, in the value of F as:

$$\sigma_F^2 = \left(\frac{\partial F}{\partial x}\right)^2 \sigma_x^2 + \left(\frac{\partial F}{\partial y}\right)^2 \sigma_y^2. \qquad \text{(B.1)}$$

In this context F represents the particle number or particle volume concentration, respectively, as given according to the power-law approach (Eqs.(26) and (33)). In the logarithmic form Eqs. (26) and (33) can be written as:

$$\log N = \log A + \log\left(\frac{Ø_2^{(1-b)} - Ø_1^{(1-b)}}{1-b}\right), \qquad \text{(B.2)}$$

and

$$\log V = \log(\pi/6) + \log A + \log\left(\frac{Ø_2^{(4-b)} - Ø_1^{(4-b)}}{4-b}\right). \qquad \text{(B.3)}$$

On the assumption that the variables x (= logA) and y (= b) are independent, the variance can then be approximated by:

$$\sigma^2 \approx \sigma^2\{\log A\} + \lambda^2 \sigma_b^2, \qquad \text{(B.4)}$$

with

$$\lambda = \frac{\partial \log N}{\partial b} = \partial/\partial b \log\left(\frac{Ø_2^{(1-b)} - Ø_1^{(1-b)}}{1-b}\right), \qquad \text{(B.5)}$$

and

$$\lambda = \frac{\partial \log V}{\partial b} = \partial/\partial b \log\left(\frac{Ø_2^{(4-b)} - Ø_1^{(4-b)}}{4-b}\right). \qquad \text{(B.6)}$$

Variances $\sigma\{\log A\}$ and σ_b result from linear regressions obtained from the power-law presentation of the particle number distributions (see Tables 6, 7, 10 and 13).

In general, the uncertainty in a parameter M (M = number and volume concentration) presented in its logarithmic form can be written as:

$$\log M \pm \sigma\{\log M\}, \tag{B.7}$$

with the median given by:

$$M = 10^{\log M}, \tag{B.8}$$

The upper M_u and lower M_l boundaries of the uncertainty range are given by:

$$M_u = 10^{\log M + \sigma \log M} \tag{B.9a}$$

$$M_l = 10^{\log M - \sigma \log M} \tag{B.9b}$$

This uncertainty can be expressed in terms of an uncertainty factor f:

$$f = 10^{\sigma \log M}, \tag{B.10}$$

with the upper and lower boundaries expressed by:

$$M_u = M \times f, \tag{B.11a}$$

$$M_l = M / f. \tag{B.11b}$$

In Table 11, upper and lower boundaries M_u and M_l of the colloid mass concentrations are listed. In Tables 14 - 17, uncertainties in the number, volume and mass concentrations are expressed in terms of the uncertainty factor f.